GATE DESIGN FOR INJECTION MOLDS

by

Jorge Echenagucia

Dissertation submitted to the Graduate Faculty of the

Virginia Polytechnic Institute and State University

in partial fulfillment of the requirements for the degree of

DOCTOR OF PHILOSOPHY

in

Chemical Engineering

APPROVED:

J. C. Hassler, Co-Chairman

A. L. Fricke, Co-Chairman

G. H. Beyer

W. C. Thomas

W. W. Stinchcomb

H. A. McGee, Jr., Dept. Head

February, 1977

Blacksburg, Virginia

ACKNOWLEDGMENTS

The path to be followed in order to obtain any graduate degree is hard and tortuous. Most times our expectations are frustrated, but we can keep on going with the help given by our friends. I have made many friends during the time I have spent in Blacksburg; to all of them, thanks very much for your help. Thanks for sharing the heavy load when it got heavier.

Thanks to my advisers Dr. J. Hassler and Dr. A. Fricke for their patience, understanding and friendship. Without their encouragement, I could not have worked as hard and with as much dedication. Thanks to Mr. B. Williams for the magnificent job done making the injection mold used in this investigation.

To my friend Mr. Tom Mason, thanks for the development of the computer software to log and plot the experimental data. Thanks for your encouragement and sincere friendship. To Mr. Russell Smith, thanks very much for helping me with the computer interfacing and in other computer related areas of this project. To Mr. Joseph Conte thanks for your help with the plotter software. You certainly should be proud of it.

To the members of my committee, thanks for the help given, especially at the beginning of this investigation.

Last, but never least, thanks to my dear wife Milagros; you really helped me with your patience, love and encouragement. God bless you!

TABLE OF CONTENTS

TABLE OF CONTENTS - continued

LIST OF FIGURES

LIST OF FIGURES - continued

LIST OF FIGURES - continued

LIST OF TABLES

I. INTRODUCTION

The basic components of any injection molding operation are the injection press, the injection mold and the mold cooling system. The injection press, either of the plunger type or the newer sliding screw type, melts and delivers the molten polymer into the injection mold. The mold basically shapes the polymer into the desired article. The cooling system removes the heat necessary to insure an optimum molding cycle time.

The hot polymer must be conveyed into the cavity by a system of channels generally of circular, half circular or square cross section that are called runners. The runners are reduced in cross sectional area and appropriately shaped near the cavity entrance in order to reduce the plunger or screw forward time, to uniformly heat the cold polymer front, to evenly distribute the polymer flow during the filling of the cavity and to ease the cleaning of the molded part. These runner reductions are called gates.

The design of gates for injection molds is a subject that is too often neglected when consideration is being given to the various problems related to product quality. The effect which gate design has on the properties of the molded part is as important as its effect on the molding cycle. Despite the vast amount of literature published on materials and their properties, little or no information is published on what happens to these materials under the conditions imposed by various types of gates.

It is the purpose of this investigation to develop a procedure for the design of gates and runner systems for injection molds for pseudoplastic materials. Special attention will be given to the design of restricted (pin) gates because of their wide use in the molding industry.

The steps to be followed in this study will include: (1) selection of a suitable polymer, (2) determination of the flow curves for the selected polymer, (3) development of a mathematical model to simulate the injection molding process. The model will be used to predict temperature and pressure profiles during the filling, packing and cooling stages of the injection molding cycle. This information will be used to determine the appropriate gate dimensions to insure an optimum part, (4) design and construction of an injection mold to validate the proposed model, (5) development of a technique to monitor the temperature and pressure in the runner(s), gate(s) and mold cavity, and (6) development of a gate design procedure based on the predictions of the model.

The mathematical model developed in this investigation should be useful not only for design purposes, but as an aid for pinpointing and correcting defects in existing molds.

II. BACKGROUND AND SURVEY OF LITERATURE

A survey of the literature pertinent to this investigation is presented in the following sections.

Gates for Injection Molds

During the flow of polymer melt in the filling stage of the injection cycle, the runners serve as conveyers of the polymer into the mold cavity. Before the melt enters the cavity, and in order to insure a high quality molded part, the cross section of the runners is changed into a wide variety of shapes. These new shaped channels are called gates.

The most commonly used type of gates are shown in figures 1, 2 and 3. Gates can be located on the side, top or bottom, depending on the shape of the article to be molded. For large hollow articles, diaphragm, spider, or ring gates should be used. For flat and wide parts, fan, flash, or multiple-edge gates are recommended. For more complicated geometries, tab or submarine gates are generally used.

It is not difficult to recognize that gates play a very important role in the production of good quality molded parts. A very narrow gate will require a high injection pressure setting to overcome the tremendous pressure drop across it. Even if the injection pressure is high enough to allow the filling of the cavity, the heat generated by viscous dissipation across the gate could raise the polymer temperature above its degradation temperature, causing polymer decomposition. A gate that is very short or too wide could allow a cold polymer front

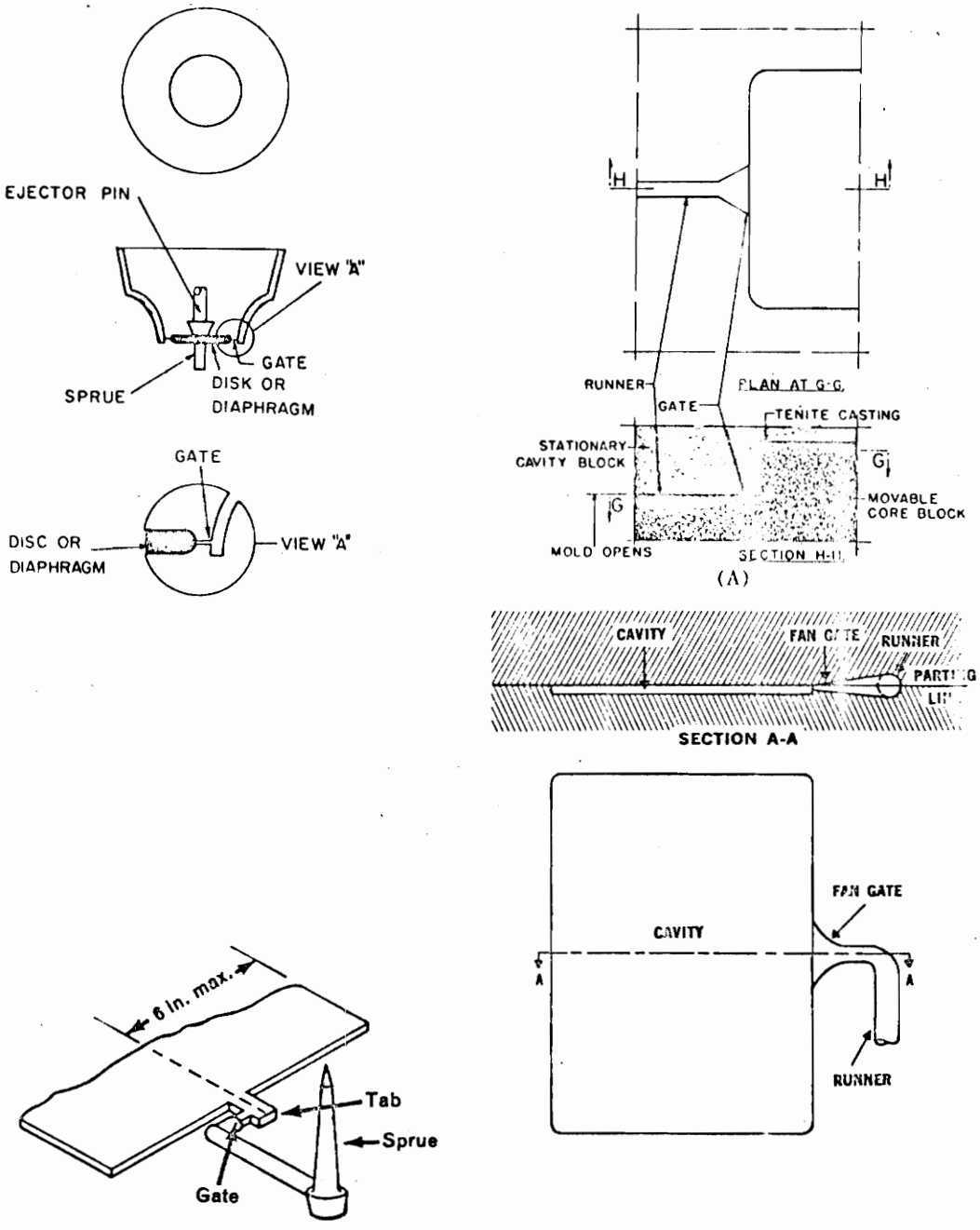

FIGURE 1. DIAPHRAGM, TAB AND FAN GATES

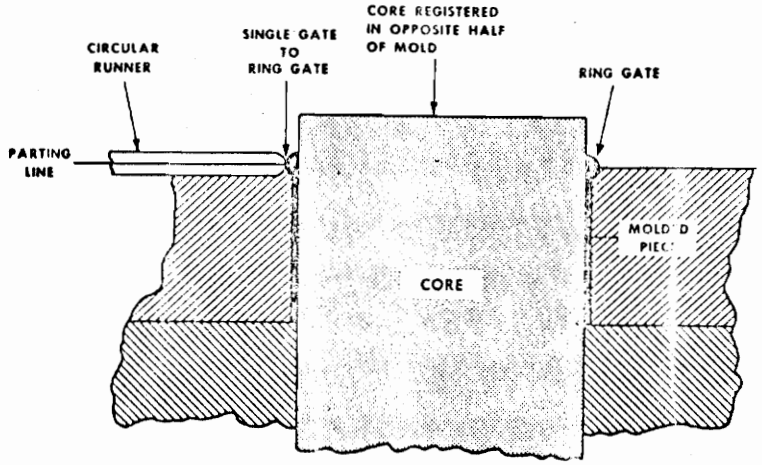

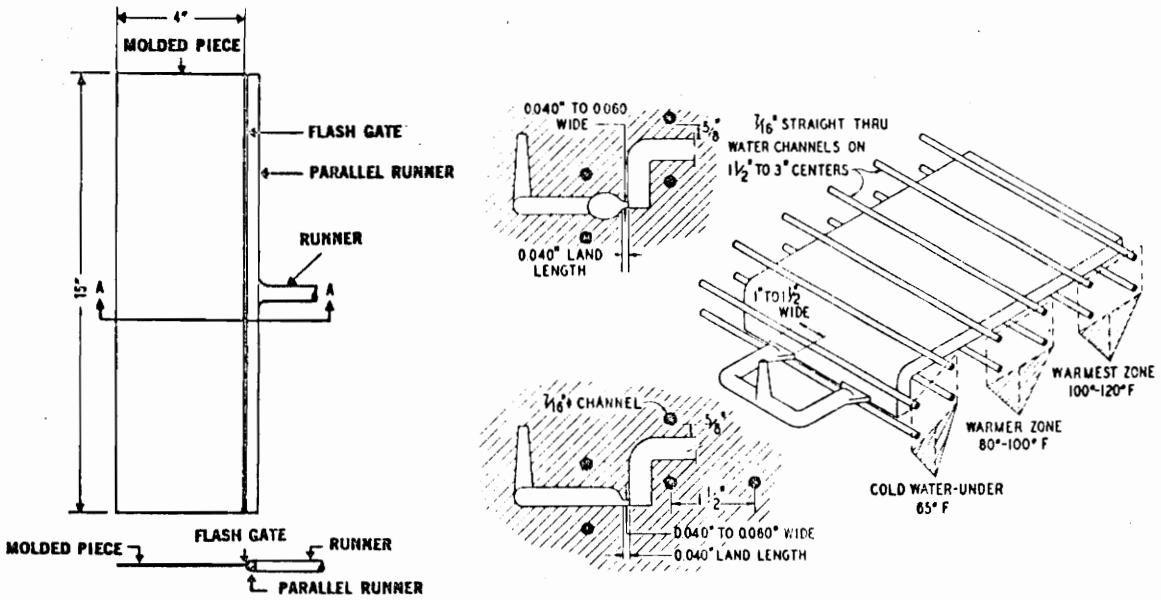

FIGURE 2. RING, FLASH AND RESTRICTED FAN GATES

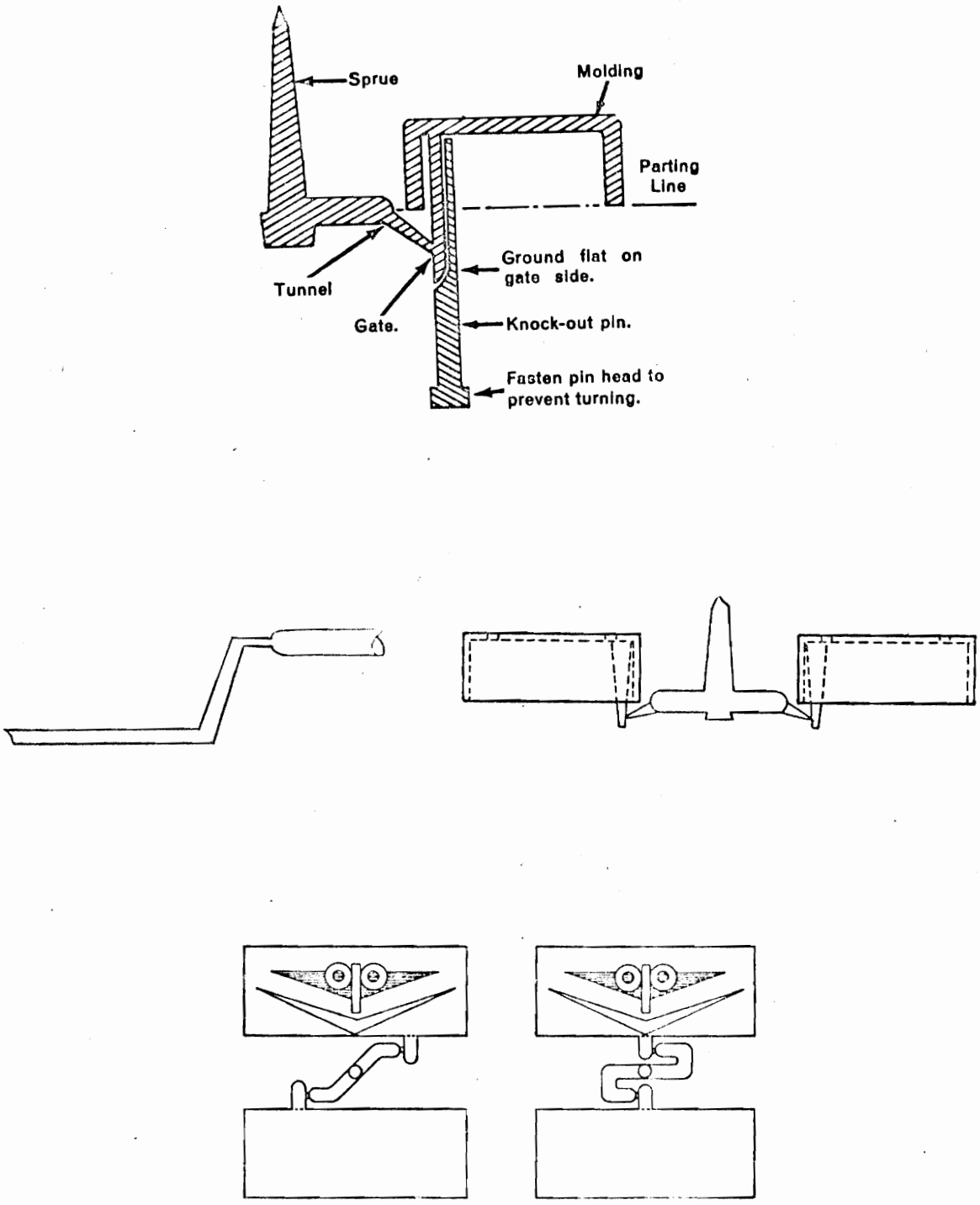

FIGURE 3. SUBMARINE, PIN, PLUG AND RESTRICTED TAB GATES

into the cavity, causing sink marks or a rough surface appearance of the molding. A very long gate will cause the viscous dissipation to increase the melt temperature beyond the decomposition temperature of the polymer, resulting in discoloration and low mechanical properties of the product.

The cross sectional shape of the gate is also critical. As an example, if a pin gate is used to fill a very wide cavity, there exists a very high probability of obtaining weld lines and surface marks in the molded part caused by the unevenness of the flow across the cavity. If a fan or a flash gate is used instead, the flow across the cavity is more evenly spread, resulting in fewer weld lines or surface marks in the molded product.

Very few papers have been written about gates or gate design, and none about gate optimization techniques, the reason being the complexity of the phenomenon occurring inside the gate during the molding cycle. The author surveyed the literature published in the period from 1950 until 1976 and found only five papers related to gates, none of which contained a design method or optimization procedure. The following paragraphs contain an analysis of these papers.

Bostwick and Joslin (9) presented the advantages of using restricted (pin) gates for molding several geometries, among them a vacuum cleaner handle. Several gate sizes and locations were considered. A mold with provision for several types of gates was built and used to produce molded parts. The parts molded using different gate sizes and geometries were compared. Restricted (pin) gates did

prove to be an improvement over the other types considered, but no reasons were given to explain this fact. Briers (10) described feeding and gating techniques for injection molds. Basically, this paper deals with the different types of gates that could be used to avoid degating (separation of the molded part from the runners) as a separate step after the part has been molded. Engman (28) gives some ideas about gate location, parameters involved in gate design, and cost estimation for different types of gates. Reference (31) shows the advantages of using flash gates for a wide variety of flat geometries. An empirical design procedure for flash gates is given and a comparison is made against experimental moldings. The results of the comparison show that the empirical method works for a very limited number of cases. Robinson (43) analyzes several gating schemes and the effect of temperature and pressure on the surfaces of the molded part. He gives empirical design data for polypropylene. Bainbrige (4) criticizes the poor planning used for gate and runner design and gives some hints for designing runner and gate systems.

By now it should be obvious that a general design and optimization procedure for gate and runner systems must be developed. In this investigation a generalized design procedure for gate and runner systems was developed. The optimization of gate dimensions using the developed design procedure will be the subject of a posterior investigation by the author.

Transient Flow in Gates

By its very nature injection molding is a transient phenomenon. During the filling stage of the injection cycle the polymer flows through the gate into the cavity. Due to the small gate cross section, the polymer is accelerated and shear-heated within a very short time interval, usually of the order of tenth of a second.

The literature is filled with numerical simulations of the filling process for the cavity (6,12,34,35,39,40,49,53), but the transient flow of polymer across the gate has been avoided in every case. the reason being the complexity of the equations of change in cylindrical co-ordinates as much as the method for their solution. Lord and Williams (40) have considered the steady flow of polymer melt through cylindrical channels. They claim that there is no need to consider the transient phenomenon, since the transient temperature profile approaches the steady profile very rapidly. They showed that the transient temperature profile will approach the steady profile when 40% of the filling time has elapsed. This figure was given for filled ABS, which is very viscous and flows very slowly. For polyethylene or polystyrene, the transient temperature profile most probably will never approach the steady profile before the filling time has elapsed. Therefore, the assumption of steady conditions during the polymer flow through runners and gates is very doubtful. This is especially true for many commercially used thermoplastics.

In order to analyze the transient flow through the gate and runer systems, it is then necessary to develop a method of solution

for the transient equations of change. In this investigation a method called nodal positioning analysis (NPA) was developed to solve the simultaneous system of equations resulting from the equations of change. This procedure is described in detail on page 59.

Computer Simulation of the Injection Molding Cycle

In order to determine the transient changes in temperature across the gate, a model for the entire molding cycle must be developed. Recently, several authors have reported computer simulations of the mold-filling process. Harry and Parrot (30) used a moving coordinate system at the flow front. With this arrangement, the transient temperatures and pressures could be determined at the flow front, but it was impossible to obtain transient changes at any other location. A power law model was used to represent the viscosity-shear rate relationship and an Arrhenius type temperature-viscosity dependence was assumed. This viscosity model and this temperature dependence are known to hold only over very narrow temperature ranges. These assumptions limited severely the use of the simulation. Echenagucia (26) modified Harry's (28) model and used it to simulate polymer flow in annular, tapered channels. Even though the modifications added stability to the solution, especially at low volumetric flow rates, the information obtained was still only at the moving front location. Berger and Gogos (6) simulated the filling of a center gated disk with crystaline Newtonian and power-law fluids, but with no dependence of melt viscosity on temperature. The pressure at the head of the sprue

was assumed to be constant during filling and the predictions of their model were not compared against experimental results. Wu, Huang and Gogos (53) solved the problem of radial filling of a circular cavity, but they used the power law-Arrhenius viscosity model and assumed constant pressure at the entrance of the cavity. Broyer (12) modelled the polymer flow in thin channels. The concept of equivalent Newtonian viscosity (ENV), which replaces the Newtonian viscosity at a particular location by an equivalent non-Newtonian viscosity, was used instead of a constitutive equation. They used the flow analysis network (Fan) for determining the flow field and an implicit Crank-Nicolson scheme for determining the temperature field. Melt solidification during flow was determined, but no comparison against experimental results was given. White (49) considered isothermal and nonisothermal flow in a rectangular cavity. Again, a power law-Arrhenius viscosity model was used. Viscous dissipation was neglected and melt solidification during flow was ignored.

In all of the references cited above only the filling stage of the injection cycle was considered. Kamal and Keing (34) are the first to include the packing and cooling stages in their model. Agreement between their model predictions and experimental data was good. The main limitations of their model are the assumption of known pressure variation with time at the entrance of the mold and the use of a power law-Arrhenius viscosity model. Kamal and Kuo (35), (39) studied the filling of a narrow gap, rectangular cavity by using the lubrication theory and the stream function approach for determining velocity and

pressure profiles. With this scheme, they were able to obtain analytical solutions of the equations of change, but their model is limited to rectangular cavities due to the complexity of these equations for other geometries. As before, the pressure distribution versus time at the cavity entrance must be known. This last requirement limits the use of the model, because experimental pressure versus time data must be obtained before the model can be used.

Since the gate is a link between the runner and the cavity, a model for the transient behavior of the polymer flow during the injection molding process must include the runner, gate and cavity geometries as well as the filling, packing and cooling stages. In other words the temperature, pressure and velocity variations in the gate at a given time depend upon what happens in the runner and in the cavity at that time. This means that the gate cannot be isolated from the runner and/or cavity, but that the effect of all three geometries must be considered simultaneously.

In this investigation a model including the runner, gate and cavity channels as well as the filling, packing and cooling stages was developed and validated with experimental data obtained from an injection mold especially designed for this purpose. Details of the mold design, data logging and model development are included in the following sections.

Constitutive Equation for Polyethylene

Due to the fact that polyethylene behaves as a non-Newtonian (pseudoplastic) fluid, its viscosity is shear rate dependent. The

flow behavior of the polymer melt through the runner, gate and cavity is determined by the changes in viscosity due to changes in temperature and shear rate. It is then necessary to obtain a relationship among viscosity, shear rate and temperature before a flow model of the polymer can be attempted. An equation describing the dependence of viscosity on temperature and shear rate is called a constitutive equation.

Constitutive equations of two types are currently in use. The first, which is purely empirical, is of the form:

$$\text{Ln } \eta' = A_0 + A_1 \text{ Ln } \dot{\gamma}'_{tw} + A_{11}(\text{Ln } \dot{\gamma}'_{tw})^2 + A_2 T' + A_{22} T'^2 + A_{12} T' \text{Ln } \dot{\gamma}'_{tw} \qquad (1)$$

where η denotes viscosity, $\dot{\gamma}'_{tw}$ the shear rate and the A's are empirically determined constants. Constitutive equations of this type have been found to provide a good fit to viscosity data of a number of commercially important polymers, polyethylene being a typical example. In addition, this type of constitutive equation has been used with considerable success in modeling the plasticating portion of the injection molding process (21). The main limitation in using equation (1) is that extrapolation to parameter ranges outside those for which data is available can produce unreasonable results. Thus, it is necessary to examine the behavior of the function over the range of temperatures and shear rates that may be encountered in injection molding and make reasonable modifications to the behavior in extrapolated regions. In particular, equation (1) is parabolic in $\text{Ln } \dot{\gamma}'_{tw}$, therefore, at a fixed temperature $\text{Ln } \eta'$ has a maximum, and for values of $\text{Ln } \dot{\gamma}'_{tw}$ smaller than

that at which the maximum occurs, the viscosity computed from equation (1) decreases as $\overset{o}{\gamma}'_{tw}$ decreases, instead of approaching some constant value, as polymer viscosities are known to do as shear rate approaches zero.

The second type of constitutive equation that is being used also fits viscosity data for some commercially important polymers, but has the advantage that it can be extrapolated to low temperatures with some theoretical justification (14,50,51,52). This equation is given by

$$\frac{\eta'}{\eta_o'} = f\left(\frac{\eta_o' \overset{o}{\gamma}'}{T'}\right) \qquad (2)$$

where η is the steady-shearing viscosity at temperature T' and shear rate $\overset{o}{\gamma}' = \frac{du'}{dr}$, η_o is the zero-shear viscosity at temperature T', and the function f is determined from the Bueche-Harding "Universal Curve" (15).

In this investigation, equation (1) was used as the constitutive equation. The empirical coefficients of equation (1) were determined using a capilary rheometer and the analysis presented on page 79.

Optimization of Gate Dimensions

The heat and momentum transfer associated with the polymer flow inside gates are complex phenomena due to the transient nature of the injection molding process. For this reason no attempt has been made by any investigator to simulate these phenomena occurring simultaneously during the complete molding cycle, much less to develop an optimization procedure for gate dimensions.

In this investigation a graphical procedure for gate optimization is outlined on page 79. This graphical procedure uses the results from the proposed computer simulation model of the complete injection cycle developed on page 52. A multivariable optimization procedure using the flow model developed in this investigation as an abstract objective function will be the subject of future research by the author.

III. EXPERIMENTAL

The purpose of the investigation, the plan of investigation, and a description of the apparatus, mold design data acquisition system, and experimental procedure are included in this section.

Purpose of Investigation

The scope of thisinvestigation was to develop a numerical simulation of the injection molding cycle, to validate the proposed simulation using experimental data obtained from an 150 ton injection press available at VPI&SU with an injection mold and data acquisition system specially designed for this application, and to use the developed simulation to determine variations of critical design parameters of gate systems in injection molds. This last step allowed for the development of a graphical optimization procedure.

Plan of the Investigation

The plan of investigation followed in this study consisted of literature review, polymer selection, experimental system, design and construction of a suitable injection mold to validate the proposed model, development of a monitoring system capable of logging data at the high speed required by the injection molding process, determination of the flow curves for the selected polymer, analysis and interpretation of the experimental data for comparison against the predicted results of the simulation, and development of a graphical optimization procedure for gate channels.

Literature Review. A survey of literature was made to acquaint the author with the transient heat and momentum transfer occurring during the flow of pseudoplastic material through different channel geometries and finite difference analysis and numerical methods for solving two dimensional partial differential equations.

Polymer Selection. Low density polyethylene was selected as the polymer to be used in this investigation because of its wide use in the polymer industry, and the extensive literature on its physical and rheological properties.

Experimental System. The experimental system consisted of an injection press, an injection mold, and the control and the analytical system. Figures 4 to 10 show the experimental system used in this study.

The injection press was a 150 ton, 10 ounce per shot hydraulic driven machine with a toggle mechanism for die plate movement. An injection mold with two square cavities in succession, the first to accommodate runner and gate inserts, the second to accommodate cavity inserts, was mounted on the die plates of the injection press.

Four I/C thermocouples were mounted inside the mold cavity, gate and runner to determine transient temperature variations during the injection cycle. Four pressure transducers were inserted in the cavity, runner and gate to determine transient pressure variations during the injection cycle.

The output signals from the thermocouples and pressure transducers were taken to a PDP 11/40 computer with A/D converter and

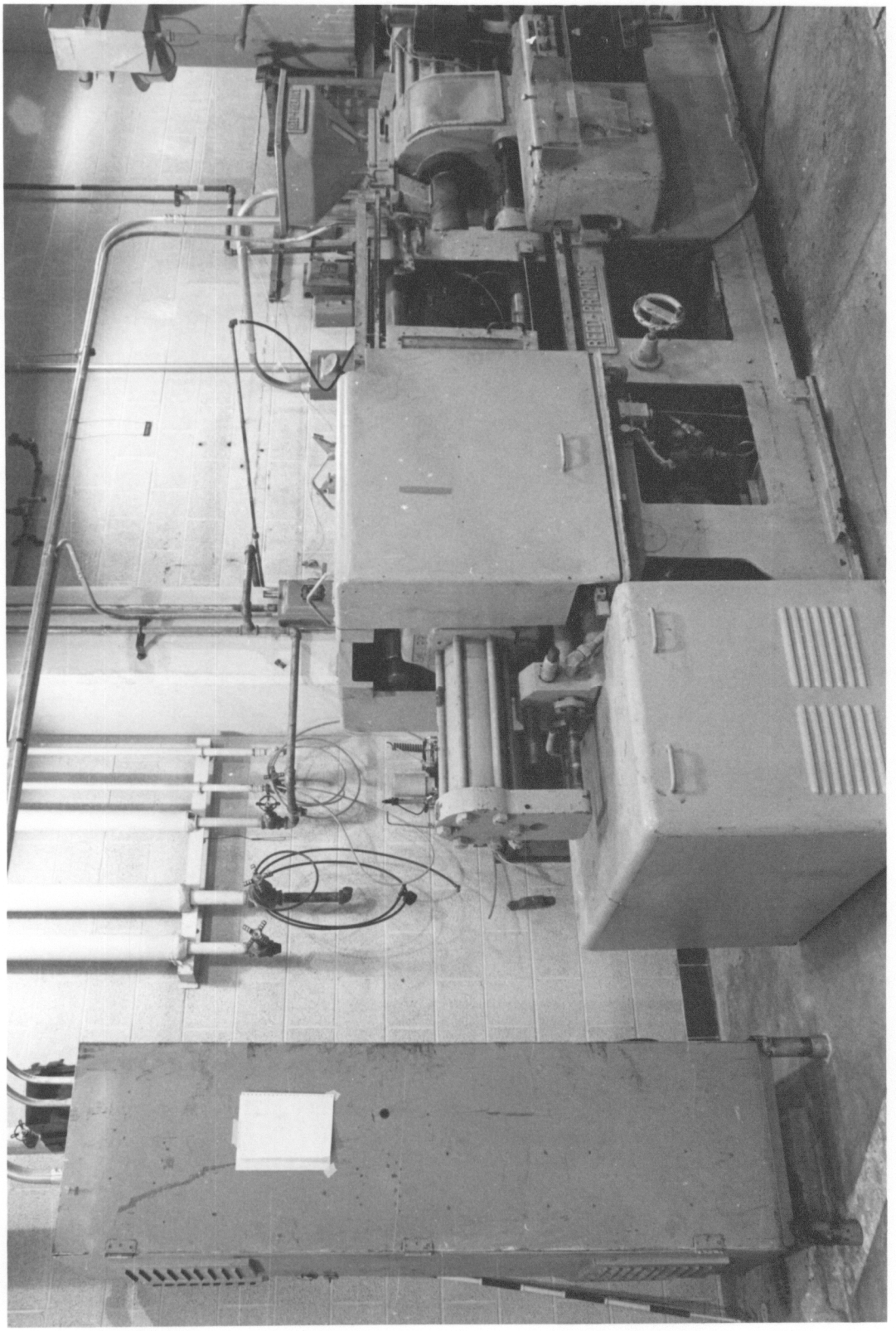

FIGURE 4. 150 TON INJECTION MOLDING PRESS

recorded on a disc unit.

The heat input to the heating cylinder of the injection press was controlled by four proportional controllers.

The apparatus used in this investigation was used in a previous work, and all equipment specifications can be found in reference (26).

Design and Modification of the Equipment. In order to measure the transient pressure and temperature changes in the runner, gate and mold cavity, a monitoring system consisting of a voltage-to-current conversion circuit and a high speed current multiplexer were designed, build, and linked to a PDP 11/40 computer with A/D converter.

An injection mold with the capability of accommodating different runner, gate, and cavity dimensions was designed, built and mounted on the injection press.

Determination of Flow Curves. Shear stress versus apparent shear rate data was obtained by running the polymer through a MRC capilary rheometer made by Instron Corporation. The experimental data was transformed into a regression equation expressing viscosity as a function of temperature and shear rate. The procedure followed is outlined on page 74.

Procedure

The operational procedure followed in the injection molding of polymer samples, in the capilary viscometer experiment, and in the injection cycle data acquisition is included in this section. Also, the mold design procedure is included.

Mold Design. The main frame of a two plate mold used in a previous investigation (26) was selected in this study because of its operational simplicity and convenience. The injection press used in this investigation has a 20,000 Psig injection pressure limit; and, based on this fact, a numerical simulation of the mold filling stage developed in a previous study (26) was used to determine the minimum gate diameter to insure cavity filling at the maximum injection pressure. It was desirable to use the smallest permissible gate size in order to validate the predictions of the numerical simulation developed in this investigation under the most severe conditions. A diameter of 1/32" inch was determined to be the minimum permissible. A 1/16" inch diameter was used in order to insure a perfectly round gate cross section and to avoid alignment problems while maintaining the intended severity of the conditions intended.

The main objective kept in mind when designing the mold was versatility. A 1/2" inch total depth square cavity was believed to be the most convenient, because many different cavity geometries could be made by using specially shaped inserts. Also, the depth of the cavity could be varied by simply "filling it", using an insert with the same cavity side length and arbitrary thickness.

Perhaps the most important mold component from the point of view of this investigation was the gate. In order to accommodate a large number of gate dimensions and geometries, provisions were made to have the gate cut on a separate square metal block with the same thickness as the cavity. This small square block could be screwed in place in a

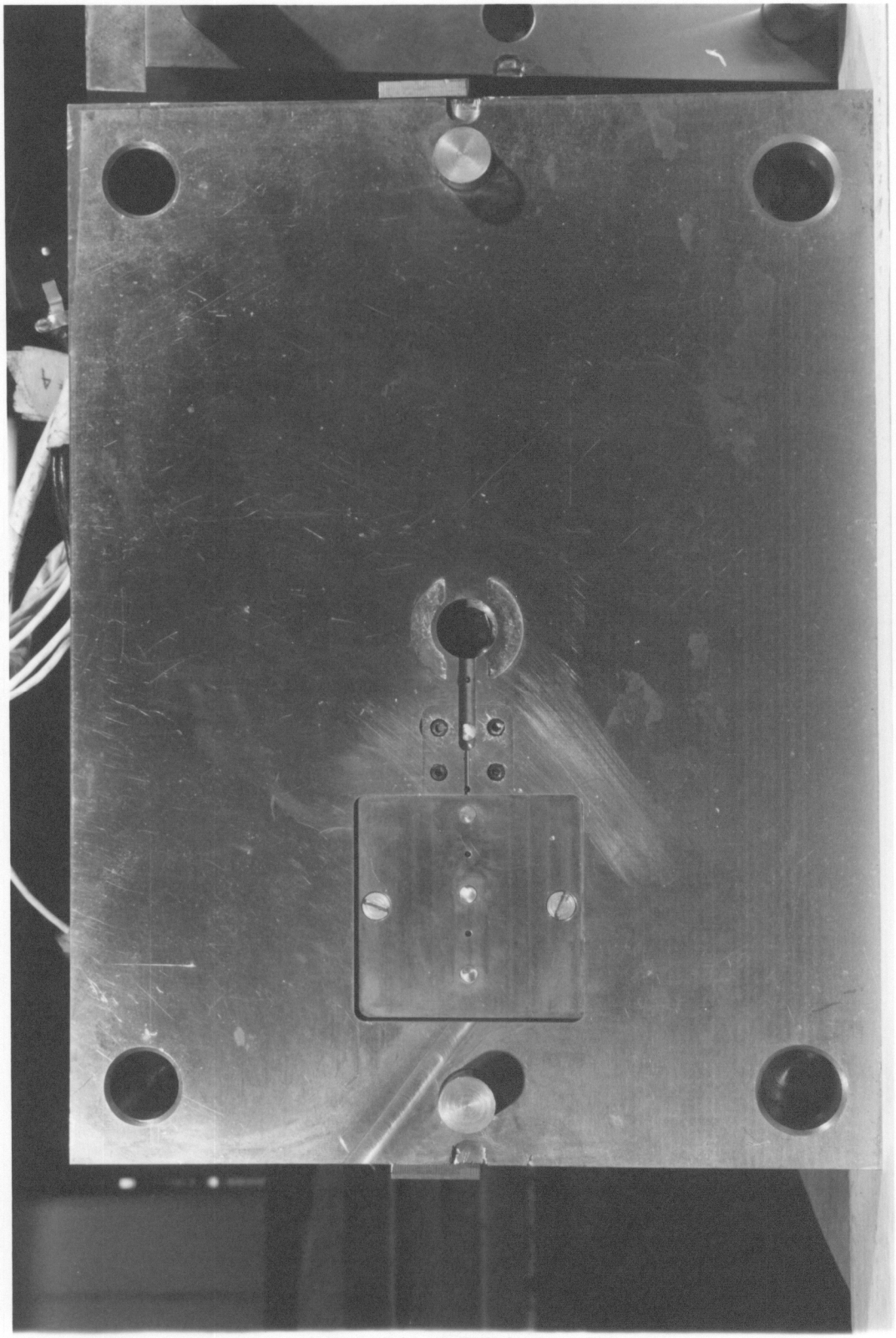

FIGURE 5. BOTTOM CAVITY PLATE OF THE INJECTION MOLD

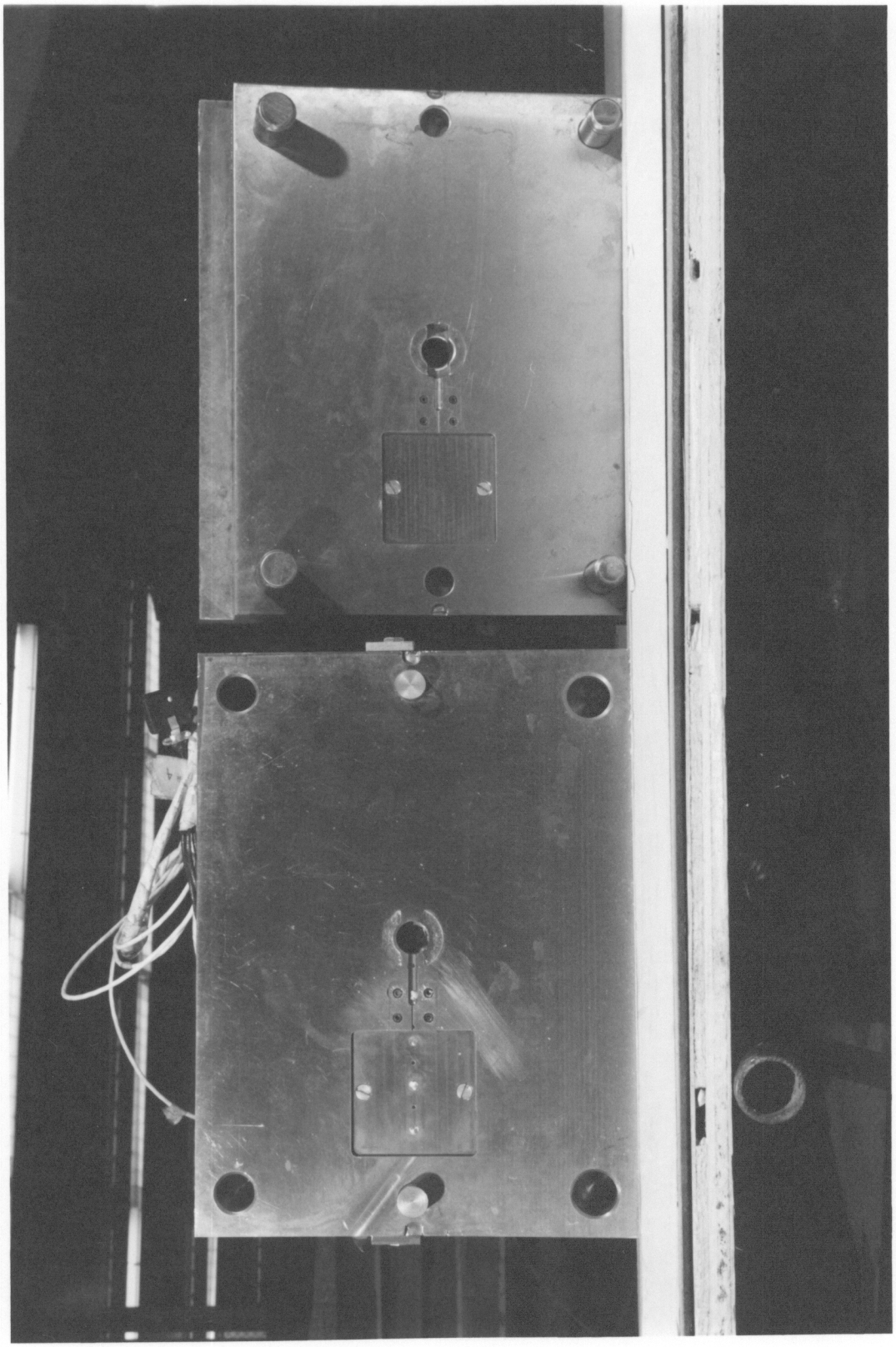

FIGURE 6. TOP AND BOTTOM CAVITY PLATES OF THE INJECTION MOLD

cavity cut on the mold plate, next to the main cavity (see figure 5, page 21). This arrangement allowed for fast gate replacement. A round runner and gate were selected in spite of the known alignment problems they create, because they offer the maximum volume to surface area. This allows the use of smaller runners and gates, which translates into polymer scrap savings. At the end of the cooling stage, provisions have to be made to eject the molding from the cavity. An automatic ejector mechanism, consisting of an ejector (movable) plate, alignment pins and knockout pins, was designed as part of the mold. In this case the knockout pins had a dual purpose; to eject the part from the cavity and to convey the cavity pressure to the pressure transducers located under their bases. Five knockout pins were provided, four of them were carefully located in the gate and main cavity to allow for maximum system flexibility. Figure 12 is a cavity layout showing the locations of the pins. Four thermocouples were also installed next to the transducers to complete the data monitoring system.

Injection Cycle Data Acquisition. The injection molding process requires a very fast data acquisition system due to the short cycle times (50-100 sec) commonly used. The monitoring system used in a previous work (26) was used in this investigation (see figure 7, page 24). Basically, the monitoring system consisted of: four type J thermocouples, five pressure transducers (load cells), the ram position detector, signal conditioning amplifiers, a current mode multiplexer, a current loop and a PDP 11/40 computer with A/D converter (see figures 7 to 11).

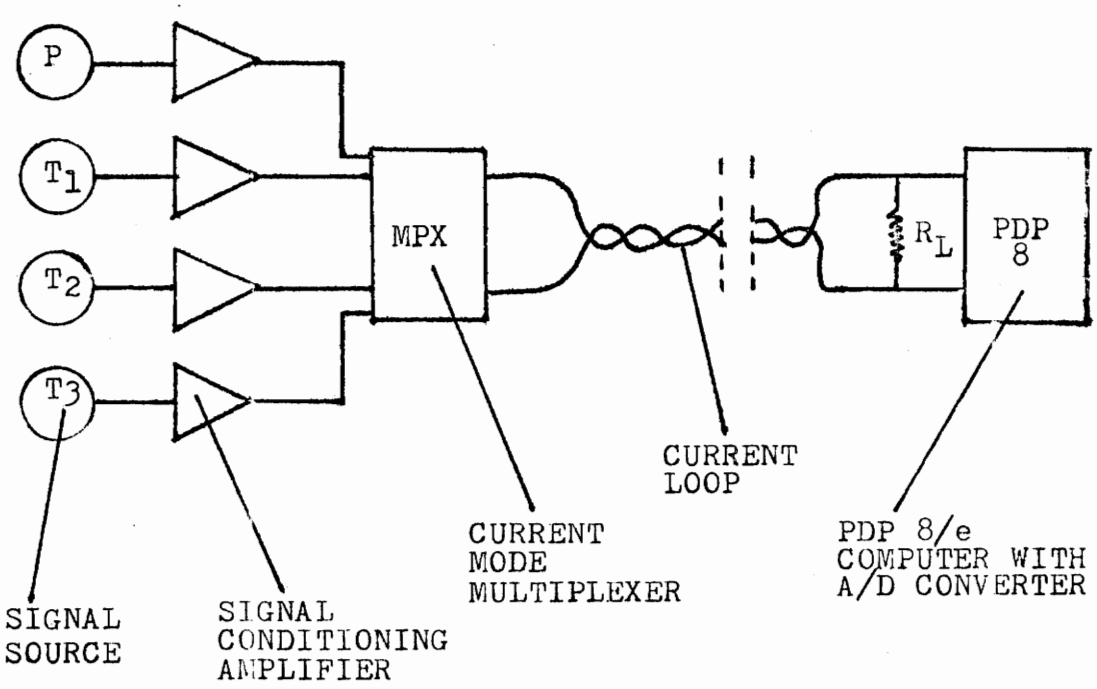

FIGURE 7-A. ANALOG DATA LINK

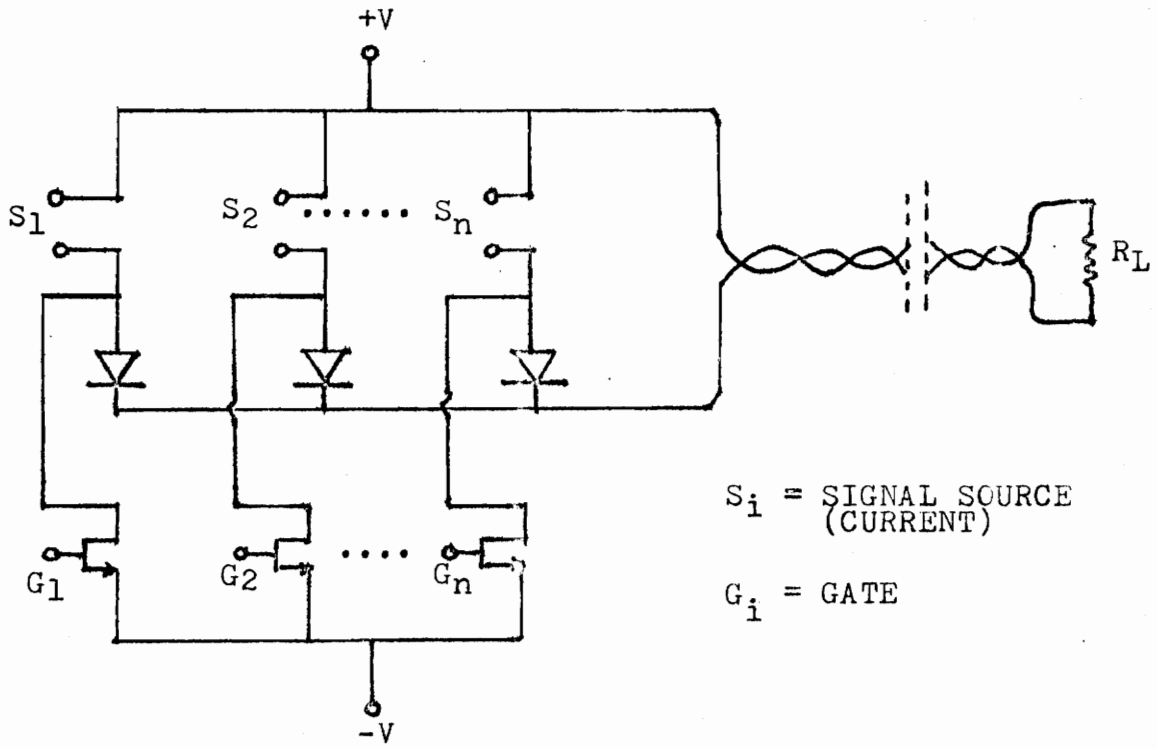

FIGURE 7-B. MULTIPLEXER

FIGURE 7. MULTIPLE DATA POINT ANALOG LINE LINK

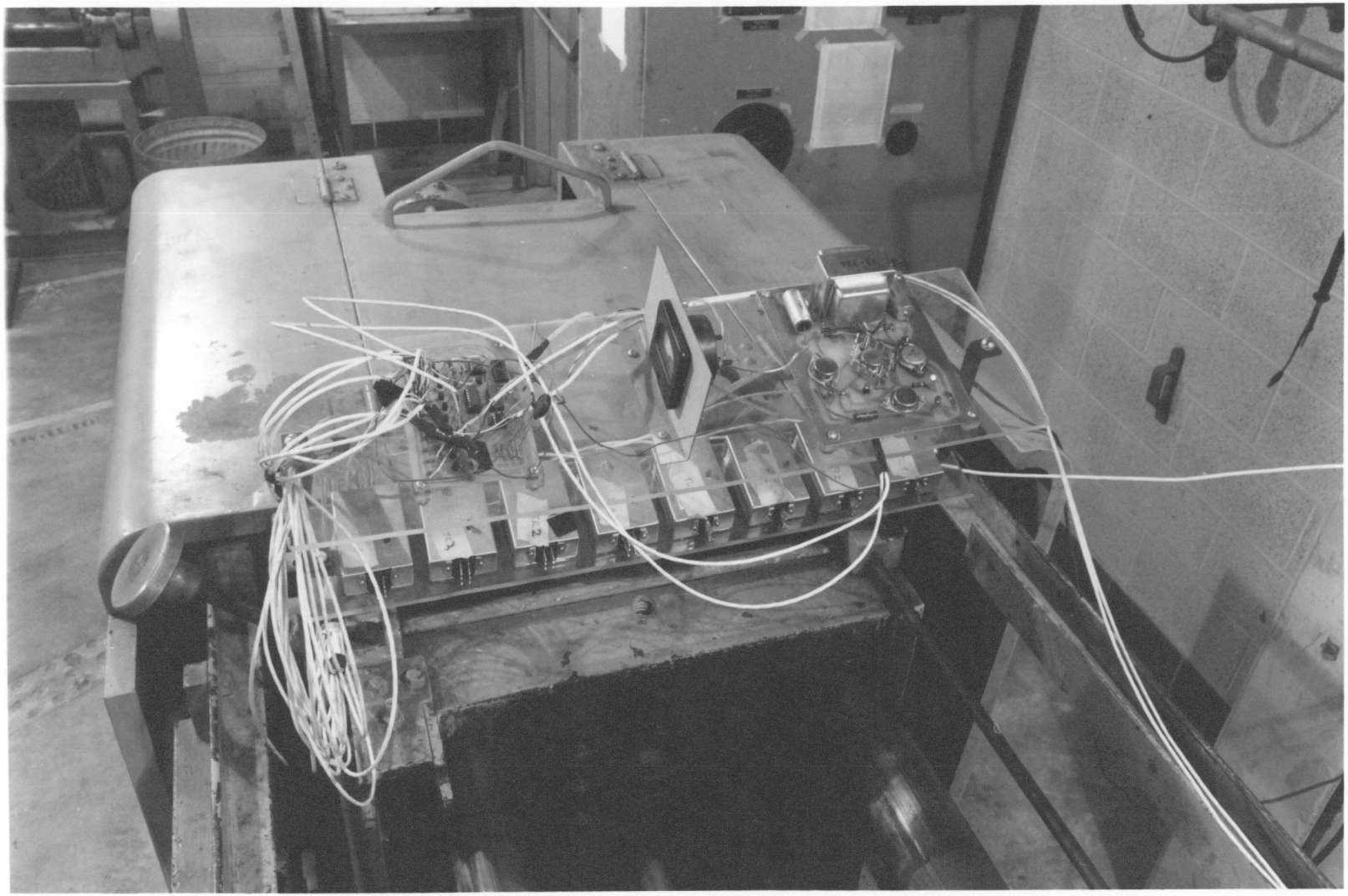

FIGURE 8a. CURRENT MODE MULTIPLEXER, TRANSDUCER TERMINALS AND POWER SUPPLY COMPONENTS OF THE DATA ACQUISITION SYSTEM

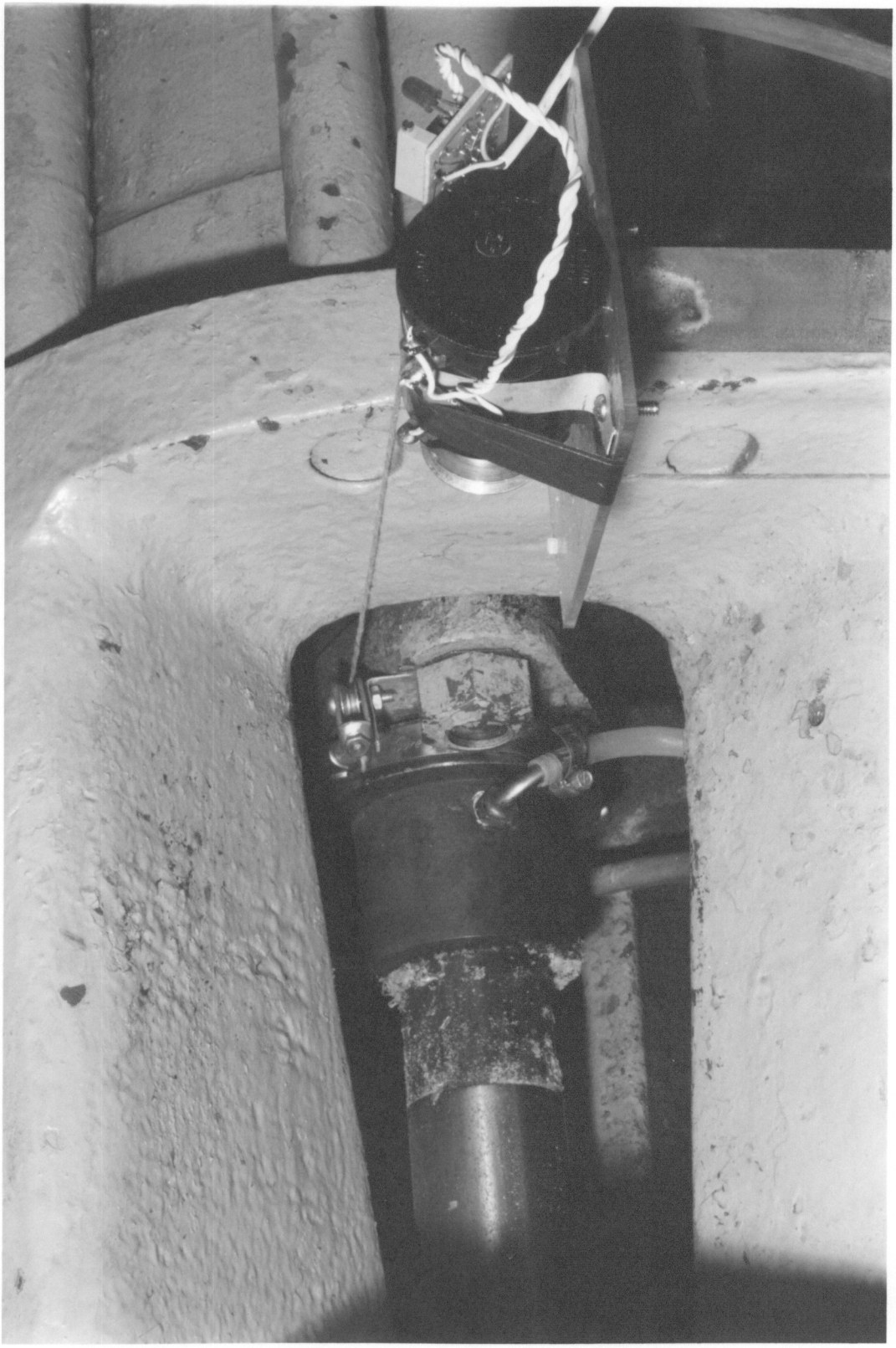

FIGURE 8b. RAM POSITION DETECTOR

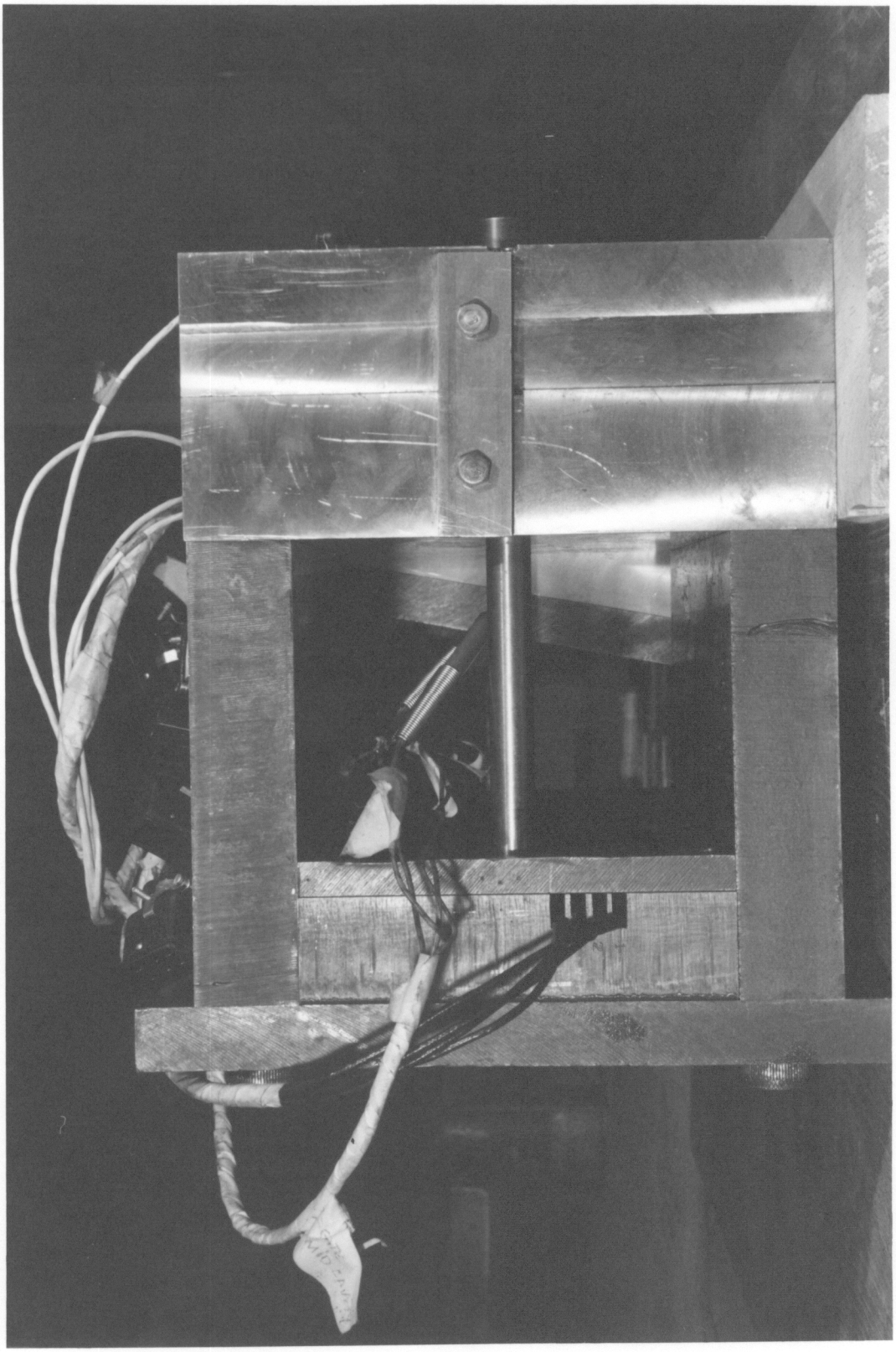

FIGURE 9. SIDE VIEW OF THE INJECTION MOLD

FIGURE 10. PDP 11/40 COMPUTER, CRT, PRINTER AND PLOTTER

The signal from the thermocouples and transducers were passed through the signal conditioning amplifiers, which converted a high impedance ("voltage") signal to a low impedance ("current") signal. The current signals were passed through a current mode multiplexer (figure 8a, page 25) which put each signal in turn into the current loop for 10 milliseconds. The analog signal was transmitted as a variable current through a current loop, which caused a voltage to appear across the load resistor RL (see figure 7, page 24). A Current loop was used to transmit the signal because it is less sensitive to induced noise signals than is a voltage loop (high impedance). The voltage across RL was read by the PDP 11/40 digital computer with A/D converter. The voltage was converted to a digital value and stored on a disc unit.

In order to calibrate the pressure temperature and position transducers, to place the data on the disc at known locations and to tabulate and/or plot the data, a special software package for the PDP 11/40 computer had to be developed. Basically, three computer programs had to be developed. The program called INJCAF was used to calibrate any desired transducer. The program used a pulse (trigger) sent from the multiplexer to synchronize the beginning of the 10 channel cycle. Next, the program took five points of the same channel, averaged them, and sent the output value to a CRT unit located near the injection molder. The data format on the screen showed digital numbers equivalent to the analog signals received from the transducers. All 10 channels were displayed in columns. The program had a limit of

10,000 lines and the CRT printed a line per second. With the digital output on the screen, the calibration data for the temperature, pressure or ram position transducers were taken.

The program called INJF, synchronized the beginning of the data set and took the analog data from the transducers, made the analog to digital conversion, smoothed the data, stored the data at known disc locations and allowed for pre and post comments in order to identify the data set (file). This program was run at the beginning of each molding cycle. The data for every run was then labeled, smoothed and stored in a known disc location.

The program INJRF2 used the data stored in the disc unit to produce the final report. Several options were available; option 1: a hard copy of the data for the whole cycle could be obtained through the printer. Option 2: plots of the output of any transducer versus time could be obtained through the printer or on the CRT screen. Option 3: the data could be sent to a digital plotter. The plotter produced a continuous ink plot of the data in labeled axis. Any section of the data could be blown up by simply selecting the desired interval.

INJRF2 uses third order calibration polynomials, which were obtained from the data supplied by INJCAF and a nonlinear regression on the data, to convert the digital output into dimensional variables e.g., temperature, pressure, etc. In this fashion all data output is in dimensional variables form. The outputs generated by INJRF2 are shown in the appendix.

TABLE I. INJCAF FLOW DIAGRAM

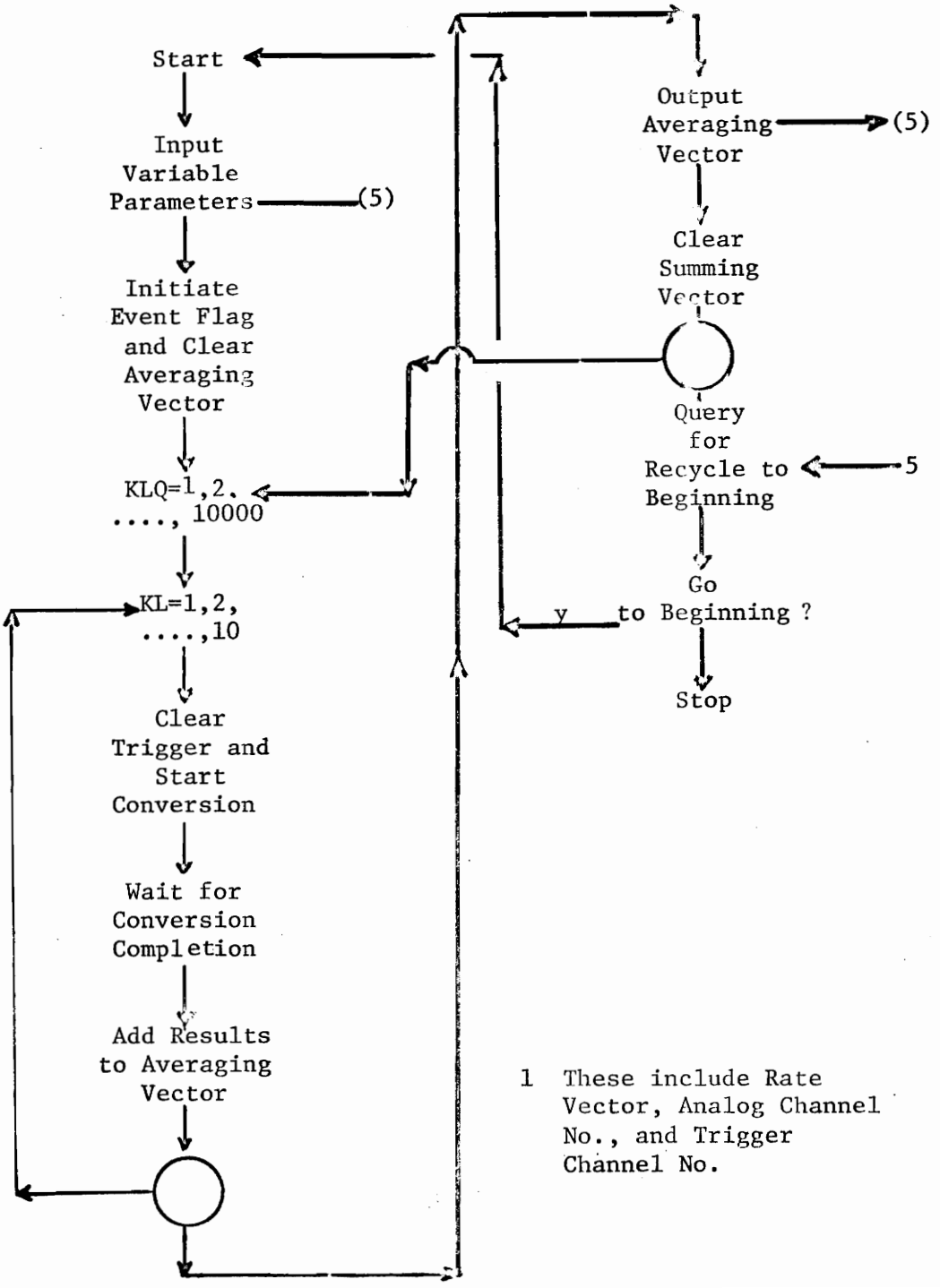

1 These include Rate Vector, Analog Channel No., and Trigger Channel No.

TABLE II. INJF FLOW DIAGRAM

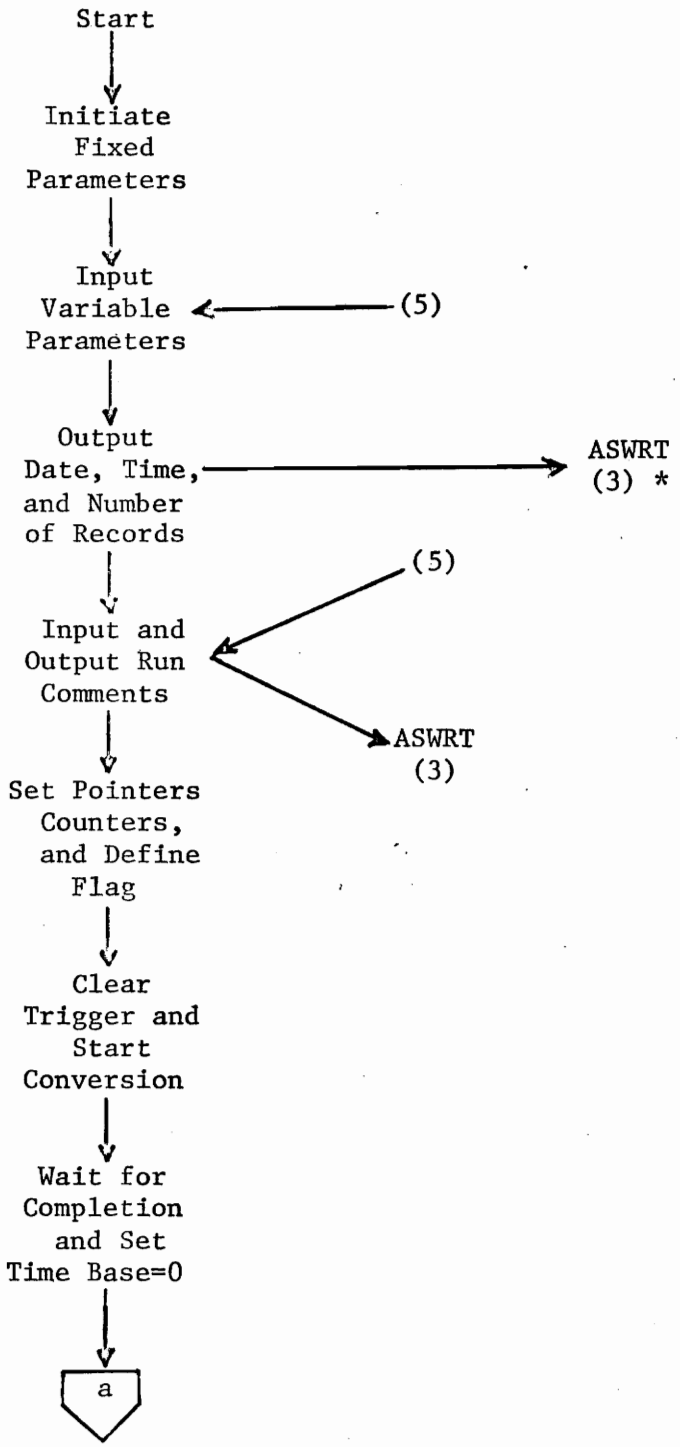

TABLE II. (continued)

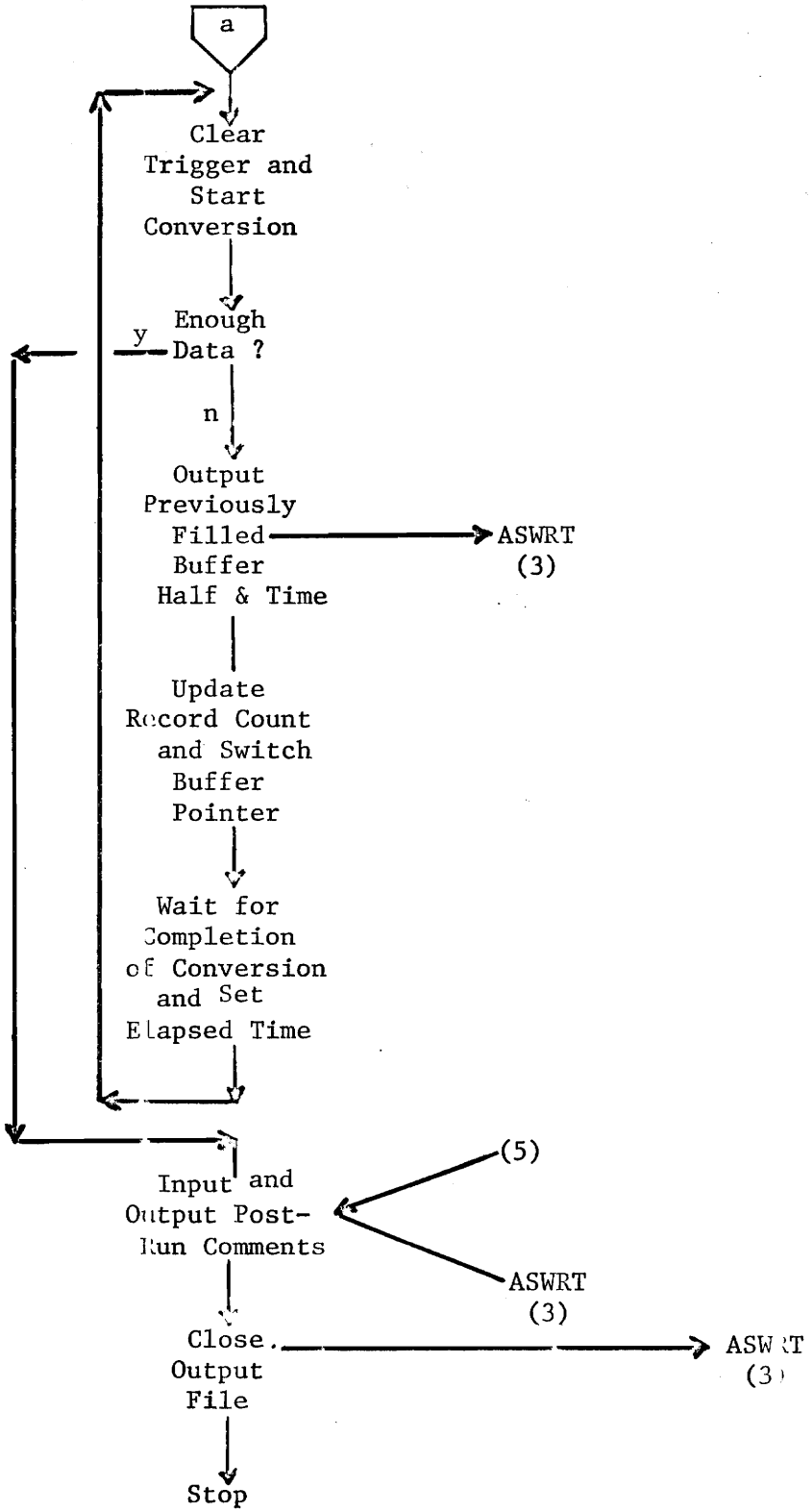

TABLE II. (continued)

Legend.

* ASWRT is a high speed data output routine

ASWRT includes Rate Vector, Analog Channel No., Trigger Channel No., and No. of data points required

(5) CRT addressed as Lun5

ASWRT (3) Disc addressed via ASWRT as Lun3

TABLE III. INJREF2 FLOW DIAGRAM

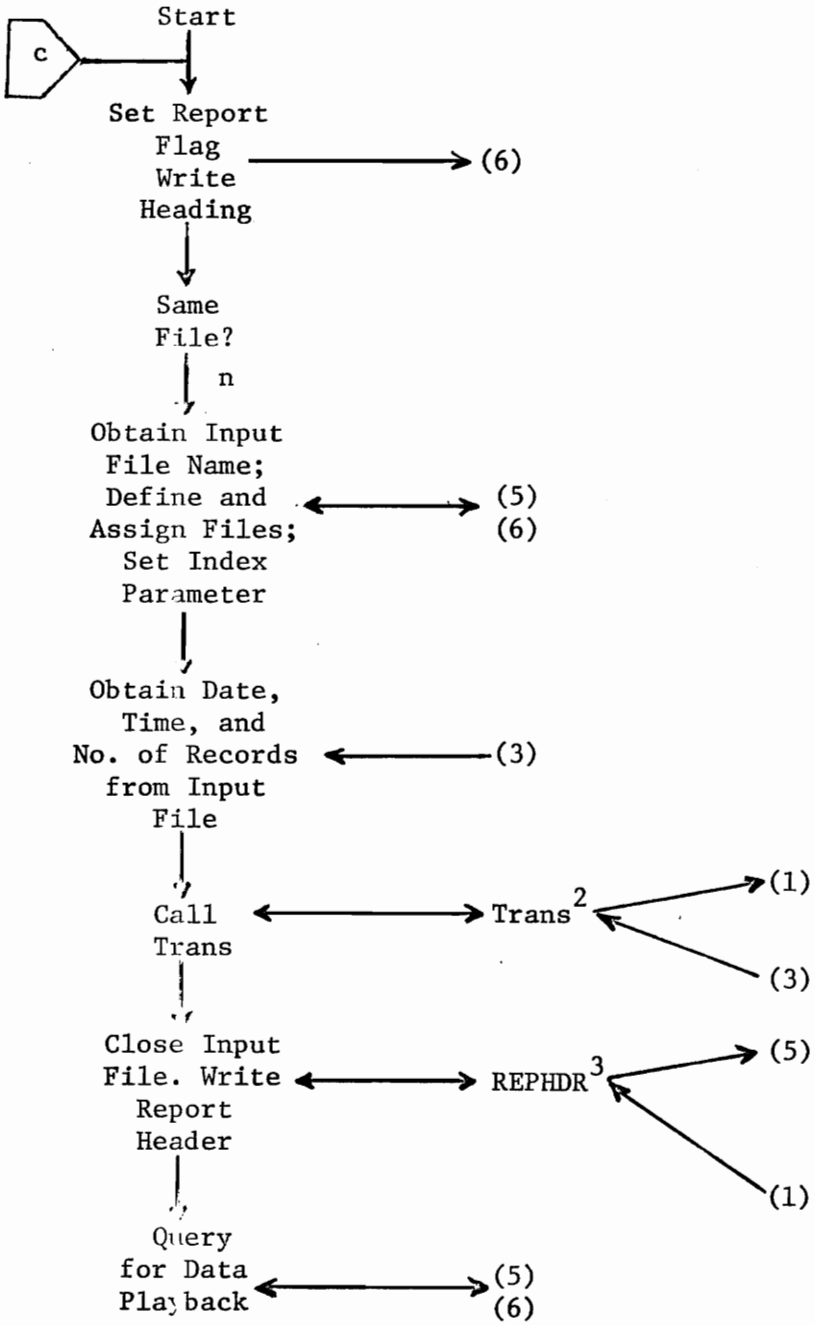

TABLE III. (continued)

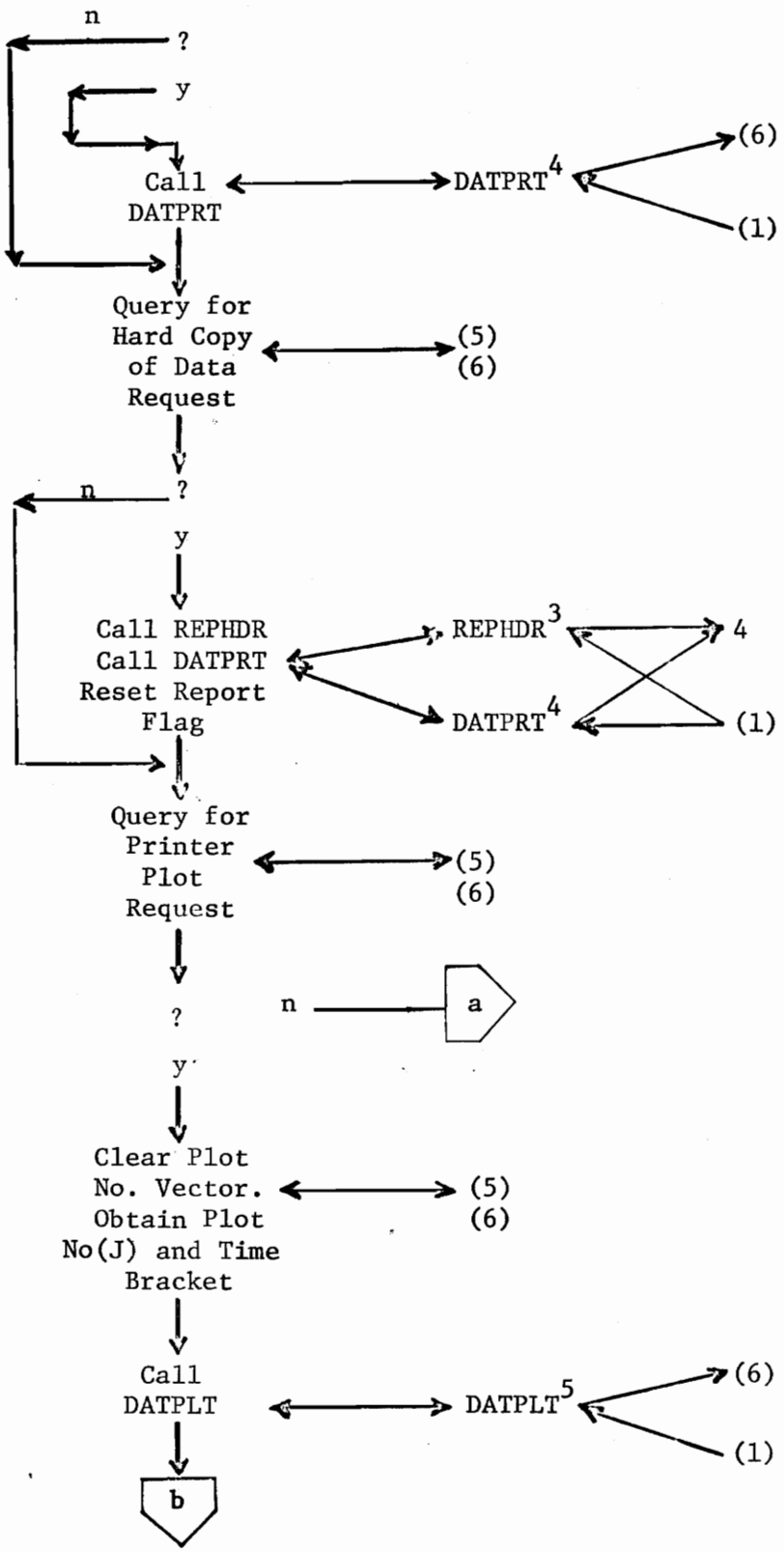

TABLE III. (continued)

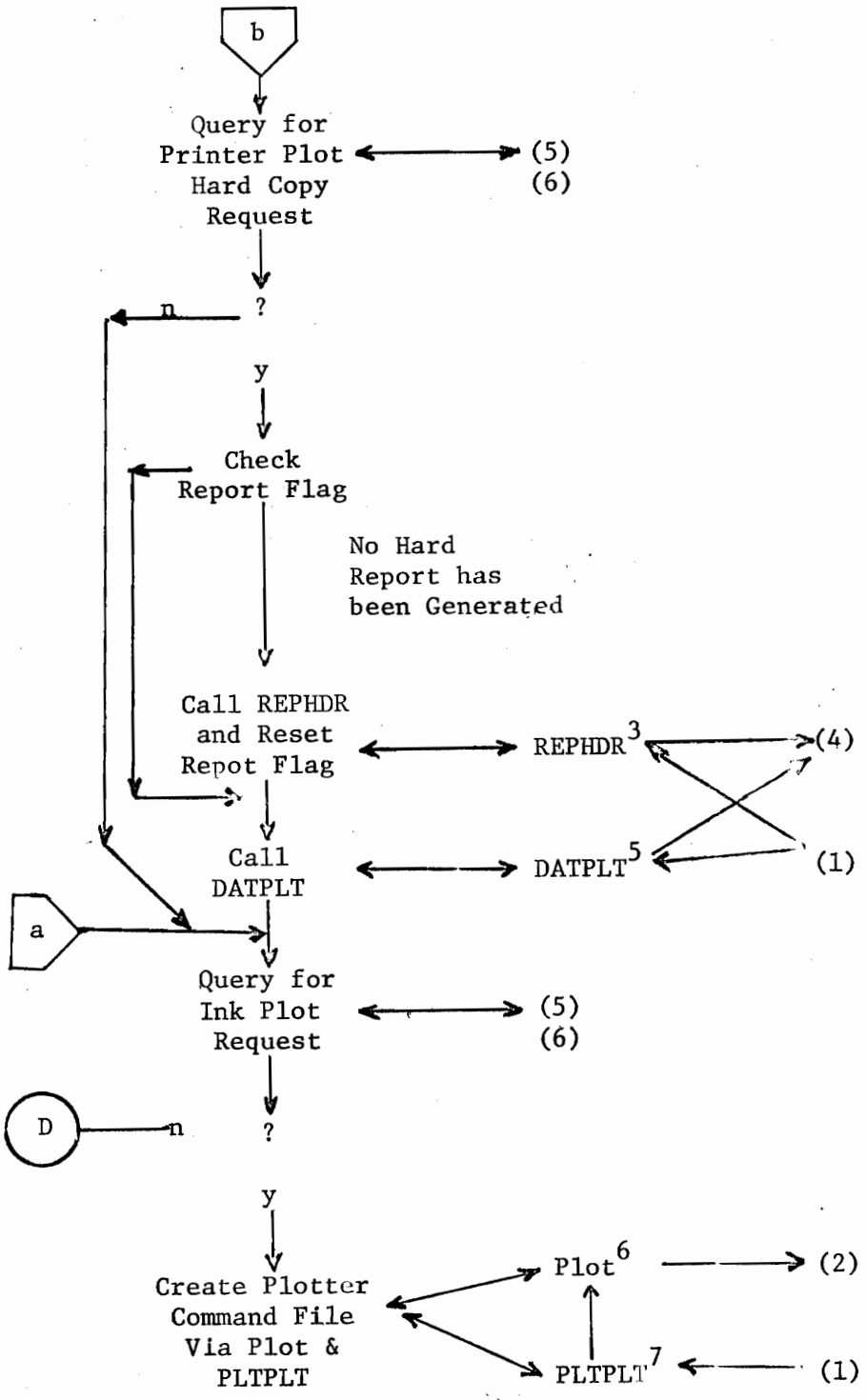

TABLE III. (continued)

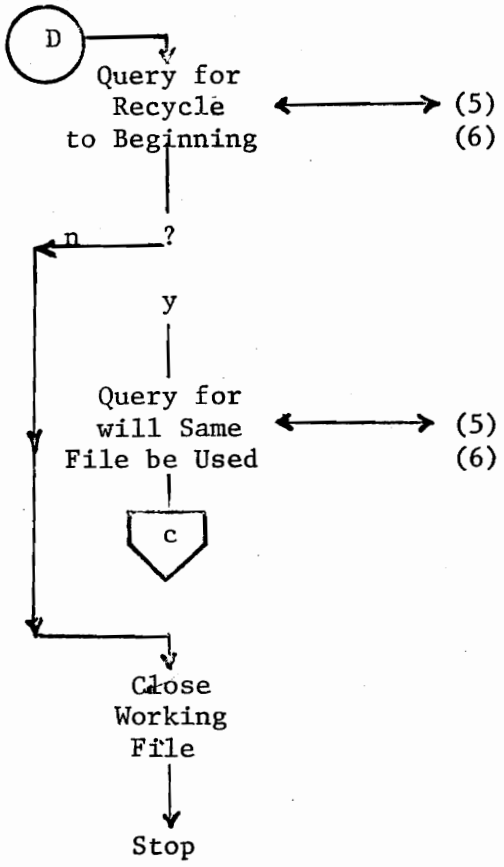

TABLE III. (continued)

Legend.

1. Always negative on first pass
2. Trans converts binary date from input file into floating point form using calibration subroutine CAL. Derivative of Ram position is also obtained using TPT Sabitsly Golay function. All of the data is rewritten on a new working file.
3. REPLIOR obtaines from working file and outputs time, date, No. of records and run comments.
4. DATPRT outputs data from working file.
5. DATPLT outputs a printer plot using data from the working file.
6. PLOT outputs actual
7. PLTPLT obtaines data from the working file

LUN index.

1. Working file
2. Ink plot command file
3. Input file
4. Hard copy output file
5. CRT input
6. CRT output

The flow diagrams for each of the above mentioned programs are shown in Tables I to III, pages 21 to 39.

Injection Molding of Samples. The desired injection temperature, pressure and volumetric flow rate were set and the machine barrel was allowed to reach a steady temperature. The timers controlling the "plunger stays forward", "mold stays closed after plunger returns" and "mold stays open at the end of cycle", were positioned at the desired set points. Several cycles were run before steady conditions were reached. This was recognized when a perfect molded part, ejected without problems, was obtained. Once at steady conditions, the data logging program was called from a computer terminal (CTR), located next to the injection press, and the instantaneous pressure, temperature and flow rate for the molding cycle were stored on the disc unit.

Immediately at the end of the molding cycle, the data was displayed on the CRT screen by simply calling the report program described before. If the data set was complete and clean, it was kept; otherwise, it was erased from the disc. The volumetric flow rate was then changed and the procedure described above was repeated. Data for three different pressures and three different volumetric flow rates at one injection temperature were recorded.

Rheological Data. The capillary rheometer consisted of the heating barrel, the plunger, the capillary (the capillary is a cylindrical channel with a very small, 0.005-0.002 inch diameter) and a PID temperature control unit. The whole capillary assembly was mounted on an Instron Universal Testing Machine (38), and the plunger was aligned to

move freely inside the barrel. A type C-F Instron compression load cell with a 0-10,000 pound force range was located at the top of the moving across head of the Instron tester; the purpose of the load cell was to record the force needed to drive the plunger into the barrel and force hot polymer through the small capilary opening. The desired run temperature was set on the PID controller and a period of about four hours was allowed for the barrel to reach a steady temperature; the reason being the large amount of heat lost by conduction and convection. The polyethylene pellets were manually fed and well packed into the barrel using a brass rod. The pellets had to be packed to avoid air bubbles in the extruded monofilament (extrudate). Once the pellets were well packed, the cross head was moved down at a fixed velocity, thus forcing the molten polymer through the capilary. The force needed for the movable cross head to drive the plunger, i.e., to force the polymer through the capilary, was recorded for different cross head speeds. The procedure described above was followed for six different temperatures and three different capillary sizes; the raw data from this experiment is shown in Table IV, page 42.

TABLE IV. RHEOLOGICAL DATA

CAPILARY DIAMETER= 0.050100 (IN)
****
CAPILARY LENGTH= 4.006000 (IN)
****

TEMPERATURE= 160.0 (DF)
****

CROSSHEAD VELOCITY (IN/MIN)	LOAD ON PLUNGER (LBF)	SHEAR STRESS AT THE WALL (PSI)	SHEAR RATE AT THE WALL (1/SEC)
0.500E-01	0.110E 03	0.320E 01	0.726E 01
0.100E 00	0.170E 03	0.494E 01	0.145E 02
0.200E 00	0.245E 03	0.712E 01	0.290E 02
0.500E 00	0.385E 03	0.112E 02	0.726E 02
0.100E 01	0.531E 03	0.154E 02	0.145E 03
0.200E 01	0.710E 03	0.206E 02	0.290E 03

TEMPERATURE= 180.0 (DF)
****

CROSSHEAD VELOCITY (IN/MIN)	LOAD ON PLUNGER (LBF)	SHEAR STRESS AT THE WALL (PSI)	SHEAR RATE AT THE WALL (1/SEC)
0.500E-01	0.850E 02	0.247E 01	0.726E 01
0.100E 00	0.120E 03	0.349E 01	0.145E 02
0.200E 00	0.178E 03	0.518E 01	0.290E 02
0.500E 00	0.288E 03	0.837E 01	0.726E 02
0.100E 01	0.410E 03	0.119E 02	0.145E 03
0.200E 01	0.585E 03	0.170E 02	0.290E 03

TABLE IV. (continued)

TEMPERATURE= 200.0 (DF)

CROSSHEAD VELOCITY (IN/MIN)	LOAD ON PLUNGER (LBF)	SHEAR STRESS AT THE WALL (PSI)	SHEAR RATE AT THE WALL (1/SEC)
0.500E-01	0.630E 02	0.183E 01	0.726E 01
0.100E 00	0.920E 02	0.268E 01	0.145E 02
0.200E 00	0.140E 03	0.407E 01	0.290E 02
0.500E 00	0.232E 03	0.675E 01	0.726E 02
0.100E 01	0.332E 03	0.965E 01	0.145E 03
0.200E 01	0.472E 03	0.137E 02	0.290E 03

TEMPERATURE= 210.0 (DF)

CROSSHEAD VELOCITY (IN/MIN)	LOAD ON PLUNGER (LBF)	SHEAR STRESS AT THE WALL (PSI)	SHEAR RATE AT THE WALL (1/SEC)
0.500E-01	0.470E 02	0.137E 01	0.726E 01
0.100E 00	0.740E 02	0.215E 01	0.145E 02
0.200E 00	0.116E 03	0.337E 01	0.290E 02
0.500E 00	0.200E 03	0.582E 01	0.726E 02
0.100E 01	0.290E 03	0.843E 01	0.145E 03
0.200E 01	0.405E 03	0.118E 02	0.290E 03

TABLE IV. (continued)

CAPILARY DIAMETER= 0.051000 (IN)
****
CAPILARY LENGTH= 2.000000 (IN)
****

TEMPERATURE= 160.0 (OF)
****

CROSSHEAD VELOCITY (IN/MIN)	LOAD ON PLUNGER (LBF)	SHEAR STRESS AT THE WALL (PSI)	SHEAR RATE AT THE WALL (1/SEC)
0.500E-01	0.600E 02	0.356E 01	0.688E 01
0.100E 00	0.900E 02	0.534E 01	0.138E 02
0.200E 00	0.130E 03	0.771E 01	0.275E 02
0.500E 00	0.205E 03	0.122E 02	0.688E 02
0.100E 01	0.280E 03	0.166E 02	0.138E 03
0.200E 01	0.485E 03	0.288E 02	0.275E 03

TEMPERATURE= 180.0 (OF)
****

CROSSHEAD VELOCITY (IN/MIN)	LOAD ON PLUNGER (LBF)	SHEAR STRESS AT THE WALL (PSI)	SHEAR RATE AT THE WALL (1/SEC)
0.500E-01	0.650E 02	0.385E 01	0.688E 01
0.100E 00	0.900E 02	0.534E 01	0.138E 02
0.200E 00	0.130E 03	0.771E 01	0.275E 02
0.500E 00	0.210E 03	0.125E 02	0.688E 02
0.100E 01	0.292E 03	0.173E 02	0.138E 03
0.200E 01	0.395E 03	0.234E 02	0.275E 03

TABLE IV. (continued)

TEMPERATURE= 200.0 (OF)

CROSSHEAD VELOCITY (IN/MIN)	LOAD ON PLUNGER (LBF)	SHEAR STRESS AT THE WALL (PSI)	SHEAR RATE AT THE WALL (1/SEC)
0.500E-01	0.450E 02	0.267E 01	0.688E 01
0.100E 00	0.680E 02	0.403E 01	0.138E 02
0.200E 00	0.102E 03	0.605E 01	0.275E 02
0.500E 00	0.167E 03	0.990E 01	0.688E 02
0.100E 01	0.240E 03	0.142E 02	0.138E 03
0.200E 01	0.325E 03	0.193E 02	0.275E 03

TEMPERATURE= 210.0 (OF)

CROSSHEAD VELOCITY (IN/MIN)	LOAD ON PLUNGER (LBF)	SHEAR STRESS AT THE WALL (PSI)	SHEAR RATE AT THE WALL (1/SEC)
0.500E-01	0.350E 02	0.208E 01	0.688E 01
0.100E 00	0.550E 02	0.326E 01	0.138E 02
0.200E 00	0.860E 02	0.510E 01	0.275E 02
0.500E 00	0.147E 03	0.872E 01	0.688E 02
0.100E 01	0.222E 03	0.132E 02	0.138E 03
0.200E 01	0.315E 03	0.187E 02	0.275E 03

TABLE IV. (continued)

TEMPERATURE= 220.0 (0F)
****

CROSSHEAD VELOCITY (IN/MIN)	LOAD ON PLUNGER (LBF)	SHEAR STRESS AT THE WALL (PSI)	SHEAR RATE AT THE WALL (1/SEC)
0.500E-01	0.310E 02	0.184E 01	0.688E 01
0.100E 00	0.480E 02	0.285E 01	0.138E 02
0.200E 00	0.750E 02	0.445E 01	0.275E 02
0.500E 00	0.130E 03	0.771E 01	0.688E 02
0.100E 01	0.193E 03	0.114E 02	0.138E 03
0.200E 01	0.275E 03	0.163E 02	0.275E 03

CAPILARY DIAMETER= 0.030100 (IN)
****
CAPILARY LENGTH= 1.997000 (IN)
****

TEMPERATURE= 160.0 (0F)
****

CROSSHEAD VELOCITY (IN/MIN)	LOAD ON PLUNGER (LBF)	SHEAR STRESS AT THE WALL (PSI)	SHEAR RATE AT THE WALL (1/SEC)
0.500E-01	0.215E 03	0.753E 01	0.335E 02
0.100E 00	0.310E 03	0.109E 02	0.669E 02
0.200E 00	0.445E 03	0.156E 02	0.134E 03
0.500E 00	0.660E 03	0.231E 02	0.335E 03
0.100E 01	0.920E 03	0.322E 02	0.669E 03
0.200E 01	0.128E 04	0.447E 02	0.134E 04

TABLE IV. (continued)

TEMPERATURE= 180.0 (DF)

CROSSHEAD VELOCITY (IN/MIN)	LOAD ON PLUNGER (LBF)	SHEAR STRESS AT THE WALL (PSI)	SHEAR RATE AT THE WALL (1/SEC)
0.500E-01	0.170E 03	0.596E 01	0.335E 02
0.100E 00	0.250E 03	0.876E 01	0.669E 02
0.200E 00	0.380E 03	0.133E 02	0.134E 03
0.500E 00	0.608E 03	0.213E 02	0.335E 03
0.100E 01	0.830E 03	0.291E 02	0.669E 03
0.200E 01	0.115E 04	0.403E 02	0.134E 04

TEMPERATURE= 200.0 (DF)

CROSSHEAD VELOCITY (IN/MIN)	LOAD ON PLUNGER (LBF)	SHEAR STRESS AT THE WALL (PSI)	SHEAR RATE AT THE WALL (1/SEC)
0.500E-01	0.135E 03	0.473E 01	0.335E 02
0.100E 00	0.210E 03	0.736E 01	0.669E 02
0.200E 00	0.310E 03	0.109E 02	0.134E 03
0.500E 00	0.500E 03	0.175E 02	0.335E 03
0.100E 01	0.710E 03	0.249E 02	0.669E 03
0.200E 01	0.100E 04	0.350E 02	0.134E 04

TABLE IV. (continued)

TEMPERATURE= 210.0 (DF)

CROSSHEAD VELOCITY (IN/MIN)	LOAD ON PLUNGER (LBF)	SHEAR STRESS AT THE WALL (PSI)	SHEAR RATE AT THE WALL (1/SEC)
0.500E-01	0.111E 03	0.389E 01	0.335E 02
0.100E 00	0.160E 03	0.561E 01	0.669E 02
0.200E 00	0.240E 03	0.841E 01	0.134E 03
0.500E 00	0.387E 03	0.136E 02	0.335E 03
0.100E 01	0.550E 03	0.193E 02	0.669E 03
0.200E 01	0.750E 03	0.263E 02	0.134E 04

TEMPERATURE= 220.0 (DF)

CROSSHEAD VELOCITY (IN/MIN)	LOAD ON PLUNGER (LBF)	SHEAR STRESS AT THE WALL (PSI)	SHEAR RATE AT THE WALL (1/SEC)
0.500E-01	0.103E 03	0.361E 01	0.335E 02
0.100E 00	0.161E 03	0.564E 01	0.669E 02
0.200E 00	0.246E 03	0.862E 01	0.134E 03
0.500E 00	0.435E 03	0.152E 02	0.335E 03
0.100E 01	0.650E 03	0.228E 02	0.669E 03
0.200E 01	0.890E 03	0.312E 02	0.134E 04

TABLE IV. (continued)

CAPILARY DIAMETER= 0.030140 (IN)
****
CAPILARY LENGTH= 4.004000 (IN)
****

TEMPERATURE= 160.0 (OF)
****

CROSSHEAD VELOCITY (IN/MIN)	LOAD ON PLUNGER (LBF)	SHEAR STRESS AT THE WALL (PSI)	SHEAR RATE AT THE WALL (1/SEC)
0.500E-01	0.430E 03	0.753E 01	0.333E 02
0.100E 00	0.622E 03	0.109E 02	0.667E 02
0.200E 00	0.870E 03	0.152E 02	0.133E 03
0.500E 00	0.144E 04	0.251E 02	0.333E 03
0.100E 01	0.205E 04	0.359E 02	0.667E 03
0.200E 01	0.285E 04	0.499E 02	0.133E 04

TEMPERATURE= 180.0 (OF)
****

CROSSHEAD VELOCITY (IN/MIN)	LOAD ON PLUNGER (LBF)	SHEAR STRESS AT THE WALL (PSI)	SHEAR RATE AT THE WALL (1/SEC)
0.500E-01	0.315E 03	0.551E 01	0.333E 02
0.100E 00	0.465E 03	0.814E 01	0.667E 02
0.200E 00	0.677E 03	0.118E 02	0.133E 03
0.500E 00	0.106E 04	0.186E 02	0.333E 03
0.100E 01	0.155E 04	0.271E 02	0.667E 03
0.200E 01	0.225E 04	0.394E 02	0.133E 04

TABLE IV. (continued)

TEMPERATURE= 200.0 (DF)

CROSSHEAD VELOCITY (IN/MIN)	LOAD ON PLUNGER (LBF)	SHEAR STRESS AT THE WALL (PSI)	SHEAR RATE AT THE WALL (1/SEC)
0.500E-01	0.250E 03	0.438E 01	0.333E 02
0.100E 00	0.380E 03	0.665E 01	0.667E 02
0.200E 00	0.597E 03	0.104E 02	0.133E 03
0.500E 00	0.964E 03	0.169E 02	0.333E 03
0.100E 01	0.135E 04	0.235E 02	0.667E 03
0.200E 01	0.187E 04	0.327E 02	0.133E 04

TEMPERATURE= 210.0 (DF)

CROSSHEAD VELOCITY (IN/MIN)	LOAD ON PLUNGER (LBF)	SHEAR STRESS AT THE WALL (PSI)	SHEAR RATE AT THE WALL (1/SEC)
0.500E-01	0.225E 03	0.394E 01	0.333E 02
0.100E 00	0.350E 03	0.613E 01	0.667E 02
0.200E 00	0.490E 03	0.858E 01	0.133E 03
0.500E 00	0.840E 03	0.147E 02	0.333E 03
0.100E 01	0.119E 04	0.208E 02	0.667E 03
0.200E 01	0.164E 04	0.287E 02	0.133E 04

TABLE IV. (continued)

TEMPERATURE= 220.0 (DF)

CROSSHEAD VELOCITY (IN/MIN)	LOAD ON PLUNGER (LBF)	SHEAR STRESS AT THE WALL (PSI)	SHEAR RATE AT THE WALL (1/SEC)
0.500E-01	0.185E 03	0.324E 01	0.333E 02
0.100E 00	0.292E 03	0.511E 01	0.667E 02
0.200E 00	0.458E 03	0.767E 01	0.133E 03
0.500E 00	0.747E 03	0.131E 02	0.333E 03
0.100E 01	0.109E 04	0.190E 02	0.667E 03
0.200E 01	0.153E 04	0.267E 02	0.133E 04

IV. DESCRIPTION AND ANALYSIS

In the following sections the mathematical developments and theoretical considerations concerning this study are presented.

Computer Simulation of the Injection Molding Cycle

A mathematical model for each of the stages of the injection molding process was developed in this investigation. The following sections summarize the mathematical developments, the fundamental assumptions and method of solution for the resulting system of partial differential equations resulting from the proposed model.

Filling Stage. The filling stage is perhaps the most difficult to model because the temperature, pressure and velocity profiles all change with time as well as with the axial movement of the polymer front inside the runner, gate or mold cavity. Also, provisions have to be made to account for changes in channel geometry (cylindrical for the runner or gate and cartesian for the cavity) and for melt solification during flow.

The simplest way to account for changes in channel geometry as well as to generate small time increments for the solution of parabolic partial differential equations is to use dimensionless variables. In this investigation the following dimensionless variables were used:

$$B1 = \frac{U'^2 \eta' R'}{T'_R K'_R} \qquad B2 = \left(\frac{K'_R}{\rho'_R C'_{PR} U' R'}\right)^2 \qquad C_P = \frac{C'_P}{C'_{PR}}$$

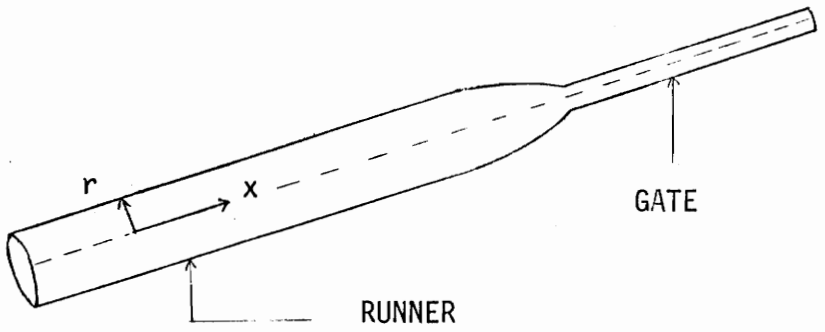

FIGURE 11a. RUNNER AND GATE COORDINATE SYSTEM

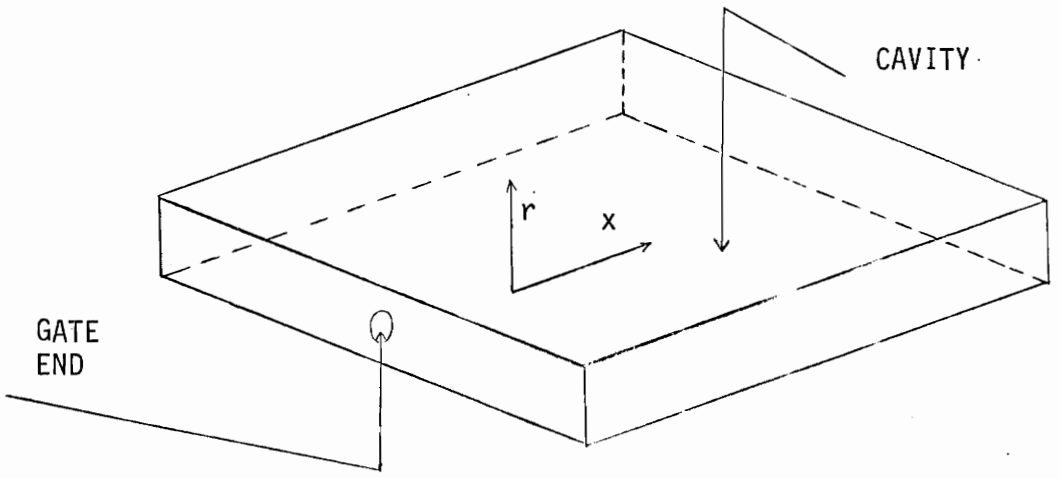

FIGURE 11b. CAVITY COORDINATE SYSTEM

FIGURE 11. EULERIAN COORDINATE SYSTEM FOR MOLD CHANNELS

TABLE V. LIST OF VARIABLES USED IN SIMULATION

VARIABLE	DIMENSIONAL SYMBOL	UNITS
Heat Capacity	C_p'	(Btu/Lb °F)
Thermal Conductivity	K'	(Btu/°F sec in)
Pressure	P'	(Psia)
Initial Volumetric Flow Rate	Q_0'	in^3/sec
Volumetric Flow Rate	Q'	in^3/sec
Radial Position	r'	(in)
Channel Inside Radius	R'	(in)
Time	t'	(sec)
Temperature	T'	(°F)
Average Temperature	T_m'	(°F)
Initial Temperature	T_I'	(°F)
Metal Temperature	T_M'	(°F)
Axial Velocity	u', V_x'	in/sec
Initial Average Velocity in Cylindrical Channel	U'	in/sec
Initial Average Velocity in Cavity	U_c'	in/sec
Average Velocity in Channel	$\bar{V}'$	in/sec
Apparent Shear Rate at the Wall	$\dot{\gamma}_w'$	sec^{-1}
True Shear Rate at the Wall	$\dot{\gamma}_{wt}'$	sec^{-1}
Density	ρ'	Lb/in^3
Viscosity	η'	Lbf-ft sec/in^2

$$K = \frac{K'}{K'_R} \qquad P = \frac{K'_R(P'-P'_0)}{2\rho'_R\, C'_{PR}\, \eta'_R\, U'^2} \qquad Q = \frac{Q'}{Q'_0}$$

$$r = \frac{r'}{R'} \qquad t = \frac{K'_R\, t'}{R'^2\, \rho'_R\, C'_{PR}} \qquad T = \frac{T' - T'_R}{T'_R}$$

$$u = \frac{u'}{QU'} \qquad U' = \frac{Q'_0}{\pi R'^2} \qquad U'_C = \frac{Q'_0}{2w'R'}$$

$$x = \frac{K'_R\, x'}{\rho'_R\, C'_{PR}\, U'\, R'^2} \qquad \eta = \frac{\eta'}{\eta'_R} \qquad \rho = \frac{\rho'}{\rho'_R}$$

where the primed variables are dimensional variables, and the subscript R means the value of a given property at any chosen reference condition. The units of each variable are shown in table V.

The filling stage was divided in two sections; the first for the runner and gate (cylindrical coordinates) and the second for the cavity (cartesian coordinates). The equations of change for both sections are described in the following sections.

Solution for the Runner and Gate. The Eulerian coordinate system used in this case is shown in figure 11, page 53. The continuity equation was written in integral form as follows

$$Q'(t) = \int_0^{R'} u'\, dA_c \qquad (3)$$

where A_c represents the cross sectional area of the channel. Using the dimensionless variables defined on page 52, equation (3) transforms to

$$\int_0^1 ur\, dr = \frac{1}{2} \tag{4}$$

Due to their high viscosity, polymers flow in the laminar regime (13). For this reason only the axial direction component of the momentum equation was considered. Because of their low thermal conductivity and relatively high heat capacity, most polymers can store heat very well, but are not able to dissipate it fast. Therefore, the velocity profile at a point approaches steady state faster than the temperature profile. Further, it is known that for Prandtl numbers greater than about 5, the velocity profile at the entrance of a cylindrical tube can be considered to have its steady state shape, i.e., the axial distance for the development of the steady profile is nearly zero (36). Polyethylene, the polymer used in this investigation, has a Prandtl number of about 9.8×10^5; this high Prandtl number justifies the assumption of a fully developed profile at the entrance of the runner.

The complete momentum equation can be written as follows (8):

$$\rho'\left(\frac{\partial v'_x}{\partial t'} + v'_r \frac{\partial v'_x}{\partial r'} + \frac{v'_\theta}{r'} \frac{\partial v'_x}{\partial \theta'} + v'_x \frac{\partial v'_x}{\partial x'}\right) = -\frac{\partial P'}{\partial x'}$$
$$-\left(\frac{1}{r'} \frac{\partial}{\partial r'} (r'\tau'_{rx}) + \frac{1}{r'} \frac{\partial \tau'_{\theta x}}{\partial \theta'} + \frac{\partial \tau'_{xx}}{\partial x'}\right) \tag{5}$$

With the above assumptions, the momentum equation transforms to:

$$-\frac{dP'}{dX'} = \frac{1}{r'} \frac{d}{dr'} (r'\tau'_{rx}) \tag{6}$$

Since the two sides of this equation vary independent of each other, direct integration can be used to give:

$$- \frac{dP'}{dX'} \frac{r'^2}{2} = r'\tau'_{rx} + C \tag{7}$$

Since at $r' = 0$; $\tau'_{rx} = 0$ then $C = 0$, and

$$\tau'_{rx} = - \frac{dP'}{dX'} \frac{r'}{2} \tag{8}$$

For the flow of non-Newtonian fluids in a tube, the relationship between shear stress and velocity is given by (8,42)

$$\tau'_{rx} = -\eta \frac{du'}{dr'} \tag{9}$$

where η (viscosity) is not a constant but depends on temperature and shear rate (du'/dr'). Combining equations (8) and (9) gives'

$$\int_{u'}^{0} du' = \frac{1}{2} \frac{dP'}{dX'} \int_{r'}^{R'} \frac{r'}{\eta'} dr' \tag{10}$$

Performing the integration, the dimensional velocity is given by

$$u' = \frac{1}{2} \frac{dP'}{dX'} \int_{r'}^{R'} \frac{r'}{\eta'} dr' \tag{11}$$

Finally, using dimensionless variables, the momentum equation reduces to

$$Qu = - \frac{dP}{dX} \int_{r}^{1} \frac{r}{\eta} dr \tag{12}$$

Under the previously stated assumptions, the resulting energy equation is (8)

$$\rho' C_v' \left(\frac{\partial T'}{\partial t'} + u' \frac{\partial T'}{\partial X'}\right) = \frac{1}{r'} \frac{\partial}{\partial r'} \left(r' K' \frac{\partial T'}{\partial r'}\right) + K' \frac{\partial^2 T'}{\partial X'^2} + \frac{\partial K'}{\partial X'} \frac{\partial T'}{\partial X'} - \tau_{rx}' \frac{du'}{dr'} \tag{13}$$

since

$$C_P' - C_v' = -T' \left(\frac{\partial V'}{\partial T'}\right)^2 \left(\frac{\partial P'}{\partial V'}\right) \tag{14}$$

where V' = volume and C_v' is the heat capacity at constant volume. The term $(\partial V'/\partial T')$ is known to be very small for most polymers (42), (51), (52). Therefore, the heat capacity at constant pressure could be assumed to be approximately equal to the heat capacity at constant volume. Substituting C_P' for C_v' and τ_{rx}' from equation (8) into the energy equation results in

$$\underbrace{\rho' C_P' \left(\frac{\partial T'}{\partial t'} + u' \frac{\partial T'}{\partial X'}\right)}_{\text{axial convection}} = \underbrace{\frac{1}{r'} \frac{\partial}{\partial r'} \left(r' K'\right) \frac{\partial T'}{\partial r'} + K' \frac{\partial^2 T'}{\partial r'^2}}_{\text{radial conduction}} + \underbrace{\frac{\partial K'}{\partial X'} \frac{\partial T'}{\partial X'} + K' \frac{\partial^2 T}{\partial X'^2}}_{\text{axial conduction}} + \underbrace{\frac{r'}{2} \frac{dP'}{dX'} \frac{du'}{dr'}}_{\text{viscous dissipation}} \tag{15}$$

Using dimensionless variables, the energy equation transforms to:

$$\frac{\partial T}{\partial t} + Qu \frac{\partial T}{\partial X} = \frac{1}{\rho C_P r} \frac{\partial (Kr)}{\partial r} \frac{\partial T}{\partial r} + \frac{K}{\rho C_P} \frac{\partial^2 T}{\partial r^2} + \frac{B2}{C_P \rho} \frac{\partial K}{\partial X} \frac{\partial T}{\partial X} + \frac{B2\ K}{\rho C_p} \frac{\partial^2 T}{\partial X^2} + \frac{B1\ rQ}{\rho C_p} \frac{dP}{dX} \frac{du}{dr} \tag{16}$$

With the boundary conditions: $T(x,1,t) = T_M$; $\frac{\partial T}{\partial r}(x,0,t) = 0$;

$$T(0,r,t) = T_I; \quad T(x,r,t) = T_m; \quad T(x,r,0) = T_I$$

The transient velocity, temperature and pressure profiles at particular points of the channel can be obtained by solving simultaneously equations (4), (12), and (16) together with the constitutive equation:

$$\text{Ln } \eta' = 3.36 - 0.57 \text{ Ln } \dot{\gamma}'_{tw} - 1.94(10)^{-2}(\ln \dot{\gamma}'_{tw})^2 + 1.02T + 4.19(10)^{-6}T' + 4.40(10)^{-4}T \text{ Ln } \dot{\gamma}'_{tw} \qquad (77)$$

developed on page 73.

Equations (4), (12), (16) and (77) are a set of relationships between velocity, temperature and pressure, which clearly cannot be solved analytically, but lend themselves relatively well to solution by numerical methods. The next section outlines a numerical procedure for the simultaneous solution of these equations.

Nodal Positioning Analysis (NPA). Equations (4), (12), (16) and (77) were solved using a technique developed in this investigation called Nodal Positioning Analysis (NPA). In NPA the position of the flow front is calculated for each time increment; then an axial node is located at the newest location of the flow front. The procedure is repeated until axial nodes have been placed throughout all of the channel or until the flow front stops. The main advantage of this technique, when compared to the fixed finite difference grid, is that computation time is saved by considering only nodes filled with the fluid. No complications due to the parabolic shape of the flow front profile are introduced, because the axial nodes are placed at average front locations determined by the average velocity at the particular time interval in consideration.

In this investigation NPA was combined with the implicit alternating direction method of solution for two dimensional parabolic partial differential equations (PDE) outlined in reference (16). After an axial node was placed using NPA, the alternating direction method was used to solve equation (16) for the temperature distribution at every radial and axial node inside the channel.

Equation (16) was written in finite difference form (using central differences) and expressed implicitly in the radial direction for the first half time interval and implicitly in the axial direction for the second half time interval as follows:

$$\frac{T^*_{ij} - T_{ij}}{\frac{\Delta t}{2}} = \frac{1}{C_p \rho r_j} \frac{r_{j+1}K_{ij+1} - r_{j-1}K_{ij-1}}{r_{j+1} - r_{j-1}} \cdot \frac{T^*_{ij+1} - T^*_{ij-1}}{r_{j+1} - r_{j-1}}$$

$$+ \frac{K_{ij}}{\rho C_p} \frac{T^*_{ij-1} - 2T^*_{ij} + T^*_{ij+1}}{r_{j+1} - r_{j-1}} + \left(\frac{B2}{C_p \rho} \cdot \frac{K_{i+1j} - K_{i-1j}}{X_{i+1} - X_{i-1}} \cdot Qu_{ij}\right)$$

$$\frac{T_{i+1j} - T_{i-1j}}{X_{i+1} - X_{i-1}} + \frac{B2\ K_{ij}}{\rho C_p} \frac{T_{i-1j} - 2T_{ij} + T_{i+1j}}{(X_{i+1} - X_i)^2}$$

$$+ \frac{B1 r_j Q}{\rho C_p} \frac{dP}{dX} \frac{u_{ij+1} - u_{ij-1}}{r_{j+1} - r_{j-1}} \qquad (17)$$

where the star temperatures are the unknowns during the first half time interval.

Define

$$AP(i,j) = \frac{(r_{j+1}K_{ij+1} - r_{j-1}K_{ij-1})\Delta t}{2C_p \rho r_j (r_{j+1} - r_j)^2} \qquad (18)$$

$$A1(i,j) = \frac{K_{ij}\Delta t}{2C_p\rho(r_{j+1}-r_j)^2} \tag{19}$$

$$A2(i,j) = \left(\frac{B2(K_{i+1j} - K_{i-1j})}{C_p\rho(X_{i+1} - X_{i-1})} - Qu_{ij}\right) \frac{\Delta t}{2(X_{i+1} - X_{i-1})} \tag{20}$$

$$A3(i,j) = \frac{B2\ K_{ij}\ \Delta t}{2C_p\rho(X_{i+1}-X_i)^2} \tag{21}$$

$$BETA(i,j) = \frac{B1\ r_j\ Q\ \Delta t}{2C_p\rho} \frac{dP}{dX} \frac{u_{ij+1} - u_{ij-1}}{r_{j+1} - r_{j-1}} \tag{22}$$

Substituting equations (18), (19), (20), (21) and (22) into equation (17) results in

$$\begin{aligned} T^*_{ij} - T_{ij} = {} & AP(i,j)(T^*_{ij+1}-T^*_{ij-1}) + A1(i,j)(T^*_{ij-1}-2T^*_{ij}+T^*_{ij+1}) \\ & + A2(i,j)(T_{i+1j}-T_{i-1j}) + A3(i,j)(T_{i-1j}-2T_{ij}+T_{i+1j}) \\ & + BETA(i,j) \end{aligned} \tag{23}$$

Expressing the star temperatures as a function of the known temperatures, the following algebraic system of equations results

$$\begin{aligned} & [AP(i,j)-A1(i,j)]T^*_{ij-1} + [2A1(i,j)+1]T^*_{ij} - [AP(i,j)+A1(i,j)]T^*_{ij+1} \\ & = A2(i,j)(T_{i+1j}-T_{i-1j}) + A3(i,j)(T_{i-1j}-2T_{ij}+T_{i+1j}) + T_{ij} + BETA(i,j) \end{aligned} \tag{24}$$

The resulting system of linear equations shown above is a tridiagonal system, which can be easily solved by a recurrence relationship as shown in reference (16).

The same procedure previously described can be followed for the axial direction, and the resulting system of equations is:

$$[A2(i,j)-A3(i,j)]T_{i-1j} + [2A3(i,j)+1]T_{ij} - [A2(i,j)+A3(i,j)]T_{i+1,j}$$
$$= AP(i,j)(T^*_{ij+1}-T^*_{ij-1}) + A1(i,j)(T^*_{ij-1}-2T^*_{ij}+T^*_{ij}+1) + BETA(i,j) + T^*_{ij} \quad (25)$$

In equation (25), the star temperatures are known temperatures calculated during the first half time interval.

If the velocity and pressure profile are known at a particular time and location, the temperature profile can be obtained by solving the system of equations shown in relationships (24) and (25).

Solution for the Cavity. The same analysis used for the runner and gate channels was used for the cavity; the only difference was the use of Cartesian instead of cylindrical coordinates.

The continuity equation in integral form can be written as follows:

$$Q'(t) = \int_0^{R'} u' \, dA'_C = \int_0^{R'} 2u'w'dr' \quad (26)$$

Using dimensionless variables equation (26) transforms into

$$\int_0^1 udr = 1 \quad (27)$$

The momentum equation for this case can be reduced, after considering the previously mentioned assumptions, to

$$-\frac{d\tau'_{rx}}{dr'} = \frac{dP'}{dX'} \quad (28)$$

Upon integration, the resulting dimensional velocity is given by

$$u' = - \frac{dP'}{dX'} \int_{r'}^{R'} \frac{r'}{\eta'} dr' \tag{29}$$

Using dimensionless variables equation (29) reduces to

$$uQ = -2 \frac{dP}{dX} \int_{r}^{1} \frac{r}{\eta} dr \tag{30}$$

The two dimensional energy equation in Cartesian coordinates is

$$\rho' C_p' \left(\frac{\partial T'}{\partial t'} + u' \frac{\partial T'}{\partial X'}\right) = \frac{\partial}{\partial X'} \left(K' \frac{\partial T'}{\partial X'}\right) + \frac{\partial}{\partial r'} \left(K' \frac{\partial T'}{\partial r'}\right) - \tau_{rx}' \frac{\partial u'}{\partial r'} \tag{31}$$

τ_{rx}' in the viscous dissipation term can be replaced by r'dP'/dX', which can be obtained by integration of equation (28). Using the dimensionless variables defined on table V , page 54 and substituting r'dP'/dX' for τ_{rx}' in the viscous dissipation term, equation (31) reduces to

$$\rho C_p \left(\frac{\partial T}{\partial t} + uQ \frac{\partial T}{\partial X}\right) = B2 \frac{\partial K}{\partial X} \frac{\partial T}{\partial X} + K\, B2 \frac{\partial^2 T}{\partial X^2} + \frac{\partial K}{\partial r} \frac{\partial T}{\partial r} + K \frac{\partial^2 T}{\partial r^2} + 2B1\, rQ \frac{dP}{dX} \frac{du}{dr} \tag{32}$$

Redefining the coefficients shown in equations (18), (19), (20), (21), and (22) as follows,

$$AP(i,j) = \frac{(K_{ij+1} - K_{ij-1})\Delta T}{2\rho C_p (r_{j+1} - r_{j-1})^2} \tag{33}$$

$$A1(i,j) = \frac{K_{ij}\,\Delta t}{2\rho C_p (r_{j+1}-r_j)^2} \tag{34}$$

$$A2(i,j) = \left(\frac{B2(K_{i+1j}-K_{i-1j})}{\rho C_p (X_{i+1}-X_{i-1})} - Qu_{ij}\right) \frac{\Delta t}{2(X_{i+1}-X_{i-1})} \tag{35}$$

$$A3(i,j) = \frac{B2\;K_{ij}\,\Delta t}{2\rho C_p (X_{i+1}-X_i)^2} \tag{36}$$

$$BETA(i,j) = \frac{B1\;r_j\,Q\,\Delta t}{\rho C_p} \frac{dP}{dX} \frac{u_{ij+1} - u_{ij-1}}{r_{j+1} - r_{j-1}} \tag{37}$$

The resulting system of tridiagonal equations is given by equation (23).

Iterative Solution Procedure for Filling Stage. Due to the complexity of the finite difference equations, the iterative solution for the equations of change was carried out on an IBM 370 computer. The solution procedure was programmed in WATFIV language.

An initial estimate of viscosity must be obtained in order to start the iterative loop. However, the temperature and shear rate have to be known before the viscosity can be calculated. An initial estimate of shear rate for a constant temperature was obtained by using the following power law relationship (42).

$$\dot{\gamma}'_w = -Q' \left(\frac{3n'+1}{n'\Pi R'^2}\right)\left(\frac{1}{R'}\right)^{\frac{n'+1}{n'}} (r')^{1/n'} \tag{38}$$

where n is the flow index of the polymer. Values of the flow index for polyethylene for different temperatures were found in references

(7) (26). A third order polynomial was fitted to these values resulting in

$$n' = 0.835 - 0.126(10)^{-2}T' + 0.179(10)^{-5}T'^{2} + 0.277(10)^{-4}T'^{3} \quad (39)$$

Using the dimensionless variables previously defined, equation (38) reduces to

$$\overset{o}{\gamma}{}'_{w} = \frac{-Q'(3n'+1)}{n'\pi R^{3}} \; r^{1/n} \quad (40)$$

Equation (40) was used to obtain the first estimate of $\overset{o}{\gamma}{}'_{w}$; then the viscosity at every radial position was obtained using equation (77).

The procedure was started at the entrance of the runner assuming a constant temperature at that location. This assumption is justified in most cases because the sprue (where the runner begins) is usually much larger than the runner. This translates into a much slower sprue cooling rate. The first axial node was divided into equally spaced radial increments. Using equations (77) and (40), an estimate of viscosity was obtained; then from equation (12), the variable V_{ij}, defined as

$$V_{ij} = \frac{-Qu}{(dP/dX)_i} = \int_{r}^{1} \frac{r_j}{\eta_{ij}} \, dr \quad (41)$$

was numerically integrated for each radial location. Next, $(dP/dX)_i$ was calculated by numerical integration of V_{ij} as follows:

$$F = \int_0^1 V_{ij} r_j dr = \int_0^1 \frac{Qu}{(dP/dX)_i} r_j dr = \frac{-Q}{(dP/dX)_i} \int_0^1 urdr$$

$$F = \frac{-Q}{2(dP/dX)_i} ; \quad \left(\frac{dP}{dX}\right)_i = \frac{-Q}{2F_i} \tag{42}$$

with $(dP/dX)_i$ known. The velocity was calculated from equation (41) as follows:

$$u_{ij} = \frac{-v_{ij}(dP/dX)_i}{Q} \tag{43}$$

An average velocity was then calculated from the definition of volumetric flow rate

$$Q' = \bar{V}' \int_0^{2\pi} \int_0^{R'} r'dr'd\theta' = \int_0^{2\pi} \int_0^{R'} u'r'dr'd\theta'$$

The average dimensional velocity $\bar{V}'$ is given by

$$\bar{V}' = \frac{\int_0^{R'} u'r'dr'}{\int_0^{R'} r'dr'}$$

Using the dimensionless variables,

$$\bar{V}' = \frac{Qu'}{2} \int_0^1 urdr$$

but from equation (4)

$$\int_0^1 urdr = \frac{1}{2}$$

then

$$\bar{V}' = QU'$$

Finally

$$\bar{V} = \frac{\bar{V}'}{QU'} = 1 \tag{44}$$

This means that the average dimensionless velocity must always be equal to one. This fact was used to check whether the dimensionless velocities at each node were being properly calculated.

Since the average velocity was equal to one, the average axial displacement was equal to the selected time increment. Using this average displacement, the next axial node was placed and divided into equally spaced radial nodes. The average temperature of the previous node was calculated as follows:

$$T'_m = \frac{1}{\pi R'^2 \bar{V}} \int_0^{R'} u'T'd(\pi r^2)$$

$$T'_m = \frac{1}{R'^2 \pi \bar{V}} \int_0^{R'} u'T'r'dr'$$

Using dimensionless variables

$$T'_m = 2T'_R \int_0^1 urTdr + T'_R$$

Finally

$$T_m = 2 \int_0^1 uTrdr \qquad (45)$$

The average temperature of the previous axial node was assigned to be the initial temperature of the newly created nodes. Next, the alternating directions implicit method was used to determine the temperatures of all nodes for the present time interval. An iterative procedure was started in which viscosity was calculated from the known temperatures; velocity was determined from the newly calculated viscosities; with these velocities a new estimate of the temperatures was obtained and compared against the temperatures previously calculated. The procedure was continued until a convergence criterion was met. Then a new axial node was created and the iterative procedure was continued. At the end of each time interval the total pressure drop was calculated by integration of $(dp/dx)_i$. This procedure was repeated until the runner, gate and cavity were full or until the total pressure drop exceeded the machine pressure setting, in which case the volumetric flow rate was reduced until the calculated entrance pressure was less or equal to the set pressure or until the flow stopped before filling the cavity, i.e., a "short-shot" occurred. It is worthwhile to point out that equations (38) to (45) apply only for cylindrical coordinates; a similar set of equations can be easily developed for Cartesian coordinates.

Flow and Static Solidification of Polyethylene. During all three stages of the injection cycle the hot polymer undergoes solidification. It then becomes necessary to include polymer solidification in the

in the simulation since changes in the channel geometry which affect the flow behavior occur during the filling stage, and the rate of solidification during the cooling stage governs the final physical and mechanical properties of the molded part.

A rigorous approach for determining the extent of solidification at any time will envolve an energy balance performed at the solid-liquid interface as follows:

$$\left(\frac{\partial T'_s}{\partial r'}\right)_{r'=\varepsilon'} - \frac{K'_m}{K'_s}\left(\frac{\partial T'_m}{\partial r'}\right)_{r'=\varepsilon'} = \rho'_s L'_f \frac{d\varepsilon'}{dt'} \tag{46}$$

where the subscripts m and s refer to melt and solid, respectively; ε' measures the extent of solidification in the radial direction; and L'_f is the latent heat of freezing.

The values of $(\partial T'_s/\partial r')_{r'=\varepsilon'}$ and $(\partial T'_m/\partial r')_{r'=\varepsilon'}$ are obtained from the solution of the energy equations (15) or (31). For the solid layer, equations (15) or (31) are solved, making the velocities zero wherever they appear. This eliminates the convection and viscous dissipation terms. At the solid-liquid polymer interface, all temperatures are assumed to be equal to the solidification temperature.

Due to the complexity of the equations of change for the injection molding model, the procedure outlined above was simplified in an attempt to decrease the computer execution time. The following procedure was used instead; first, the crystallinity of the polymer was defined as

$$\beta = \frac{L'_f - C'_{pa}(\Delta T')}{L'_f} \tag{47}$$

where β is the fraction of crystalline material; $\Delta T'$ is the solidification temperature range and C'_{pa} is an average heat capacity. Values for L'_f and C'_{pa} are given in reference (21).

The percent crystallinity β and the upper limit temperature of the solidification range were determined in a previous work (26). Equation (47) can be solved for $\Delta T'$ to give

$$\Delta T' = \frac{L'_f\ (1-\beta')}{C'_{pa}} \tag{48}$$

Substituting in values gives

$$\Delta T' = \frac{55.8\ \frac{Btu}{26}\ (1-0.47)}{0.62\ \frac{Btu}{26°F}} = 47.7°F$$

Then the lower limit temperature of the solidification range is:

$$\Delta T' = T'_{UL} - T'_{LL} = 47.7°F = 8.7°C$$

$$T'_{LL} = 110°C - 8.7°C = 101.3°C$$

where T'_{UL} and T'_{LL} are the upper and lower temperature limits, respectively.

The solidification temperature was taken as 101.3°C. In the simulation, whenever the temperature of a given node reaches this value, the solidification front is moved to this node and the velocity of the node is set equal to zero. In this way the zero velocity boundary condition is satisfied. T'_{LL} introduces a time delay in the movement of the solidification front since the lower limit temperature of the solidification range is used instead of an average solidification temperature.

Packing Stage. In the event that a short-shot did not occur, the following model was used to simulate the additional polymer fed into the cavity before the gate solidified.

The average pressure in the cavity was calculated as follows:

$$P'_a = \frac{\int_0^{L'} P_x(x,t)w'dX'}{w'L'} \tag{49}$$

where P'_a is the average pressure of the cavity and L' is the cavity length. Using dimensionless variables:

$$P_a = \frac{1}{L} \int_0^L P_x dx \tag{50}$$

Once the average pressure is known the volumetric flow rate can be calculated by using the power-law relationship

$$Q_i = Q_0 \left(\frac{\Delta P_t}{\Delta P_0}\right)^{1/n} \tag{51}$$

where Q_0 and ΔP_0 are the volumetric flow rate and total pressure drop at a particular node in the cavity at the beginning of the packing stage.

The average density at any given time was given by

$$\rho'_{ia} = \rho'_0 + \Delta\rho'_i \tag{52}$$

where ρ'_{ia} is the average density at a given time; ρ'_0 is the average cavity density at the beginning of the packing stage; and $\Delta\rho'_i$ is the density change during the present time increment. Using known

parameters, equation (52) can be written as follows:

$$\rho'_{i^a} = \rho'_0 + \frac{\int_0^{t'} \rho_{i-1^a} Q'_i \, dt'}{V'} \tag{53}$$

where ρ'_{i-1^a} is the average density at the end of the previous time increment. In dimensionless form equation (53) is given by

$$\rho_{i^a} = 1 + \frac{1}{L} \int_0^t Q_i \, \rho_{i-1^a} \, dt \tag{54}$$

where

$$\rho_{i^a} = \frac{\rho'_{i^a}}{\rho'_0}$$

At the beginning of the packing stage equations (49) and (50) were used to determine the initial average temperature and pressure in the cavity. These values were used in conjunction with the following equation of state proposed by Donovan (21).

$$\rho' = 53.76 + 0.000252 \, P' - 0.0465 \, T' \tag{55}$$

where ρ' is in Lb/ft^3; P' is in psia; and T' is in °F.

This equation was found to give more accurate results than the commonly used equation of state proposed by Gilmore (45) when comparison of the predictions of equation (55) against the experimental density data found in reference (7) was made. Equation (55) was used to determine ρ'_0, the average density in the cavity at the beginning of

the packing stage. The initial flow rate Q_0' was assumed to be the same as the volumetric flow rate at the end of the filling stage.

With all initial values known, the energy equation was solved using the alternating directions scheme described before to obtain the temperature at every node. The average temperature, pressure and volumetric flow rate were calculated for this new time increment, and the new average density was calculated from equation (54). An iterative procedure was started in which for every time increment, the average temperature and average density were determined; equation (55) was used to obtain the new cavity pressure and equation (51) was used to determine the new volumetric flow rate. The iterative loop was stopped when the pressure at the entrance of the runner reached the machine injection pressure setting.

Cooling Stage. Once the flow of polymer into the cavity stopped, the cooling stage was begun. Equations (45) and (55) were used to calculate average temperature and pressure at a given time, and the energy equation was solved including only radial and axial conduction terms. In this way, temperature and pressure profiles were determined for each time increment until the preset molding cycle time was reached.

The calculated pressure and temperature values for each of the molding stages were stored in memory and at the end of the molding cycle were printed and plotted versus axial and radial position in the runner, gate and cavity.

Development of a Constitutive Equation for Polyethylene. As mentioned on page 14, a constitutive equation of the form of equation (1) was used in this investigation. Data from the capillary viscometer

(table IV) was converted to apparent shear rate and apparent shear stress using the following relationship developed from the analysis of Newtonian fluid flow through cylindrical channels.

$$\dot{\gamma}'_N = \frac{2}{15} \frac{V'_{xH} D'^2_P}{D'^3_C} \tag{56}$$

$$\tau'_w = \frac{F'}{4A'_P \left(\frac{LC'}{DC'}\right)} \tag{57}$$

where

$\dot{\gamma}'_N$ = Newtonian shear rate (sec^{-1})

V'_{xh} = cross head velocity (in/min)

D'_P = plunger diameter (in)

D'_C = capillary diameter (in)

τ'_w = shear stress (psia)

F' = force on plunger (Lbf)

LC = length of capillary (in)

Viscosity was assumed to be pressure dependent using the equation

$$\eta' = \eta'_a \, EXP(b'P'^*) \tag{58}$$

where η'_a is the viscosity at atmospheric pressure, P'^* is the pressure above atmospheric, and b' is a pressure coefficient which is characteristic of the material.

The momentum equation was used in order to obtain a relationship between shear stress and pressure drop as follows:

$$\frac{1}{\eta'} \frac{dP'}{dX'} = \frac{1}{r'} \left[\frac{d}{dr'} \left(r' \frac{du'}{dr'}\right)\right] \tag{59}$$

In the above equation it is assumed that the polymer behaves as an incompressible fluid; the acceleration terms are negligible; the flow is assumed unidimensional, laminar, and isothermal. Equation (59) can be integrated as follows

$$\int_{P'_i}^{P'} \frac{dP'}{\eta'} = \int_{0}^{L'_i} C'dx' \tag{60}$$

Let $P^* = P - P_{atm}$; then $dP^* = dP$. Then substituting equation (58) into equation (60) results in

$$\int_{P^*_i}^{P^*} \frac{dP^*}{\eta'_a EXP(b'P^*)} = C'L'_i \tag{61}$$

where

$$C' = \frac{1}{r'}\left[\frac{d}{dr'}\left(r' \frac{du'}{dr'}\right)\right]$$

Then

$$-\frac{1}{b'\eta'_a} EXP(-b'P^*)\Big]_{P^*_i}^{P^*} = C'L'_i$$

or

$$\frac{1}{b'\eta'_a}\left[EXP(-b'P^*) - EXP(-b'P^*_i)\right] = \frac{1}{r'}\left[\frac{d}{dr'}\left(r' \frac{du'}{dr'}\right)\right] L'_i$$

then

$$\frac{-R'^2}{2b'\eta'_a}\left[EXP(-b'P^*) - EXP(-bP^*_i)\right] = L'_i R' \frac{du'}{dr'} \tag{62}$$

Substituting equation (9) into (62) and rearranging terms yields:

$$\tau_w' = \frac{D_C'}{4b'L_C'}\left(\frac{EXP(b'\Delta P') - 1}{EXP(b'P_i')}\right) \tag{63}$$

An explicit relationship for ΔP can be obtained from equation (63) as follows:

$$EXP(-b\Delta P') = 1 - \frac{4\,\tau_w'b'L_C'}{D_C'}$$

$$-b'\Delta P' = Ln\left(1 - \frac{4\tau_w'b'L_C'}{D_C'}\right)$$

$$\Delta P' = \frac{-1}{b'} Ln\left(1 - \frac{4\tau_w'b'L_C'}{D_C'}\right) \tag{64}$$

Using a logarithmic series expansion for the right hand side of equation (64) results in

$$\Delta P' = 4\tau_w'\left(\frac{L_C'}{D_C'}\right) + 8b'\tau_w'^2\left(\frac{L_C'}{D_C'}\right)^2 \tag{65}$$

where the higher order terms have been neglected.

Equation (62) can be used together with the experimental data to obtain the constitutive equation. The procedure followed to obtain the constitutive equation is outlined in the following paragraphs.

Equation (65) can be written as follows:

$$\Delta P' = A_0' + A_1'\left(\frac{L_C'}{D_C'}\right) + A_2'\left(\frac{L_C'}{D_C'}\right)^2 \tag{66}$$

where the coefficients A_0', A_1' and A_2' are functions of the shear rate at the wall and temperature, and the coefficient A_0' has been

introduced to account for capillary end effects in accordance with Bagley correction (3).

The coefficients A_0', A_1' and A_2' can be expressed as a function of $\dot{\gamma}_N'$ and T as follows (38).

$$A_0' = C_0' + C_1' Ln\dot{\gamma}_N' + C_2 T' Ln^2\dot{\gamma}_N' + C_7 Ln^3\dot{\gamma}_N' \quad (67)$$

$$A_1' = C_3' + C_4' Ln\dot{\gamma}_N' + C_5 Ln^2\dot{\gamma}_N' \quad (68)$$

$$A_2' = C_6' Ln^3\dot{\gamma}_N' \quad (69)$$

Comparing equations (65) and (66) the following relationships are obtained

$$\tau_w' = \frac{A_1'}{4} \quad (70)$$

$$b' = \frac{2A_2'}{(A_1')^2} \quad (71)$$

Since equation (56) only applies for Newtonian fluids, the Rabinowitsch (42) correction shown in equation (72) should be used in order to transform the Newtonian shear rate at the wall given in equation (56) into the non-Newtonian shear rate at the wall needed in this case. The Rabinowitsch correction can be written as follows:

$$\dot{\gamma}_{tw}' = \frac{1}{4}\left[3 + 1/\frac{d(Ln\tau_w')}{d(Ln\dot{\gamma}_N')}\right] \dot{\gamma}_N' \quad (72)$$

where $\dot{\gamma}_{tw}'$ is the true, non-Newtonian shear rate at the wall.

The term $d(Ln\tau_w')/d(Ln\dot{\gamma}_N')$ can be obtained directly from the coefficients of equation (66)

$$\frac{\partial(\mathrm{Ln}\tau_w')}{\partial(\mathrm{Ln}\overset{\circ}{\gamma}_w')} = \frac{1}{\tau_w'}\frac{\partial\tau_w'}{\partial(\mathrm{Ln}\overset{\circ}{\gamma}_N')} = \frac{1}{A_1'}\frac{\partial A_1'}{\partial(\mathrm{Ln}\overset{\circ}{\gamma}_N')} \tag{73}$$

Computation Procedure.

1. For a constant temperature and shear rate, a regression analysis is performed on the data of table IV. From this analysis the coefficients A_0', A_1' and A_2' are obtained for each temperature and shear rate.

2. With the values of A_0', A_1' and A_2', a regression analysis is used to determine the coefficients of equations (67), (68) and (69). In this fashion the coefficients A_0', A_1' and A_2' can be easily obtained for any given set of experimental conditions.

3. With A_0', A_1' and A_2' known, equations (70), (71) and (72) are used to obtain the shear stress at the wall, the pressure correction coefficient and the true shear rate at the wall. Next, the viscosity at every experimental point was obtained from

$$\eta' = \frac{\tau_w'}{\overset{\circ}{\gamma}_{tw}'} \tag{74}$$

4. With the viscosity calculated from equation (74) a final regression analysis was performed to obtain the coefficients of the relationships

$$\mathrm{Ln}\,\eta' = E_0 + E_1\mathrm{Ln}\overset{\circ}{\gamma}_{tw}' + E_2\mathrm{Ln}^2\overset{\circ}{\gamma}_{tw}' + E_3T\,\mathrm{Ln}\overset{\circ}{\gamma}_{tw}' + E_4T' + E_5T'^2 \tag{75}$$

and

$$b = B_0 + B_1 Ln\dot{\gamma}'_{tw} + B_2 Ln^2\dot{\gamma}'_{tw} + B_3 T\, Ln\dot{\gamma}'_{tw} + B_4 T' + B_5 T'^2 \quad (76)$$

The steps outlined above were programmed in Fortran language, and the program was run in an IBM 370 computer. The resulting constitutive equation was

$$\begin{aligned} Ln\,\eta' = {} & 3.3568 - 0.57483\, Ln\dot{\gamma}'_{tw} - 0.019462(Ln\dot{\gamma}'_{tw})^2 \\ & - 0.010242\, T' + 4.186(10)^{-6}(T')^2 + 4.402(10)^{-4} T' Ln\dot{\gamma}'_{tw} \end{aligned} \quad (77)$$

and the pressure coefficient was

$$\begin{aligned} b' = {} & [-4.3216 + 2.0314\, Ln\dot{\gamma}'_{tw} - 0.1342(Ln\gamma'_{tw})^2 \\ & - 0.001986\, T' Ln\gamma'_{tw} + 0.024043\, T' \\ & - 3.9654(10)^{-6}(T')^2] \times 10^{-5} \end{aligned} \quad (78)$$

Equations (77) and (78) were used together with equation (58) in the proposed injection molding model described in previous sections of this work.

Graphical Optimization Procedure for Gates. One of the end uses of the numerical simulation developed in this investigation is the optimization of gate dimensions. As mentioned earlier, gates are presently designed by trial and error using experience as the only guidance. Up until now the money spent during the long trials to obtain a working gate was totally recovered because of the large profit margin that plastic articles yield; however, with the tremendous jump in oil prices and the ever increasing access to digital computers, a numerical optimization designed to cut labor costs is in demand. Several types of optimization techniques could be used to determine

the optimum gate dimensions. Since an objective function does not exist in this case, an analytical approach could not be used. Instead, a numerical optimization with a "black box" objective function, generated from the simulation, has to be followed. In this investigation a graphical optimization technique was considered. The numerical optimization will be developed in a future investigation by the author.

An optimum gate should offer the fastest freeze off, i.e., should solidify in the shortest time, with the minimum diameter before melt fracture occurs, the minimum pressure drop, and the maximum shear rate which will still keep the polymer under its degradation temperature.

In other words, a well designed gate should be able to freeze fast to avoid energy wasted by keeping the plunger forward longer than necessary, should have a diameter large enough to avoid melt fracture which is the cause of sink marks, weld lines and non-homogeneous surface gloss on the finished article, should develop the smallest possible pressure drop during filling in order to save energy during the plunger forward movement, and should offer the maximum shear rate, which will insure a maximum temperature below the degradation temperature of the polymer. A maximum temperature is desired because less pressure drop is generated by friction, which shortens the filling time and the complete molding cycle.

In the graphical procedure, maximum solid thickness in channel, maximum temperature in channel, pressure drop and maximum shear rate in channel can be plotted versus time with gate diameter and length (L/D) ratio as a parameter for fixed operational conditions, i.e., injection

pressure, temperature and volumetric flow rate. Generally, the injection temperature and pressure are kept constant to insure good product moldability (26). Then only the volumetric flow rate should be changed.

Figure 34, page 124 shows a plot for a set of conditions. Different (L/D) can be plotted on the same graph and the optimum gate can be selected for a specific volumetric flow rate in accordance with the constraints previously mentioned.

V. RESULTS AND DISCUSSION

A summary of the experimental and predicted results is outlined in the following paragraphs. A detailed interpretation of the results is also included.

In order to get a better understanding of the results presented in this section, the exact location of the thermocouples and pressure transducers must be known. Figure 12, page 83, shows the cavity layout of the injection mold used in this investigation. Referring to Figure the thermocouples and pressure transducers were numbered from right to left, i.e., thermocouple 1 is located closest to the sprue channel (located at the center of the figure), while pressure transducer 4 is located nearest to the left end of the cavity.

Before discussing the results in detail, the difference in the time frame of work between the experimental and the model-predicted results should be explained (refer to Tables VI to VIII and the appendix). The experimental data were recorded for each cycle when the plunger started its forward movement. This introduced a variable time lag between the starting of the plunger forward movement and the beginning of the flow inside the runner. On the other hand the simulation was started assuming that the flow front was already at the entrance of the runner. In order to compare the experimental and model-predicted results, a common time basis had to be selected. The time at which the experimental data showed the highest temperature value for thermocouple 1 was selected as the common "zero" time basis. This particular value was selected in order to eliminate the response lag time generated by the

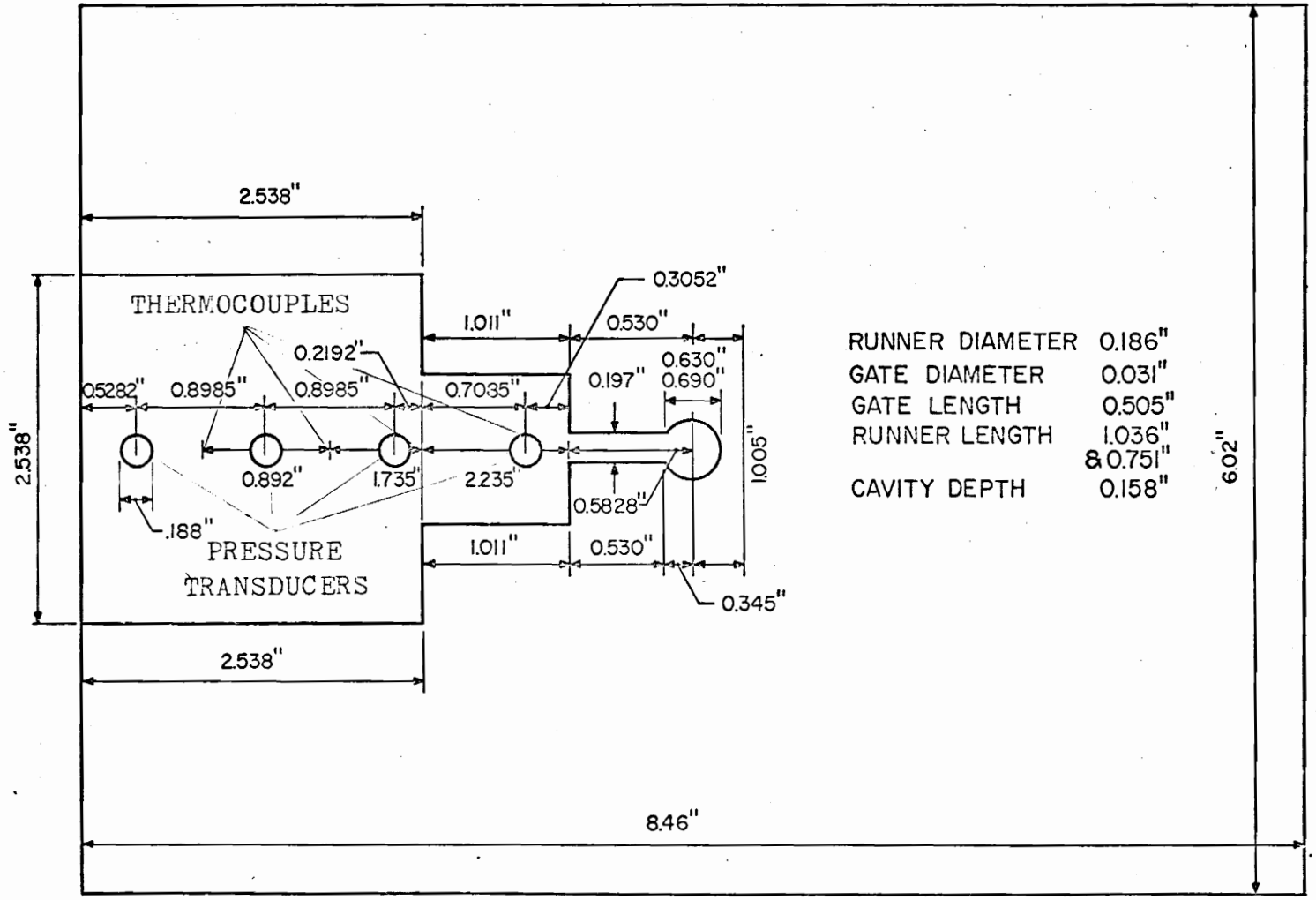

FIGURE 12. MOLD CAVITY LAYOUT

epoxy coating placed at the tip of the thermocouples for protection purposes, and by the change in thermocouple location due to pressure deformation. Even though the thermocouples were bolted to the back-up mold plate using special fittings, the tremendous pressures developed during the injection cycle, ranging from 2,000 to 20,000 psig, moved the tight fitted thermocouples inside their cavities. The deformation measured never exceeded 0.020 in. but even this small deformation allowed the thermocouple to move enough nearer to the wall of its cavity, that the conduction of heat from the hot polymer to the cold thermocouple cavity walls was translated into a time delay. This ended after a moderate increase in the runner pressure.

Figures 13-28, pages 88-108 and Tables VI and VII, pages 96-113 show the experimental results for two injection cycles run at 400°F, 12,000 psig, 1.83 in^3/sec and 388°F, 13,500 psig and 1.30 in^3/sec respectively. As expected, both the experimental and model-predicted results show the highest pressure and temperature readings for pressure transducer 1 and thermocouple 1 located closest to the runner entrance. The computer output of the simulation contains the following information pertinent to a given run: injection conditions (set points), length (in) traveled by the flow front vs time (sec), channel transition (e.g., from gate to cavity) node, dimensionless movement of the solidification front, measured from the channel wall, vs. time, volumetric flow rate vs time, and average temperature and pressure readings during the packing stage.

Generally the model-predicted temperatures proved to be higher than the experimental, while the pressures tended to be lower than the experimental for the following reasons.

1. An average volumetric flow rate had to be used as the initial volumetric flow rate because the actual rate could not be determined from the experimentally measured ram velocity vs time. As mentioned on page 23, a potentiometer was used to determine the position of the plunger with time. By taking the first derivative of the ram displacement vs time, the ram velocity at any given time was determined. It was thought that after the molder reached steady conditions, for a particular set of conditions, the volumetric flow rate could be determined by multiplying the cross sectional area of the nozzle by the ram velocity. This assumption was proved not to be valid, since experimental measurements of the volumetric flow rate revealed deviations of over 200%. Instead, an average volumetric flow rate was determined by dividing the sum of the volumes of the runner, gate and cavity by the filling time. The filling time was in turn determined from the experimental data by subtracting the time values associated with the first temperature change observed in thermocouples 1 and 4 using an average flow rate, which is lower than the true initial volumetric flow rate value gave a lower polymer velocity in the channels, which allowed more solidification to occur due to the larger polymer residence time in the channels before the filling stage was ended. The high flow resistance, caused by the greater channel solidification, was translated into a high

pressure build-up at the runner, and a low pressure build-up in the subsequent channels. For this reason the agreement between the experimental and model-predicted values for the pressure transducer 1 is better than for the other transducers.

2. The constitutive equation developed in page 73 is good for shear rate values up to 4000 sec^{-2}. Outside this upper limit, the values of viscosity given by the constitutive equation are lower than the true viscosity values when comparison was made against viscosity data given in reference (7). At the walls of the narrow gate used in this investigation shear rate values as high as 26,000 sec^{-1} were calculated by the model. These high shear rates were translated in the simulation into low viscosities, which resulted in the consistently higher temperatures and lower pressures predicted by the model.
3. The solution of equation (15) was programmed to include non-constant heat capacity and thermal conductivity. Due to the lack of good experimental data, only two values for these properties were used; one for the molten state and the other for the solid state. Polyethylene has the lowest thermal conductivity and heat capacity when it is in its liquid state. This means that a high thermal diffusivity was used until solidification occurred at a particular location, which resulted in higher temperature values, as can be deduced from equation (17).

4. As was explained earlier, the thermocouples were moved inside their cavities due to the high pressure developed during the injection cycle. Then, due to the heat conduction from the polymer to the wall, lower temperature readings were recorded. An estimate of the difference in temperature readings with position was obtained, for a particular thermocouple, by taking two readings with the thermocouple located at different positions. Differences in temperature readings of up to 20°C were recorded.
5. The use of ram operated injection molders ceased about 10 years ago because of the non-uniform injection temperatures and mass rates they delivered. The injection molder used in this investigation was ram operated. Moderate differences in polymer mass fed per molding cycle were detected when the mass of polymer fed per shot was experimentally measured. This was quite apparent experimentally since pressure readings for the same injection conditions could differ by as much as 2,000 psig.
6. As mentioned during the development of the packing model, average pressure and density had to be used in this stage. This implies that the pressure at every mode increased by an average value instead of by its corresponding exact value. The use of the average pressure increase resulted in lower calculated pressure values.

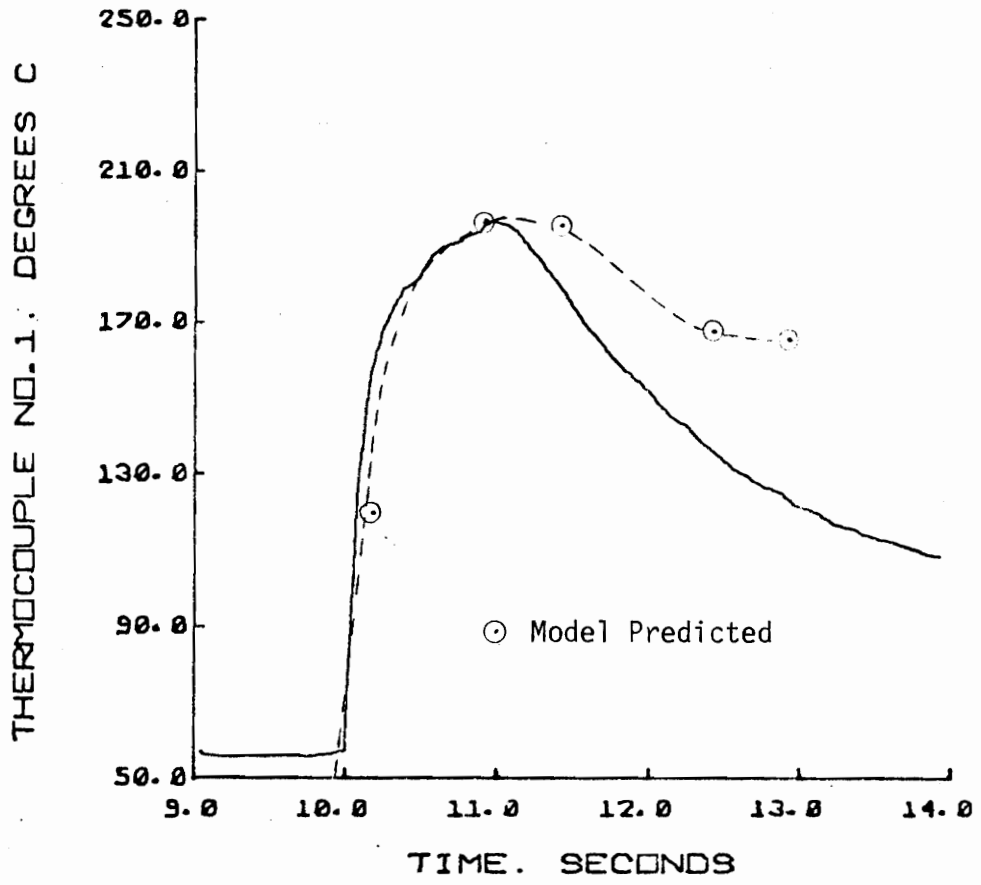

FIGURE 13. RUNNER ENTRANCE TEMPERATURE FOR A CYCLE RUN AT T'=388.0 P'=13500 Q_0'=1.30

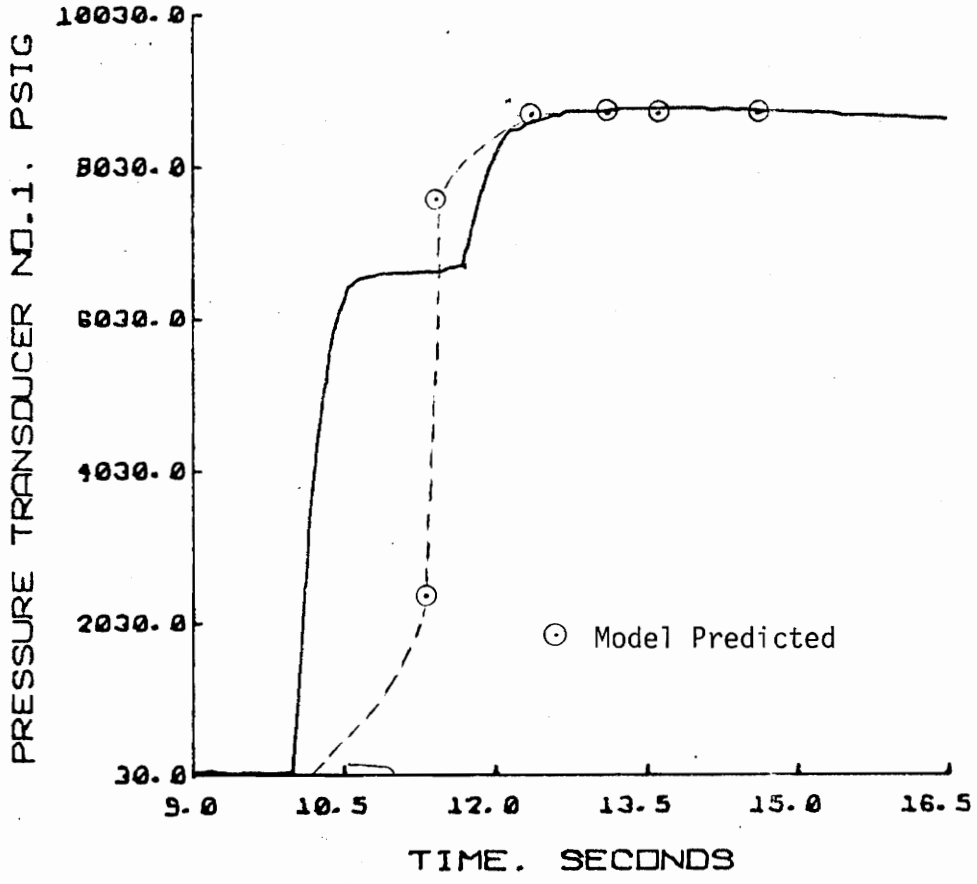

FIGURE 14. RUNNER ENTRANCE PRESSURE FOR A CYCLE RUN AT T'=388.0 P'=13500 Q_0'=1.30

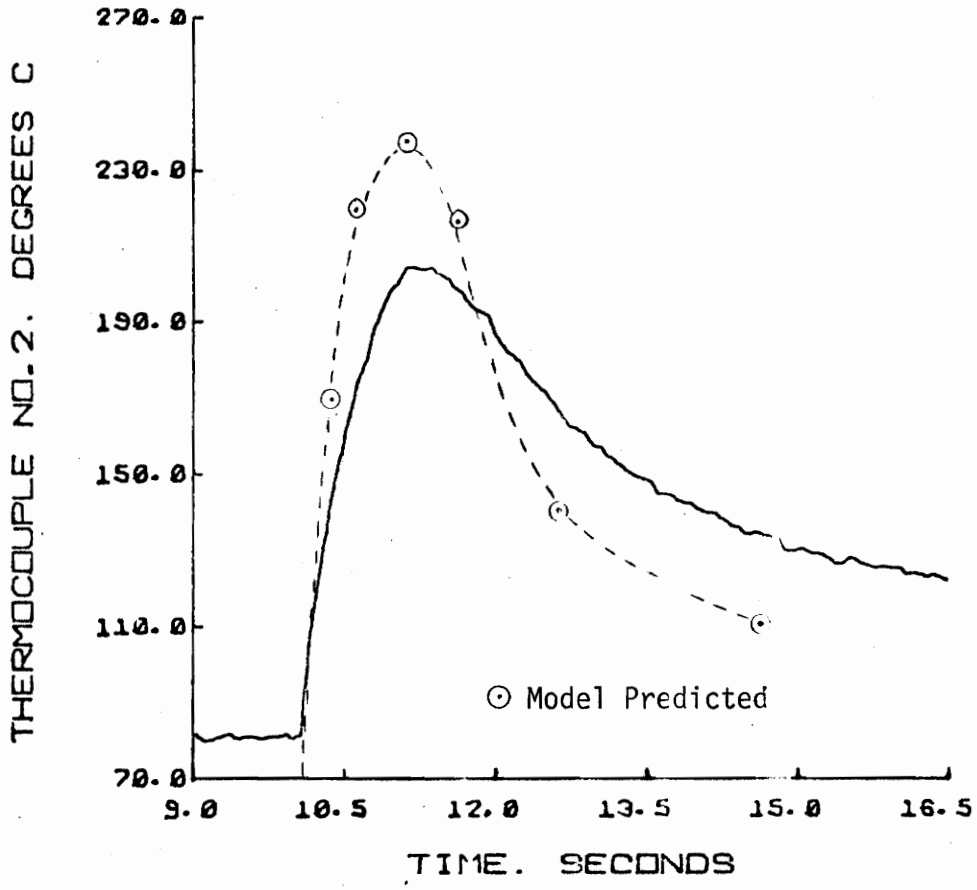

FIGURE 15. GATE EXIT TEMPERATURE FOR A CYCLE RUN AT T'=388.0 P'=13500 Q_0'=1.30

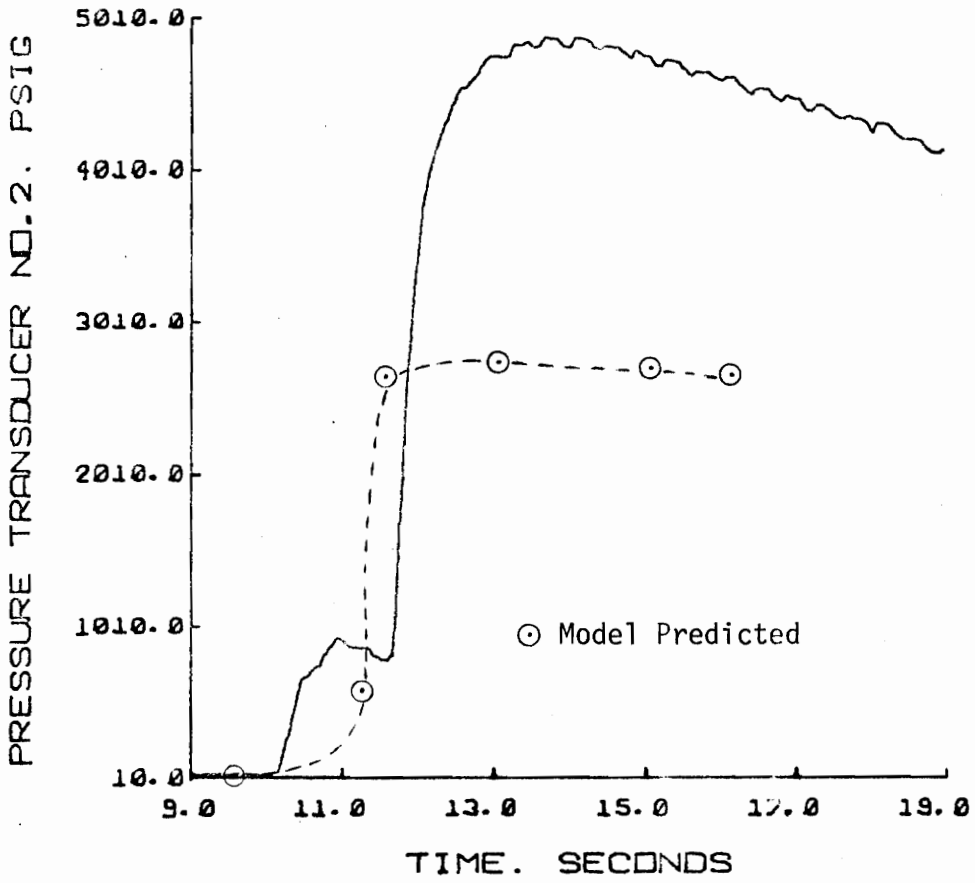

FIGURE 16. GATE EXIT PRESSURE FOR A CYCLE RUN AT T'=388.0 P'=13500 Q_0'=1.30

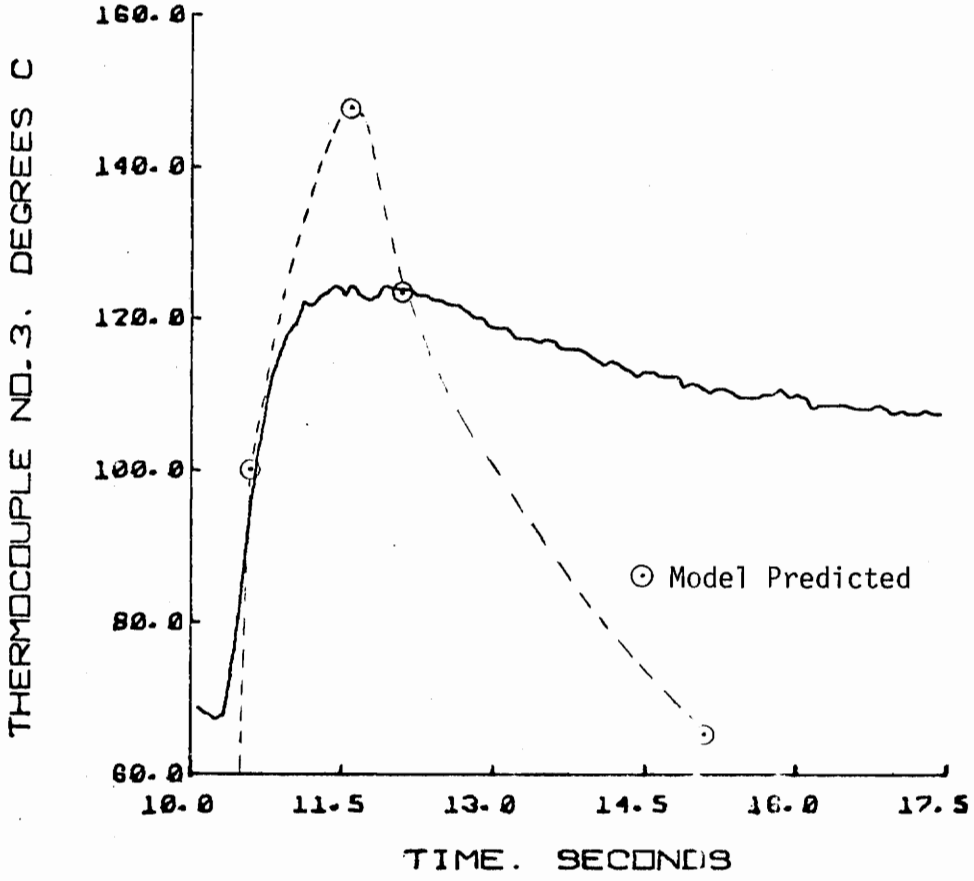

FIGURE 17. MIDDLE OF CAVITY TEMPERATURE FOR A CYCLE RUN AT T'=388.0 P'=13500 Q_0'=1.30

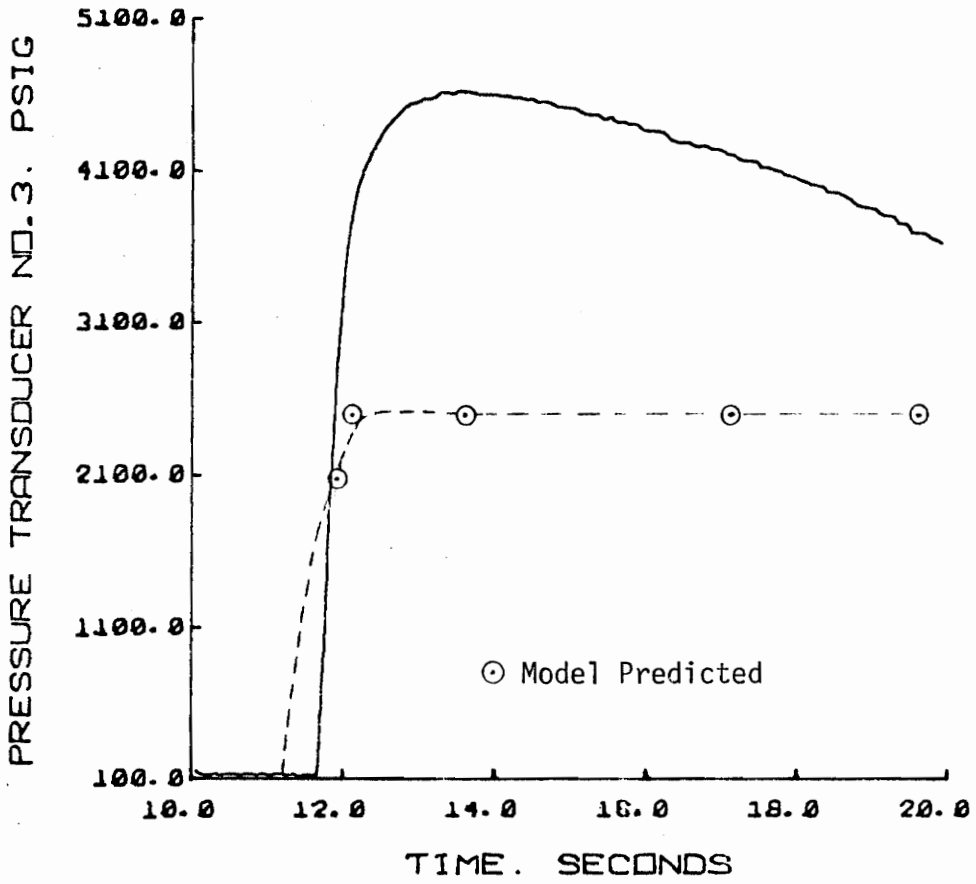

FIGURE 18. MIDDLE OF CAVITY PRESSURE FOR A CYCLE RUN AT T'=388.0 P'=13500 Q_0'=1.30

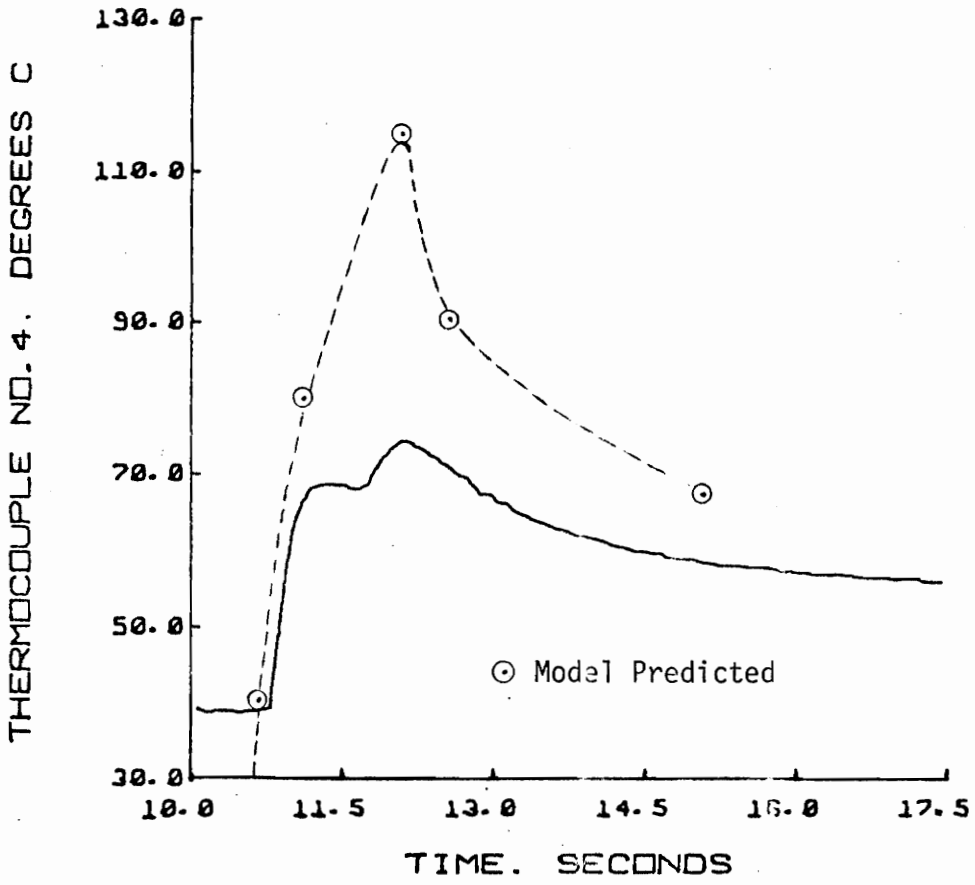

FIGURE 19. END OF CAVITY TEMPERATURE FOR A CYCLE RUN AT T'=388.0 P'=13500 Q_0'=1.30

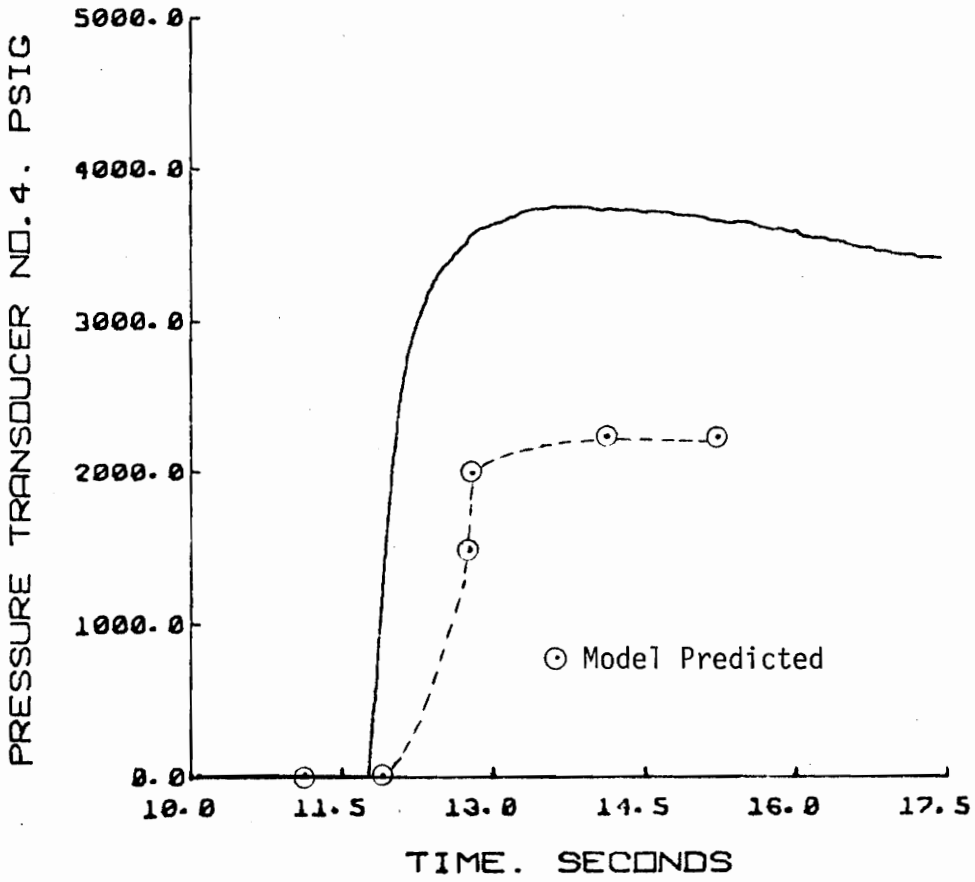

FIGURE 20. END OF CAVITY PRESSURE FOR A CYCLE RUN AT T'=388.0 P'=13500 Q_0'=1.30

TABLE VI. SIMULATION RESULTS FOR MOLDING CYCLE RUN AT T'=388.0 P'=13500 Q_0'=1.30

INITIAL TEMPERATURE= 388.00
PRESSURE SETTING= 13500.00
INITIAL FLOW RATE= 1.30
METAL TEMPERATURE= 86.00
TOTAL CAVITY LENGTH= 4.08

LENGTH ******	TIME ****	NODES *****	SOLIDIFICATION LOCATION IN GATE CHANNEL **********						
0.207E 00	0.433E-02	2	0.00	0.00	0.00	0.00	0.00	0.00	0.004
0.414E 00	0.966E-02	3	0.00	0.00	0.00	0.00	0.00	0.00	0.009
0.622E 00	0.130E-01	4	0.00	0.00	0.00	0.00	0.00	0.00	0.013
0.829E 00	0.173E-01	5	0.00	0.00	0.00	0.00	0.00	0.00	0.017
0.104E 01	0.217E-01	6	0.00	0.00	0.00	0.00	0.00	0.00	0.022
CHANNEL TRANSITION: ******************	NODE= 6 ****	ZONE= 2 ****							
0.114E 01	0.219E-01	7	0.00	0.00	0.00	0.00	0.00	0.00	0.022
0.124E 01	0.221E-01	8	0.00	0.00	0.00	0.00	0.00	0.00	0.022
0.134E 01	0.224E-01	9	0.00	0.00	0.00	0.00	0.00	0.00	0.022
0.144E 01	0.226E-01	10	0.00	0.00	0.00	0.00	0.00	0.00	0.023
0.154E 01	0.228E-01	11	0.00	0.00	0.00	0.00	0.00	0.00	0.023
CHANNEL TRANSITION: ******************	NODE= 11 ****	ZONE= 3 ****							
0.205E 01	0.179E 00	12	0.00	0.00	0.00	0.00	0.00	0.00	0.179
0.256E 01	0.335E 00	13	0.00	0.00	0.00	0.00	0.00	0.00	0.335
0.306E 01	0.491E 00	14	0.00	0.00	0.00	0.00	0.00	0.00	0.491

FLOW RATE REDUCED TO= 0.704 DIMENSIONAL FLOW RATE= 0.916 TIME= 0.4908
PE(1)= 0.158E 05 VAVP= 2.29

TABLE VI. (continued)

0.357E 01 0.789E 00 15

FLOW RATE REDUCED TO= 0.523 DIMENSIONAL FLOW RATE= 0.690 TIME= 0.4908
PE(1)= 0.144E 05 VAVP= 1.70

0.00 0.00 0.00 0.00 0.00 0.00 0.789

FLOW RATE REDUCED TO= 0.352 DIMENSIONAL FLOW RATE= 0.457 TIME= 0.7489
PE(1)= 0.163E 05 VAVP= 1.14

FLOW RATE REDUCED TO= 0.251 DIMENSIONAL FLOW RATE= 0.326 TIME= 0.7889
PE(1)= 0.147E 05 VAVP= 0.82

FLOW RATE REDUCED TO= 0.183 DIMENSIONAL FLOW RATE= 0.238 TIME= 0.7989
PE(1)= 0.136E 05 VAVP= 0.60

0.10 0.10 0.00 0.00 0.00 0.00 1.641

TABLE VI. (continued)

PACKING STAGE
****

VOL.FLOW R **********	AV.TEMP. *********	AV.DENSITY **********	INIT.DENS *********	AV.PRESS. RUNNER *********	AV.PRESS. GATE *********	AV.PRESS. CAVITY *********	ENTRANCE PRESSURE *********
0.183E 00	0.293E 03	0.100E 01	0.493E 02	0.825E 04	0.259E 04	0.137E 04	0.129E 05
0.364E-01	0.293E 03	0.100E 01	0.493E 02	0.827E 04	0.261E 04	0.139E 04	0.128E 05
0.363E-01	0.293E 03	0.100E 01	0.493E 02	0.832E 04	0.265E 04	0.143E 04	0.128E 05
0.361E-01	0.293E 03	0.100E 01	0.493E 02	0.839E 04	0.273E 04	0.151E 04	0.129E 05
0.358E-01	0.293E 03	0.100E 01	0.493E 02	0.850E 04	0.284E 04	0.162E 04	0.130E 05
0.353E-01	0.293E 03	0.100E 01	0.493E 02	0.863E 04	0.297E 04	0.175E 04	0.132E 05
0.348E-01	0.293E 03	0.100E 01	0.493E 02	0.880E 04	0.313E 04	0.192E 04	0.133E 05
0.341E-01	0.293E 03	0.100E 01	0.493E 02	0.897E 04	0.331E 04	0.209E 04	0.135E 05

0.10	0.10	0.00	0.00	0.00	0.00	1.641
0.10	0.10	0.00	0.00	0.00	0.00	1.643
0.10	0.10	0.00	0.00	0.00	0.00	1.645
0.10	0.10	0.00	0.00	0.00	0.00	1.648
0.10	0.10	0.00	0.00	0.00	0.00	1.651
0.10	0.10	0.00	0.00	0.00	0.00	1.656
0.10	0.10	0.10	0.00	0.00	0.00	1.661

TABLE VI. (continued)

COOLING STAGE
****

0.10	0.10	0.10	0.00	0.00	0.00	1.665
0.10	0.10	0.10	0.00	0.00	0.00	1.726
0.10	0.10	0.10	0.00	0.00	0.00	1.[illegible]
0.10	0.10	0.10	0.00	0.00	0.00	2.005
0.10	0.10	0.10	0.00	0.00	0.00	2.225
0.10	0.10	0.10	0.00	0.00	0.00	2.483
0.10	0.10	0.10	0.00	0.00	0.00	2.836
0.10	0.10	0.10	0.00	0.00	0.00	3.207
0.10	0.10	0.10	0.00	0.00	0.00	3.642
0.10	0.10	0.10	0.00	0.00	0.00	4.130

CYCLE HAS BEEN COMPLETED
****

TABLE VI. (continued)

T1 ****	T2 ****	T3 ****	T4 ****	P1 ****	P2 ****	P3 ****	P4 ****	P5 ****	TIME ******	FLOW RATE **********
30.000	30.000	30.000	30.000	14.700	14.700	14.700	14.700	14.700	0.0000	1.3000
30.000	30.000	30.000	30.000	14.700	14.700	14.700	14.700	14.700	0.0043	1.3000
197.335	30.000	30.000	30.000	14.700	14.700	14.700	14.700	14.700	0.0087	1.3000
196.997	30.000	30.000	30.000	14.700	14.700	14.700	14.700	14.700	0.0130	1.3000
196.737	30.000	30.000	30.000	202.407	14.700	14.700	14.700	14.700	0.0173	1.3000
196.539	30.000	30.000	30.000	390.566	14.700	14.700	14.700	14.700	0.0217	1.3000
196.387	30.000	30.000	30.000	578.277	14.700	14.700	14.700	14.700	0.0219	1.3000
196.326	30.000	30.000	30.000	918.349	14.700	14.700	14.700	14.700	0.0221	1.3000
196.274	30.000	30.000	30.000	1350.159	14.700	14.700	14.700	14.700	0.0224	1.3000
196.228	30.000	30.000	30.000	1532.596	14.700	14.700	14.700	14.700	0.0226	1.3000
196.188	204.672	30.000	30.000	1965.171	14.700	14.700	14.700	591.447	0.0228	1.3000
196.154	207.799	30.000	30.000	2438.710	588.682	14.700	14.700	777.365	0.1784	1.3000
195.813	238.918	149.653	30.000	7622.063	5398.012	14.700	14.700	5586.754	0.3348	1.3000
195.994	219.505	123.045	30.000	5270.383	2655.255	2277.914	14.700	2843.713	0.4908	1.3000
188.807	193.623	94.967	115.299	4596.609	2383.813	2065.311	14.700	2546.058	0.7584	0.6801
172.761	111.246	64.132	66.880	8016.371	2028.008	1776.212	1507.418	2160.151	1.6409	0.2389
172.610	111.207	64.125	66.893	8033.223	2044.960	1793.064	1524.270	2177.004	1.6413	0.0364
172.159	111.089	64.104	66.931	8079.277	2090.917	1839.121	1570.327	2223.060	1.6426	0.0363
171.412	110.894	64.068	66.993	8155.980	2167.623	1915.827	1647.033	2299.767	1.6446	0.0361
170.373	110.621	64.019	67.076	8262.551	2274.196	2022.400	1753.606	2406.340	1.6475	0.0358
169.063	110.272	63.959	67.177	8397.785	2409.432	2157.636	1888.843	2541.576	1.6512	0.0353
167.495	109.848	63.883	67.291	8560.824	2572.473	2320.677	2051.883	2704.616	1.6558	0.0349
165.676	109.349	63.793	67.415	8734.473	2746.121	2494.325	2225.531	2878.265	1.6611	0.0341
165.675	109.349	63.798	67.415	8734.418	2746.029	2494.217	2225.470	2878.192	1.6665	0.0000
165.663	109.346	63.797	67.415	8734.289	2745.930	2494.157	2225.455	2878.063	1.7255	0.0000
165.640	109.340	63.796	67.417	8734.035	2745.722	2494.043	2225.455	2877.840	1.8382	0.0000
165.607	109.331	63.794	67.420	8733.668	2745.435	2493.884	2225.440	2877.507	2.0046	0.0000
165.563	109.319	63.792	67.423	8733.138	2745.037	2493.676	2225.440	2877.042	2.2247	0.0000
165.508	109.304	63.789	67.426	8732.578	2744.557	2493.419	2225.421	2876.447	2.4984	0.0000
165.443	109.286	63.785	67.431	8731.875	2743.966	2493.101	2225.406	2875.927	2.9258	0.0000
165.367	109.265	63.781	67.436	8731.031	2743.293	2492.734	2225.376	2875.043	3.2069	0.0000
165.280	109.241	63.776	67.442	8730.086	2742.509	2492.317	2225.342	2874.166	3.6416	0.0000
165.182	109.214	63.771	67.449	8729.016	2741.646	2491.837	2225.311	2873.159	4.1300	0.0000

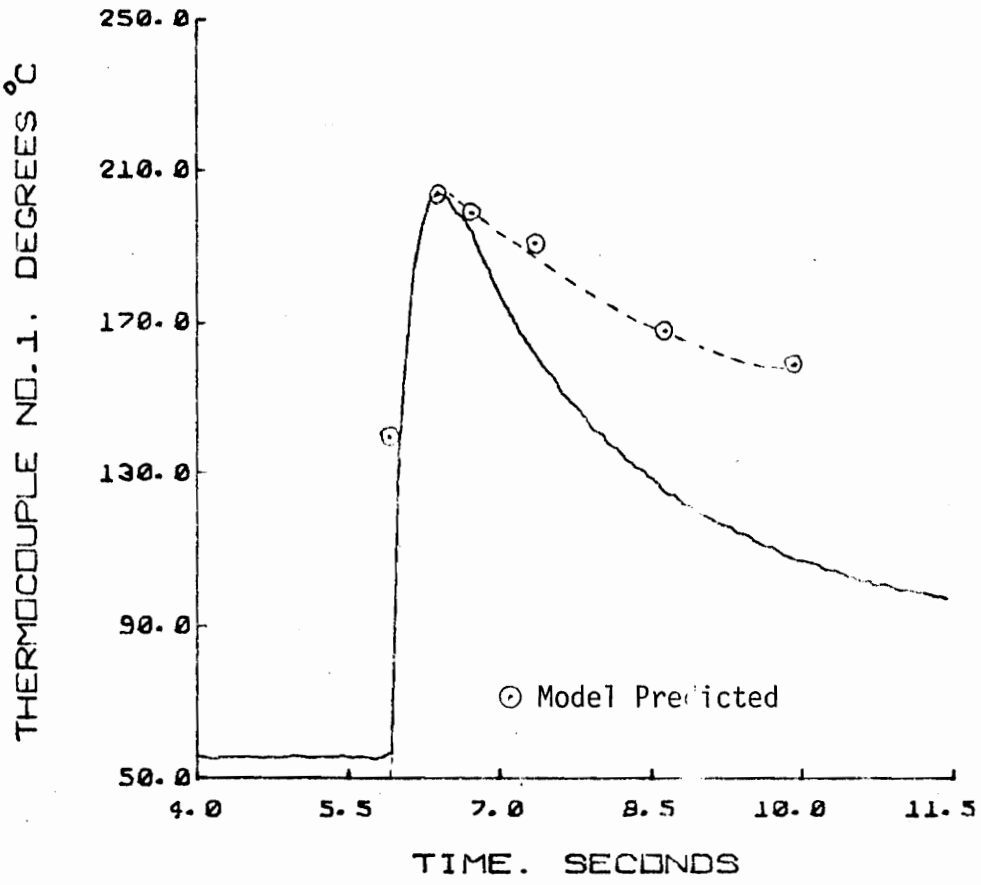

FIGURE 21. RUNNER ENTRANCE TEMPERATURE FOR A CYCLE RUN AT T'=400.0 P'=12000 Q_0'=1.83

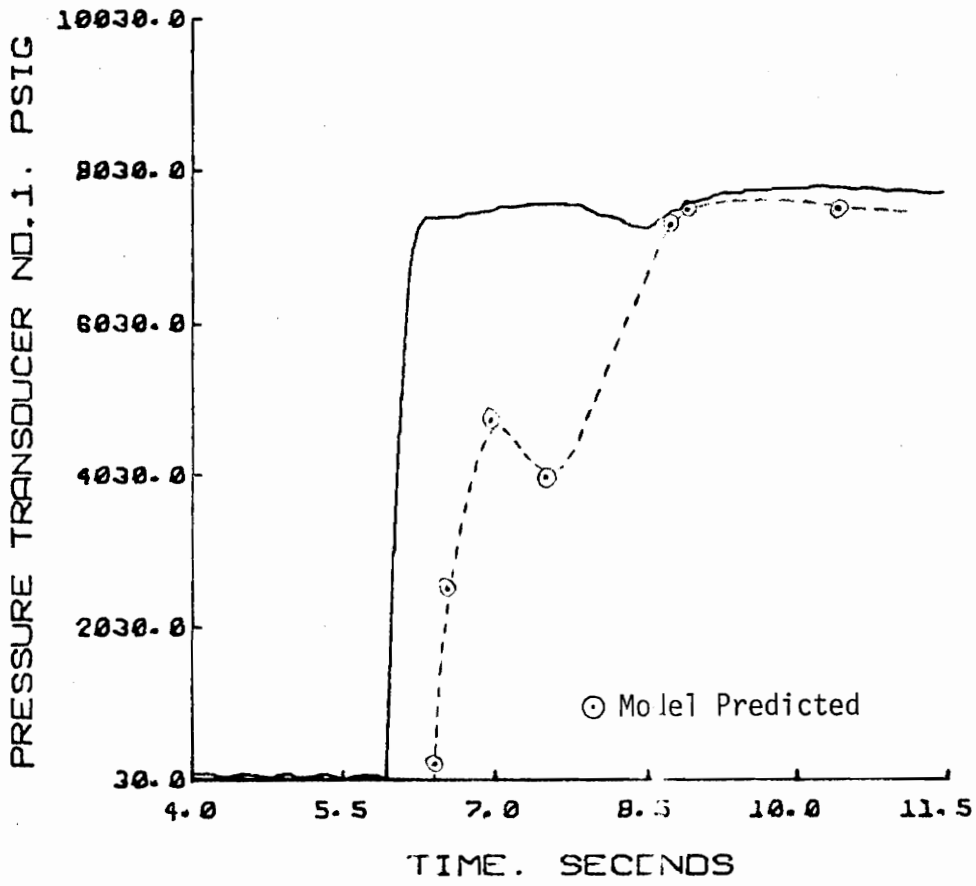

FIGURE 22. RUNNER ENTRANCE PRESSURE FOR A CYCLE RUN AT T'=400.0 P'=12000 Q_0'=1.83

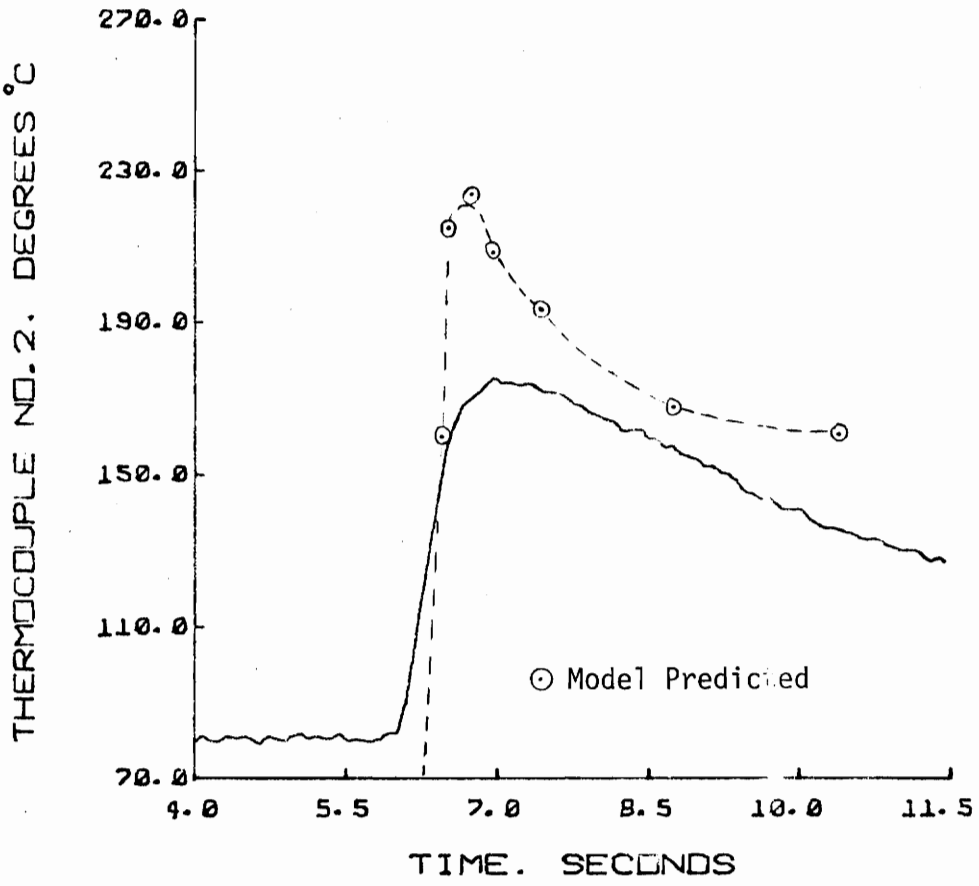

FIGURE 23. GATE EXIT TEMPERATURE FOR A CYCLE RUN AT T'=400.0 P'=12000 Q_o'=1.83

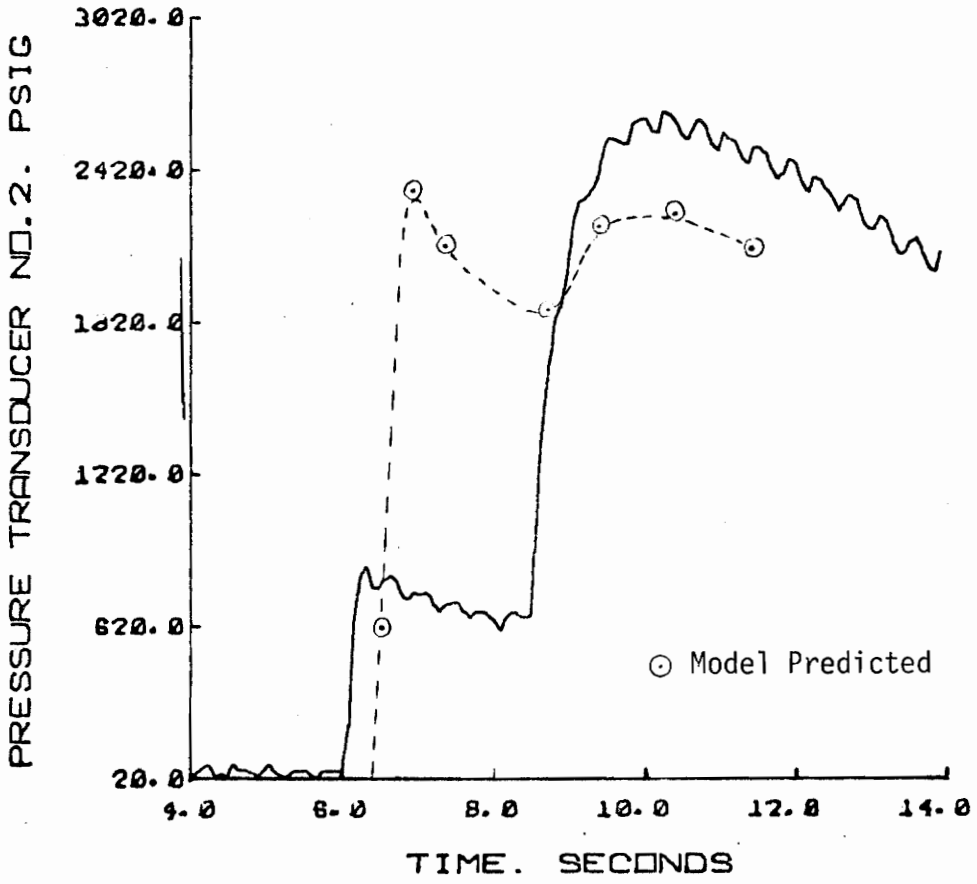

FIGURE 24. GATE EXIT PRESSURE FOR A CYCLE
RUN AT T'=400.0 P'=12000 Q_0'=1.83

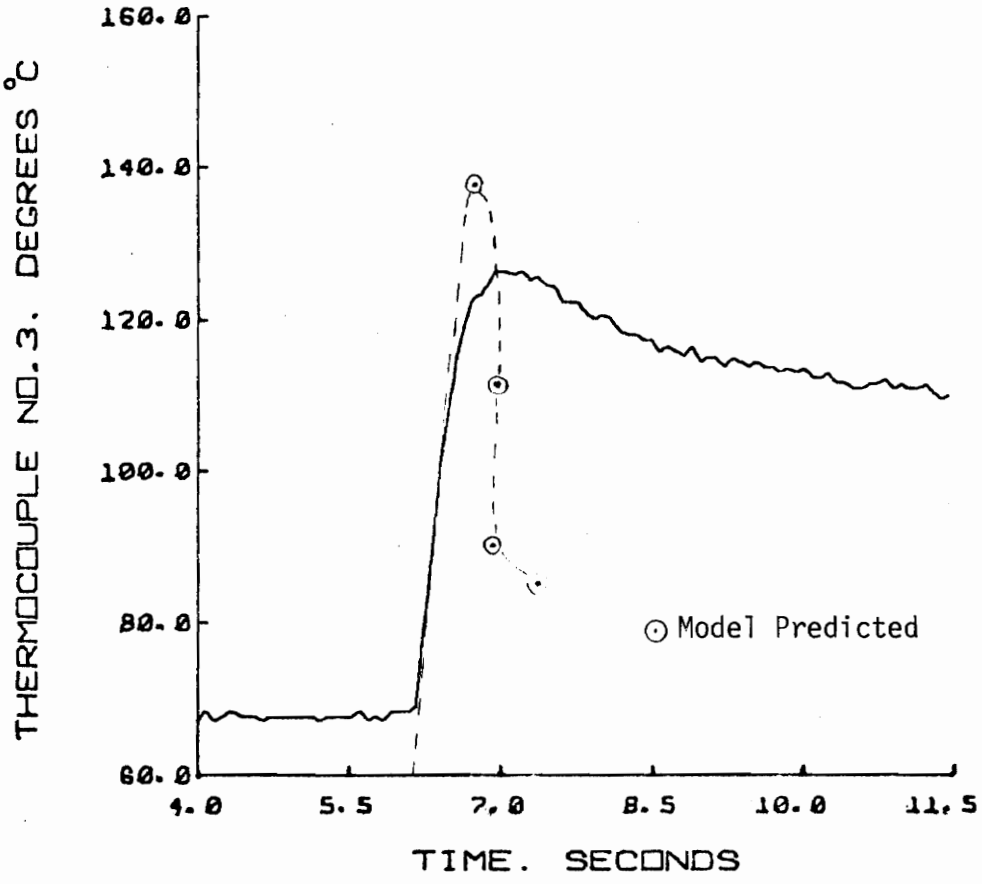

FIGURE 25. MIDDLE OF CAVITY TEMPERATURE FOR A CYCLE RUN AT T'=400.0 P'=12000 Q_0'=1.83

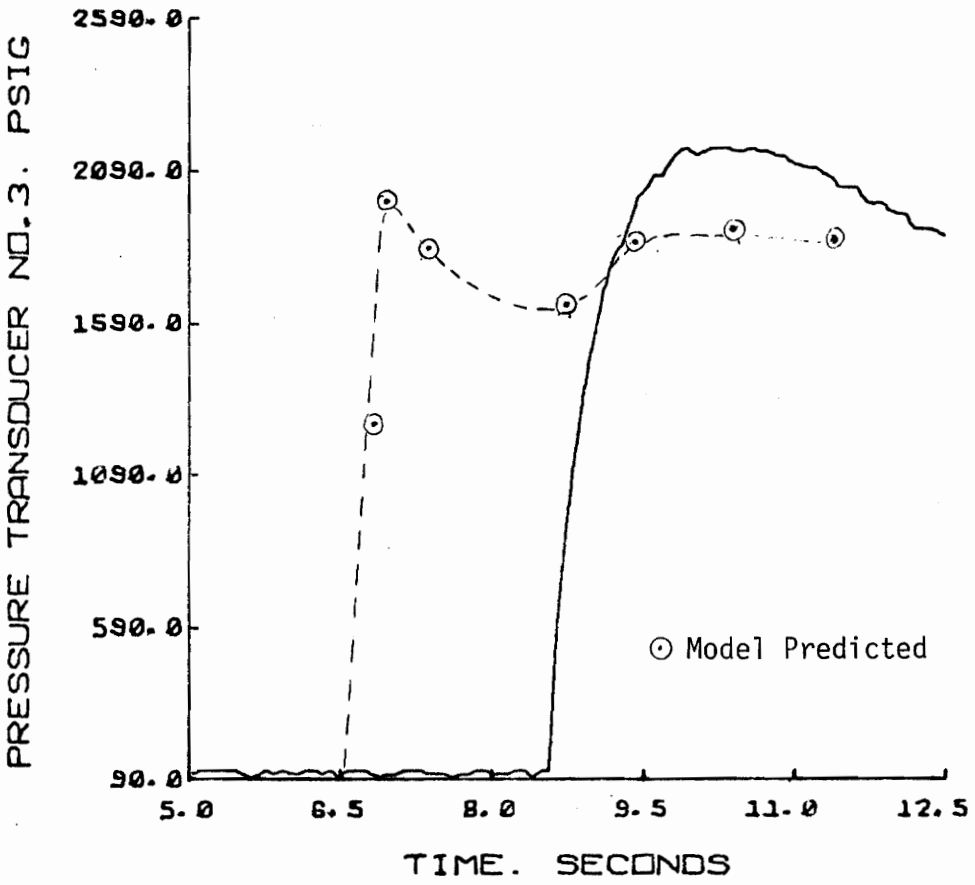

FIGURE 26. MIDDLE OF CAVITY PRESSURE FOR A CYCLE RUN AT T'=400.0 P'=12000 Q_0'=1.83

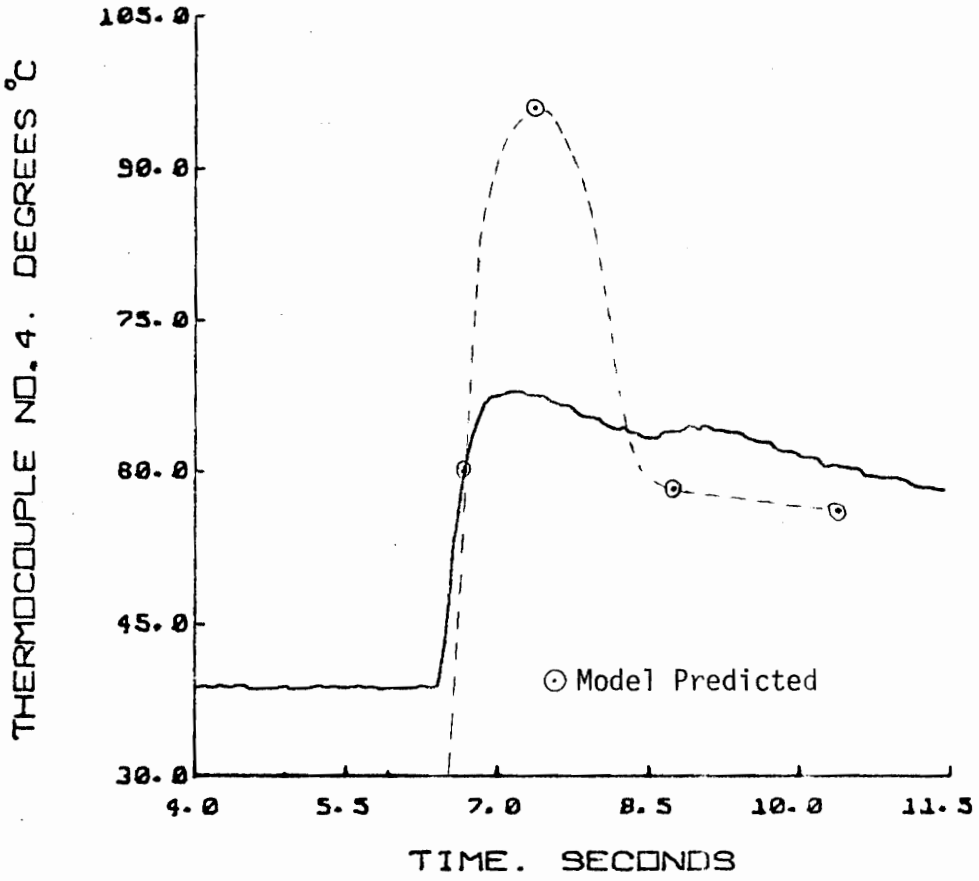

FIGURE 27. END OF CAVITY TEMPERATURE FOR A CYCLE RUN AT T'=400.0 P'=12000 Q_0'=1.83

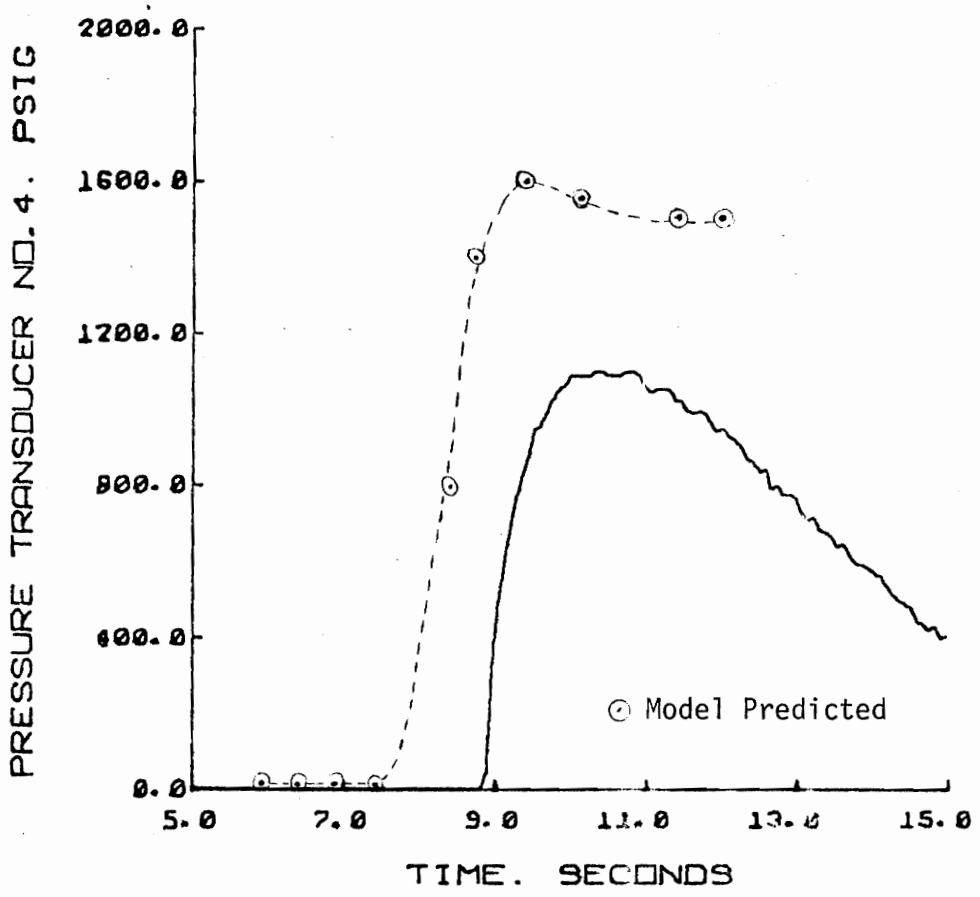

FIGURE 28. END OF CAVITY TEMPERATURE FOR A CYCLE RUN AT T'=400.0 P'=12000 Q_0'=1.83

TABLE VII. SIMULATION RESULTS FOR MOLDING CYCLE RUN AT T'=400.0 P'=12000 Q_0'=1.83

INITIAL TEMPERATURE= 400.00
PRESSURE SETTING= 12000.00
INITIAL FLOW RATE= 1.83
METAL TEMPERATURE= 86.00
TOTAL CAVITY LENGTH= 4.08

LENGTH ******	TIME ****	NODES *****	SOLIDIFICATION LOCATION IN GATE CHANNEL **********
0.207E 00	0.308E-02	2	0.00 0.00 0.00 0.00 0.00 0.00 0.003
0.414E 00	0.615E-02	3	0.00 0.00 0.00 0.00 0.00 0.00 0.006
0.622E 00	0.923E-02	4	0.00 0.00 0.00 0.00 0.00 0.00 0.009
0.829E 00	0.123E-01	5	0.00 0.00 0.00 0.00 0.00 0.00 0.012
0.104E 01	0.154E-01	6	0.00 0.00 0.00 0.00 0.00 0.00 0.015
CHANNEL TRANSITION: **********	NODE= 6 ****	ZONE= 2 ****	
0.114E 01	0.156E-01	7	0.00 0.00 0.00 0.00 0.00 0.00 0.016
0.124E 01	0.157E-01	8	0.00 0.00 0.00 0.00 0.00 0.00 0.016
0.134E 01	0.159E-01	9	0.00 0.00 0.00 0.00 0.00 0.00 0.016
0.144E 01	0.161E-01	10	0.00 0.00 0.00 0.00 0.00 0.00 0.016
0.154E 01	0.162E-01	11	0.00 0.00 0.00 0.00 0.00 0.00 0.016
CHANNEL TRANSITION: **********	NODE= 11 ****	ZONE= 3 ****	
0.205E 01	0.127E 00	12	0.00 0.00 0.00 0.00 0.00 0.00 0.127

FLOW RATE REDUCED TO= 0.713 DIMENSIONAL FLOW RATE= 1.304 TIME= 0.1270
PE(1)= 0.140E 05 VAVP= 3.26

FLOW RATE REDUCED TO= 0.526 DIMENSIONAL FLOW RATE= 0.963 TIME= 0.1270
PE(1)= 0.128E 05 VAVP= 2.41

0.256E 01	0.338E 00	13	0.00 0.00 0.00 0.00 0.00 0.00 0.338

TABLE VII. (continued)

0.306E 01	0.548E 00	14	0.00 0.00 0.00 0.00 0.00 0.00 0.548
			FLOW RATE REDUCED TO= 0.364 DIMENSIONAL FLOW RATE= 0.666 TIME= 0.5482 PE(1)= 0.143E 05 VAVP= 1.67
			FLOW RATE REDUCED TO= 0.266 DIMENSIONAL FLOW RATE= 0.487 TIME= 0.5482 PE(1)= 0.129E 05 VAVP= 1.22
0.357E 01	0.964E 00	15	0.00 0.00 0.00 0.00 0.00 0.00 0.964
			FLOW RATE REDUCED TO= 0.171 DIMENSIONAL FLOW RATE= 0.312 TIME= 0.9643 PE(1)= 0.150E 05 VAVP= 0.78
			FLOW RATE REDUCED TO= 0.116 DIMENSIONAL FLOW RATE= 0.213 TIME= 0.9643 PE(1)= 0.135E 05 VAVP= 0.53
			FLOW RATE REDUCED TO= 0.081 DIMENSIONAL FLOW RATE= 0.148 TIME= 0.9643 PE(1)= 0.125E 05 VAVP= 0.37
			0.10 0.10 0.10 0.10 0.10 0.10 2.331

TABLE VII. (continued)

PACKING STAGE

VOL.FLOW R	AV.TEMP.	AV.DENSITY	INIT.DENS	AV.PRESS. RUNNER	AV.PRESS. GATE	AV.PRESS. CAVITY	ENTRANCE PRESSURE
0.811E-01	0.284E 03	0.100E 01	0.494E 02	0.759E 04	0.238E 04	0.127E 04	0.118E 05
0.100E-01	0.284E 03	0.100E 01	0.494E 02	0.761E 04	0.239E 04	0.129E 04	0.119E 05
0.100E-01	0.284E 03	0.100E 01	0.494E 02	0.765E 04	0.244E 04	0.133E 04	0.119E 05
0.996E-02	0.284E 03	0.100E 01	0.494E 02	0.773E 04	0.252E 04	0.141E 04	0.119E 05
0.986E-02	0.284E 03	0.100E 01	0.494E 02	0.780E 04	0.259E 04	0.149E 04	0.120E 05

0.10	0.10	0.10	0.10	0.10	0.10	2.332
0.10	0.10	0.10	0.10	0.10	0.10	2.334
0.10	0.10	0.10	0.10	0.10	0.10	2.337
0.10	0.10	0.10	0.10	0.10	0.10	2.342

TABLE VII. (continued)

COOLING STAGE
****

0.10	0.10	0.10	0.10	0.10	0.10	2.346
0.10	0.10	0.10	0.10	0.10	0.10	2.497
0.10	0.10	0.10	0.10	0.10	0.10	2.495
0.10	0.10	0.10	0.10	0.10	0.10	2.539
0.10	0.10	0.10	0.10	0.10	0.10	2.529
0.10	0.10	0.10	0.10	0.10	0.10	3.065
0.10	0.10	0.10	0.10	0.10	0.10	3.446
0.10	0.10	0.10	0.10	0.10	0.10	3.677
0.10	0.10	0.10	0.10	0.10	0.10	4.053
0.10	0.10	0.10	0.10	0.10	0.10	4.475

CYCLE HAS BEEN COMPLETED
****

TABLE VII. (continued)

T1 ****	T2 ****	T3 ****	T4 ****	P1 ****	P2 ****	P3 ****	P4 ****	P5 ****	TIME ******	FLOW RATE *********
30.000	30.000	30.000	30.000	14.700	14.700	14.700	14.700	14.700	0.0000	1.8300
30.000	30.000	30.000	30.000	14.700	14.700	14.700	14.700	14.700	0.0031	1.8300
204.422	30.000	30.000	30.000	14.700	14.700	14.700	14.700	14.700	0.0062	1.8300
204.405	30.000	30.000	30.000	14.700	14.700	14.700	14.700	14.700	0.0092	1.8300
204.392	30.000	30.000	30.000	213.659	14.700	14.700	14.700	14.700	0.0123	1.8300
204.382	30.000	30.000	30.000	413.119	14.700	14.700	14.700	14.700	0.0154	1.8300
204.375	30.000	30.000	30.000	611.703	14.700	14.700	14.700	14.700	0.0156	1.8300
204.372	30.000	30.000	30.000	964.039	14.700	14.700	14.700	14.700	0.0157	1.8300
204.369	30.000	30.000	30.000	1413.791	14.700	14.700	14.700	14.700	0.0159	1.8300
204.367	30.000	30.000	30.000	1607.028	14.700	14.700	14.700	14.700	0.0161	1.8300
204.365	212.012	30.000	30.000	1951.892	14.700	14.700	14.700	611.957	0.0162	1.8300
204.364	215.618	30.000	30.000	2544.940	609.362	14.700	14.700	809.364	0.1270	1.8300
198.147	224.828	138.905	30.000	6820.219	4756.383	14.700	14.700	4923.535	0.3376	0.9628
201.353	208.928	111.241	30.000	4775.953	2343.997	1995.455	14.700	2510.545	0.5482	0.9629
190.143	172.422	84.841	96.913	4179.940	2109.097	1830.370	14.700	2253.143	0.9643	0.4874
166.797	74.946	56.905	57.992	7331.190	1860.819	1644.570	1399.552	1975.906	2.3312	0.1483
166.576	75.055	56.908	57.976	7348.137	1877.778	1661.528	1416.511	1992.865	2.3319	0.0100
165.916	75.378	56.911	57.927	7394.535	1924.179	1707.929	1462.912	2039.266	2.3339	0.0100
164.829	75.897	56.916	57.852	7471.727	2001.373	1785.124	1540.107	2116.460	2.3372	0.0100
163.331	76.582	56.928	57.759	7545.434	2075.080	1858.831	1613.814	2190.167	2.3418	0.0099
163.330	76.582	56.928	57.759	7545.355	2075.070	1858.779	1613.791	2190.075	2.3464	0.0000
163.321	76.587	56.923	57.758	7545.270	2075.040	1858.749	1613.806	2190.029	2.3974	0.0000
163.302	76.596	56.923	57.757	7545.098	2074.975	1858.699	1613.870	2189.916	2.4948	0.0000
163.274	76.610	56.929	57.755	7544.874	2074.881	1858.605	1613.949	2189.757	2.6385	0.0000
163.239	76.628	56.923	57.753	7544.473	2074.737	1858.491	1614.063	2189.549	2.8287	0.0000
163.193	76.650	56.929	57.749	7544.039	2074.578	1858.366	1614.188	2189.276	3.0651	0.0000
163.139	76.677	56.929	57.746	7543.531	2074.385	1858.188	1614.351	2188.958	3.3480	0.0000
163.076	76.708	56.930	57.742	7542.941	2074.162	1857.995	1614.525	2188.587	3.6772	0.0000
163.005	76.743	56.930	57.737	7542.250	2073.889	1857.791	1614.733	2188.156	4.0527	0.0000

Figures 29 to 32, pages 115 to 118, and Table VIII page 119, show the results for an injection cycle run at 290.0°F, 11,000 psig. and 0.63 in^3/sec. This particular run resulted in a short shot, i.e., the flow resistance due to solidification was so high that the cavity was not completely filled. The distance traveled by the front was measured experimentally to be 3.129 in. The value predicted by the model was 3.064 in. This gives a 2% deviation between the experimental and the model-predicted position value. This deviation can be explained in terms of the number of equally spaced nodes used (only five per channel). If more nodes are used, the deviation between experimental and model-predicted values should decrease.

Should we expect better than 2% — I think that good agreement is too good to be expected

Figure 33, page 123, shows the flow front displacement vs time during the filling stage. As shown, a short shot occurs at 3.064 in. from the runner entrance.

Figure 34, page 124, shows the graphical optimization plot discussed on page 79. The results shown in Figure 34 correspond to a cycle run at 400°F, 12,000psig, and 1.83 in^3/sec. For a gate L/D of 8.08. Under these conditions the temperature in the gate channel is always below the degradation temperature for polyethylene (600°F), but the shear rate far exceeded the critical shear rate for polyethylene (1500 sec^{-1}). This resulted in the presence of jetting which was experimentally observed during the experimental run.

Figure 35 page 125 shows a flow front displacement sequence obtained by slowly decreasing the pressure at a given temperature, and a jetting sequence obtained by increasing the ram speed at fixed injection conditions. Complete molded parts are also shown.

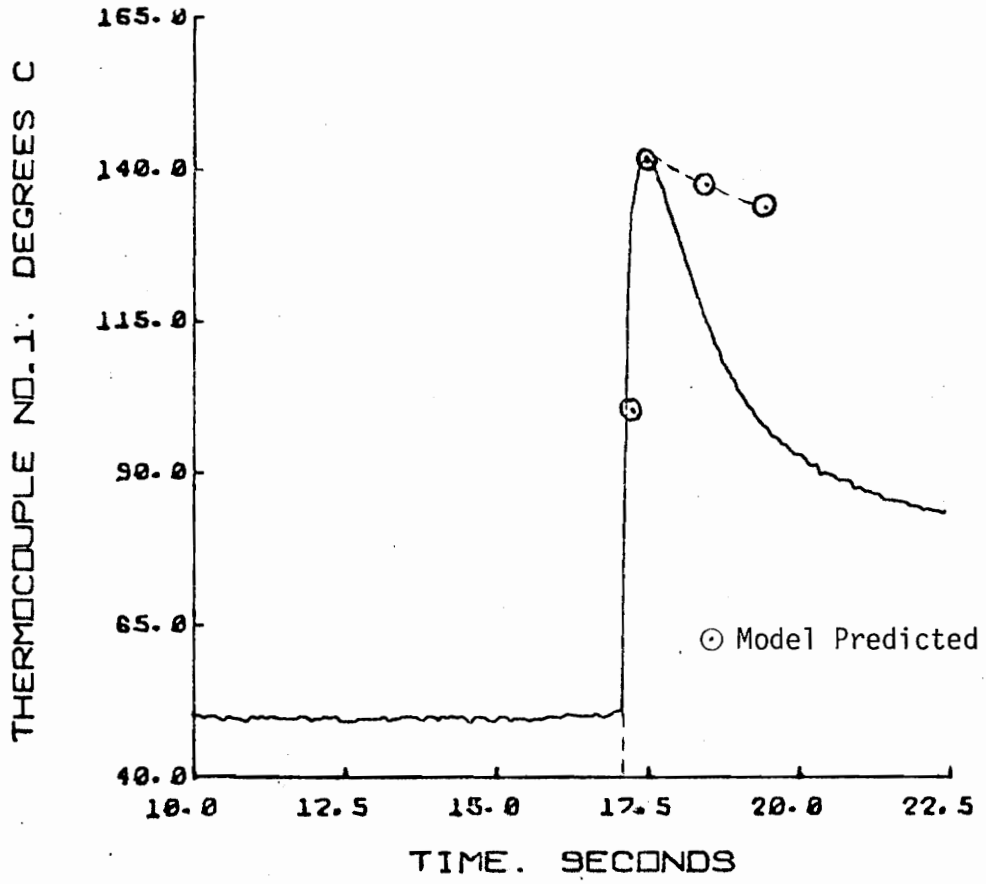

FIGURE 29. RUNNER ENTRANCE TEMPERATURE FOR A CYLCE RUN AT T'=290.0 P'=11000 Q_0'=0.63

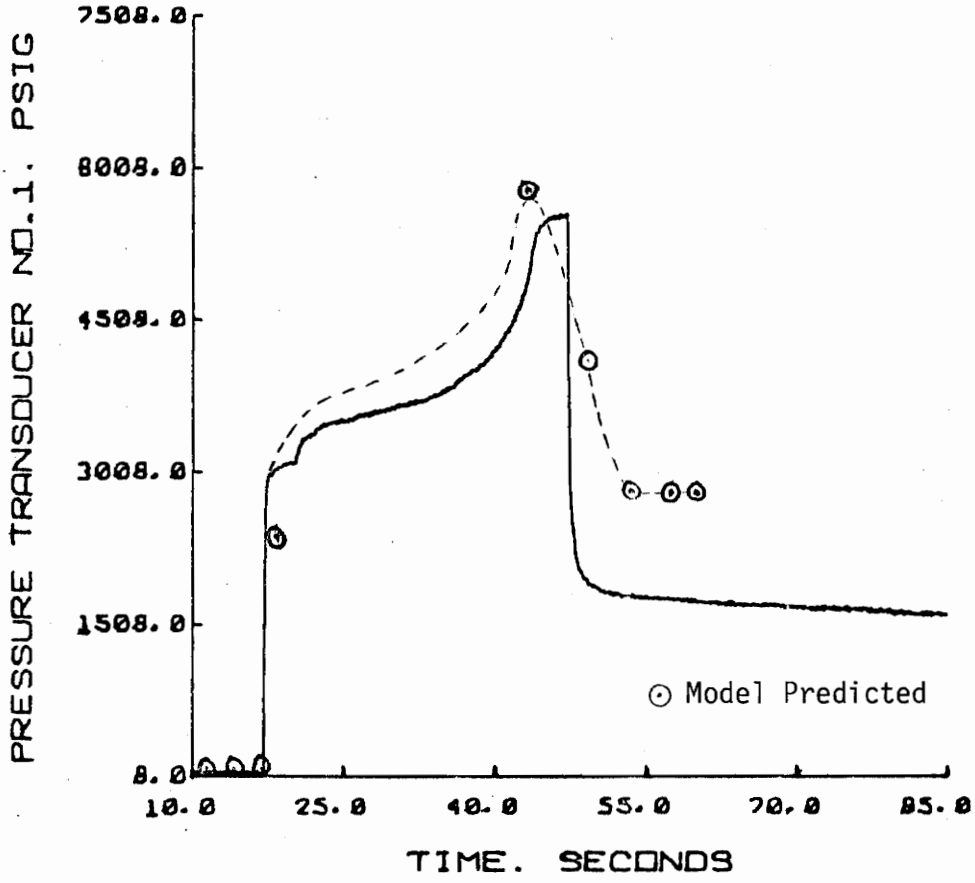

FIGURE 30. RUNNER ENTRANCE PRESSURE FOR A CYCLE RUN AT T'=290.0 P'=11000 Q_0'=0.63

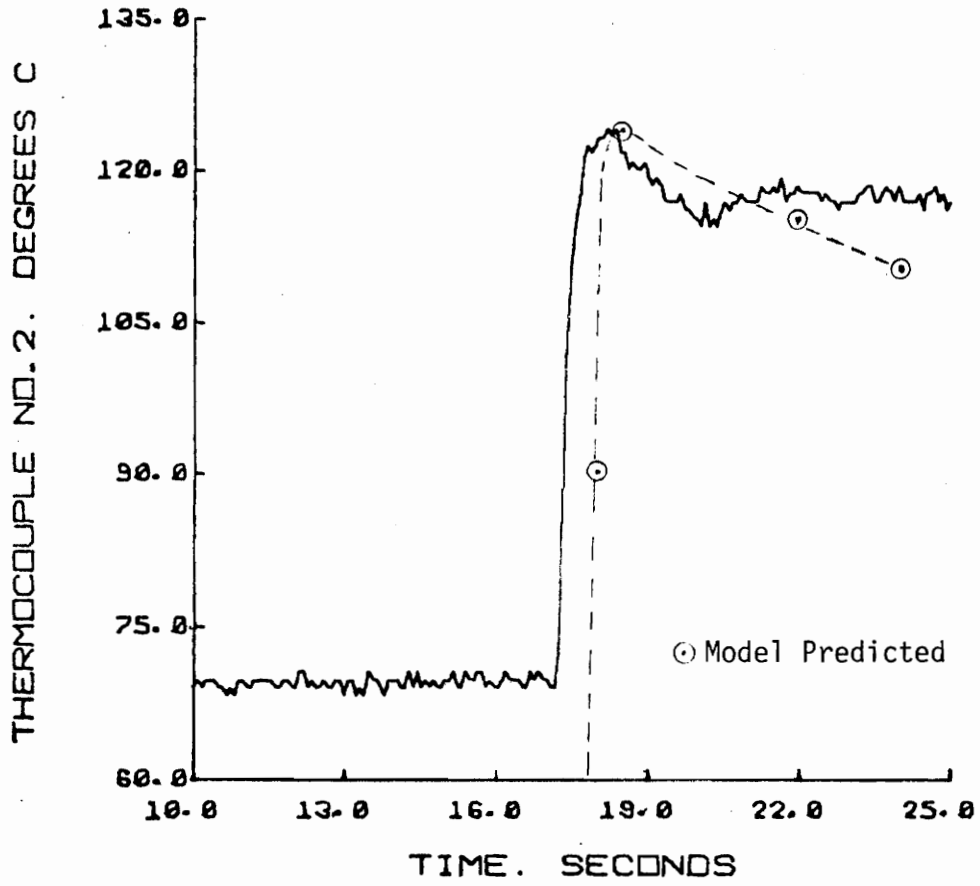

FIGURE 31. GATE EXIT TEMPERATURE FOR A CYCLE RUN AT T'=290.0 P'=11000 Q_0'=0.63

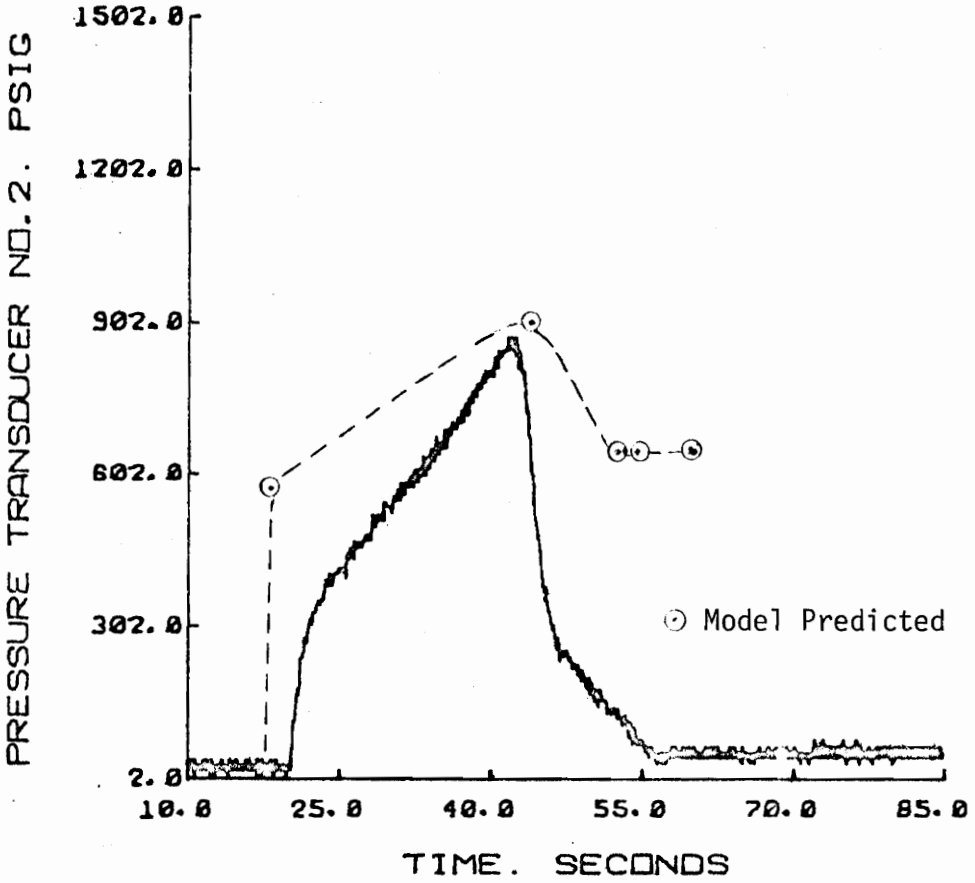

FIGURE 32. GATE EXIT PRESSURE FOR A CYCLE
RUN AT T'=290.0 P'=11000 Q_0'=0.63

TABLE VIII. SIMULATION RESULTS FOR MOLDING CYCLE RUN AT T'=290.0 P'=11000 Q_0'=0.63

INITIAL TEMPERATURE= 290.00
PRESSURE SETTING= 11000.00
INITIAL FLOW RATE= 0.63
METAL TEMPERATURE= 86.00
TOTAL CAVITY LENGTH= 4.08

LENGTH ******	TIME ****	NODES *****	SOLIDIFICATION LOCATION IN GATE CHANNEL **********						
0.207E 00	0.901E-02	2	0.00	0.00	0.00	0.00	0.00	0.00	0.009
0.414E 00	0.180E-01	3	0.00	0.00	0.00	0.00	0.00	0.00	0.018
0.622E 00	0.273E-01	4	0.00	0.00	0.00	0.00	0.00	0.00	0.027
0.829E 00	0.368E-01	5	0.00	0.00	0.00	0.00	0.00	0.00	0.037
0.104E 01	0.468E-01	6	0.00	0.00	0.00	0.00	0.00	0.00	0.047
CHANNEL TRANSITION: **********	NODE= 6 ****	ZONE= 2 ****							
0.114E 01	0.474E-01	7	0.00	0.00	0.00	0.00	0.00	0.00	0.047
0.124E 01	0.481E-01	8	0.00	0.00	0.00	0.00	0.00	0.00	0.048
0.134E 01	0.487E-01	9	0.00	0.00	0.00	0.00	0.00	0.00	0.049
0.144E 01	0.495E-01	10	0.00	0.00	0.00	0.00	0.00	0.00	0.050
0.154E 01	0.505E-01	11	0.00	0.00	0.00	0.00	0.00	0.00	0.050
CHANNEL TRANSITION: **********	NODE= 11 ****	ZONE= 3 ****							
0.205E 01	0.811E 00	12	0.00	0.00	0.00	0.00	0.00	0.00	0.811

FLOW RATE REDUCED TO= 0.215 DIMENSIONAL FLOW RATE= 0.134 TIME= 0.8111
PE(1)= 0.138E 05 VAVP= 0.34

FLOW RATE REDUCED TO= 0.137 DIMENSIONAL FLOW RATE= 0.085 TIME= 0.8111
PE(1)= 0.129E 05 VAVP= 0.21

FLOW RATE REDUCED TO= 0.086 DIMENSIONAL FLOW RATE= 0.054 TIME= 0.3111

TABLE VIII. (continued)

PE(1)= 0.122E 05 VAVP= 0.13

FLOW RATE REDUCED TO= 0.052 DIMENSIONAL FLOW RATE= 0.032 TIME= 0.8111
PE(1)= 0.117E 05 VAVP= 0.08

FLOW RATE REDUCED TO= 0.030 DIMENSIONAL FLOW RATE= 0.019 TIME= 0.8111
PE(1)= 0.114E 05 VAVP= 0.05

			0.20	0.20	0.20	0.20	0.20	0.20	26.678
0.256E 01	0.267E 02	13							
			0.30	0.30	0.30	0.30	0.30	0.30	35.806
0.306E 01	0.358E 02	14							

SHORT SHOT
****

LENGTH= 3.064
ENTRANCE PRESSURE= 9166.49
TIME= 35.8055

TABLE VIII. (continued)

COOLING STAGE **********							
	0.30	0.30	0.30	0.30	0.30	0.30	35.633
	0.30	0.30	0.30	0.30	0.30	0.30	35.985
	0.30	0.30	0.30	0.30	0.30	0.30	36.274
	0.30	0.30	0.30	0.30	0.30	0.30	36.701
	0.30	0.30	0.30	0.30	0.30	0.30	37.257
	0.30	0.30	0.30	0.30	0.30	0.30	37.970
	0.30	0.30	0.30	0.30	0.30	0.30	38.810
	0.30	0.30	0.30	0.30	0.30	0.30	39.789
	0.30	0.30	0.30	0.30	0.30	0.30	40.906
	0.30	0.30	0.30	0.30	0.30	0.30	42.160
CYCLE HAS BEEN COMPLETED **********							

TABLE VIII. (continued)

T1 ****	T2 ****	T3 ****	T4 ****	P1 ****	P2 ****	P3 ****	P4 ****	P5 ****	TIME ******	FLOW RATE **********
30.000	30.000	30.000	30.000	14.700	14.700	14.700	14.700	14.700	0.0000	0.6250
30.000	30.000	30.000	30.000	14.700	14.700	14.700	14.700	14.700	0.0090	0.6250
142.533	30.000	30.000	30.000	14.700	14.700	14.700	14.700	14.700	0.0180	0.6245
141.972	30.000	30.000	30.000	14.700	14.700	14.700	14.700	14.700	0.0273	0.6098
141.439	30.000	30.000	30.000	238.381	14.700	14.700	14.700	14.700	0.0368	0.5886
140.935	30.000	30.000	30.000	460.284	14.700	14.700	14.700	14.700	0.0468	0.5617
140.418	30.000	30.000	30.000	672.647	14.700	14.700	14.700	14.700	0.0474	0.5302
140.129	30.000	30.000	30.000	1040.203	14.700	14.700	14.700	14.700	0.0481	0.4951
139.746	30.000	30.000	30.000	1489.214	14.700	14.700	14.700	14.700	0.0487	0.4496
139.194	30.000	30.000	30.000	1634.052	14.700	14.700	14.700	14.700	0.0495	0.3890
138.414	123.779	30.000	30.000	1909.058	14.700	14.700	14.700	601.077	0.0505	0.3265
137.331	124.741	30.000	30.000	2389.203	575.524	14.700	14.700	779.488	0.8111	0.2666
103.777	30.000	30.000	30.000	5800.000	902.630	14.700	14.700	4598.434	26.6775	0.0187
76.521	44.429	40.746	30.000	3829.722	842.654	14.700	14.700	1924.186	35.8033	0.0034
75.732	42.980	40.495	30.000	3829.722	642.654	14.700	14.700	1924.186	35.8193	0.0001
75.732	42.979	40.495	30.000	2829.686	642.582	14.700	14.700	1924.125	35.8331	0.0000
75.727	42.970	40.493	30.000	2829.671	642.570	14.700	14.700	1924.079	35.9847	0.0000
75.717	42.953	40.489	30.000	2829.645	642.544	14.700	14.700	1924.003	36.2742	0.0000
75.703	42.928	40.484	30.000	2829.603	642.506	14.700	14.700	1923.886	36.7015	0.0000
75.684	42.895	40.478	30.000	2829.550	642.457	14.700	14.700	1923.739	37.2666	0.0000
75.660	42.854	40.470	30.000	2829.486	642.396	14.700	14.700	1923.549	37.9696	0.0000
75.632	42.805	40.460	30.000	2829.403	642.324	14.700	14.700	1923.326	38.8104	0.0000
75.600	42.750	40.449	30.000	2829.304	642.241	14.700	14.700	1923.065	39.7891	0.0000
75.562	42.687	40.436	30.000	2829.187	642.146	14.700	14.700	1922.766	40.9056	0.0000
75.521	42.617	40.421	30.000	2829.047	642.037	14.700	14.700	1922.429	42.1599	0.0000

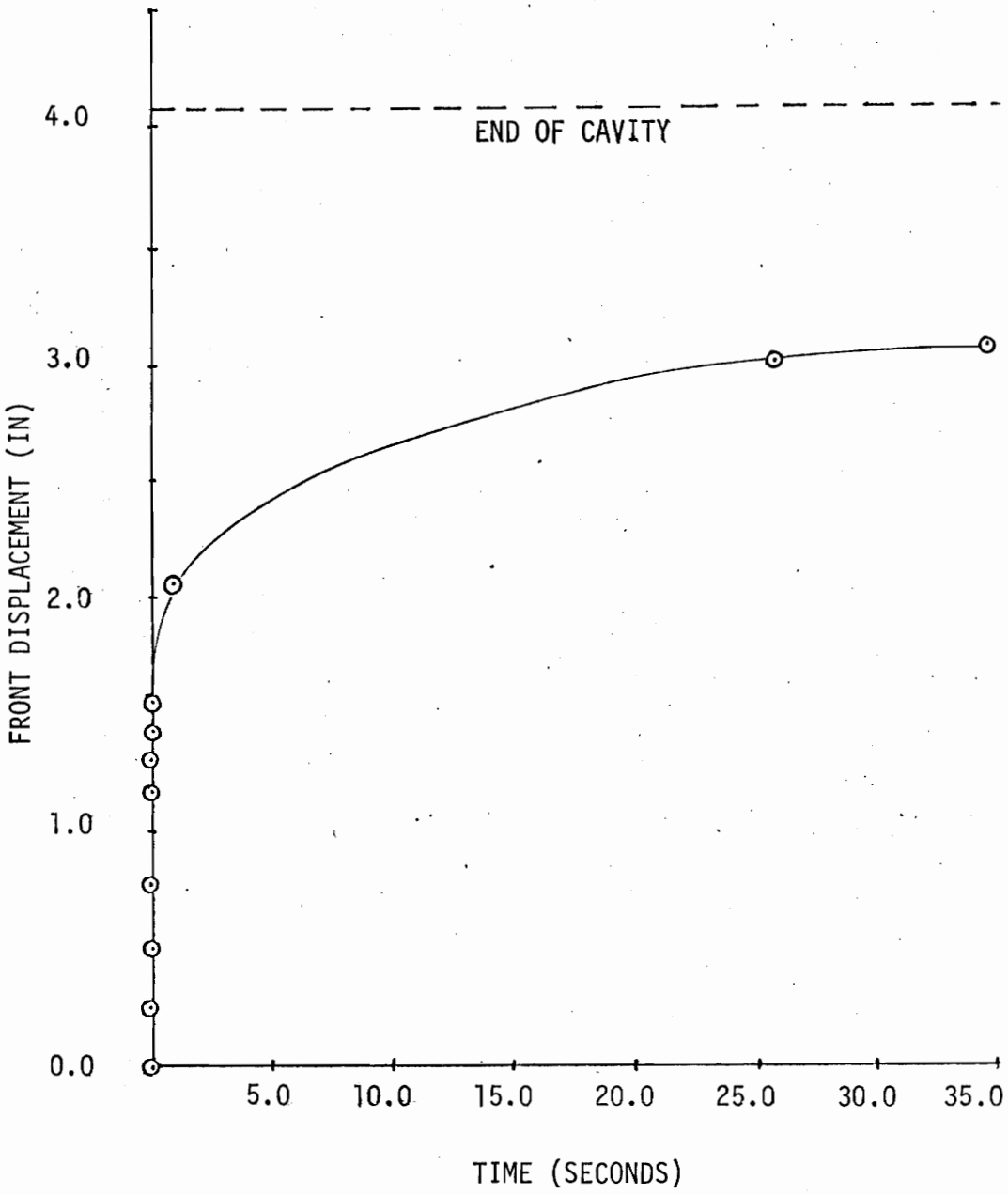

FIGURE 33. FLOW FRONT DISPLACEMENT IN MOLD CHANNELS VS TIME

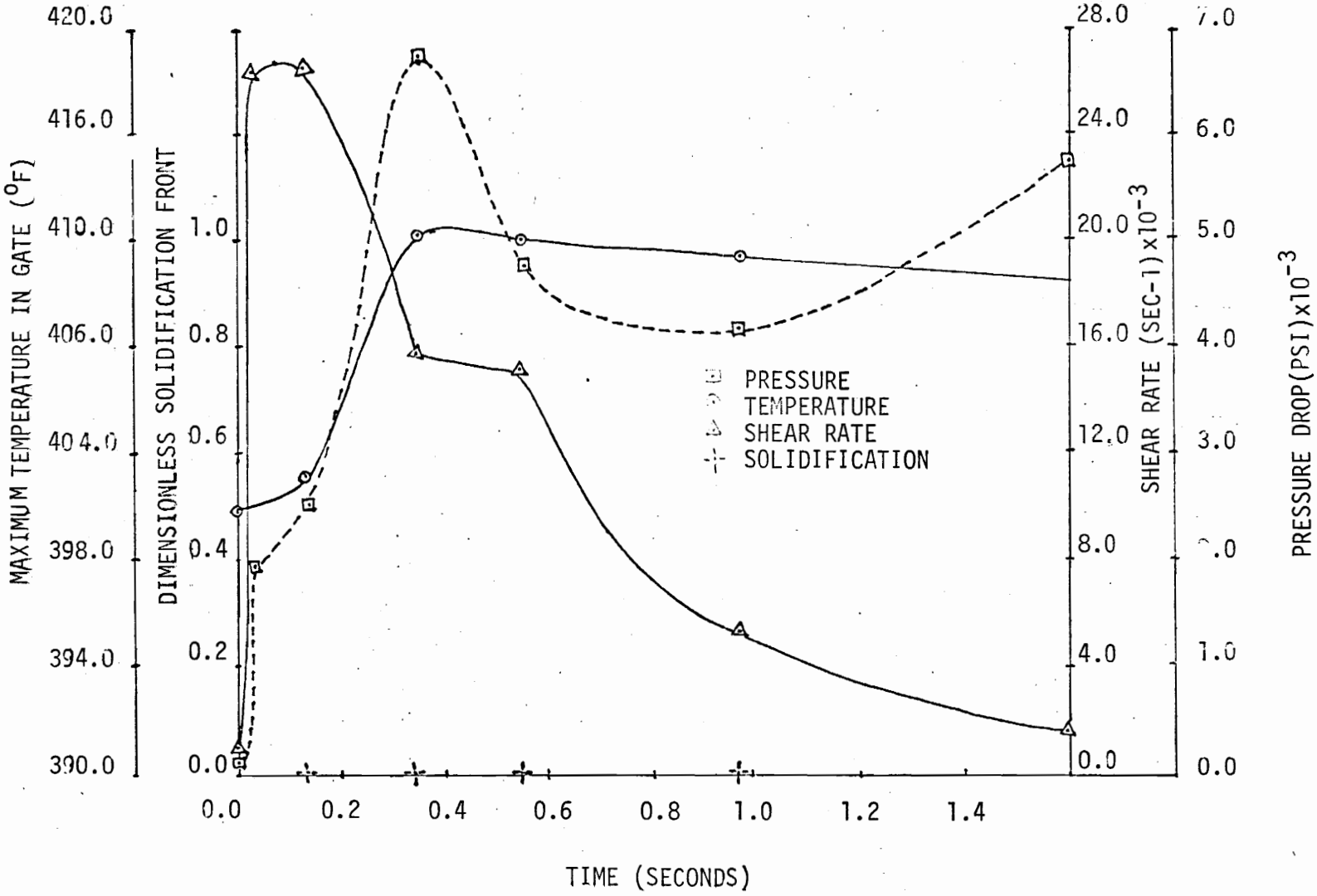

FIGURE 34. GRAPHICAL OPTIMIZATION OF GATE DIMENSIONS

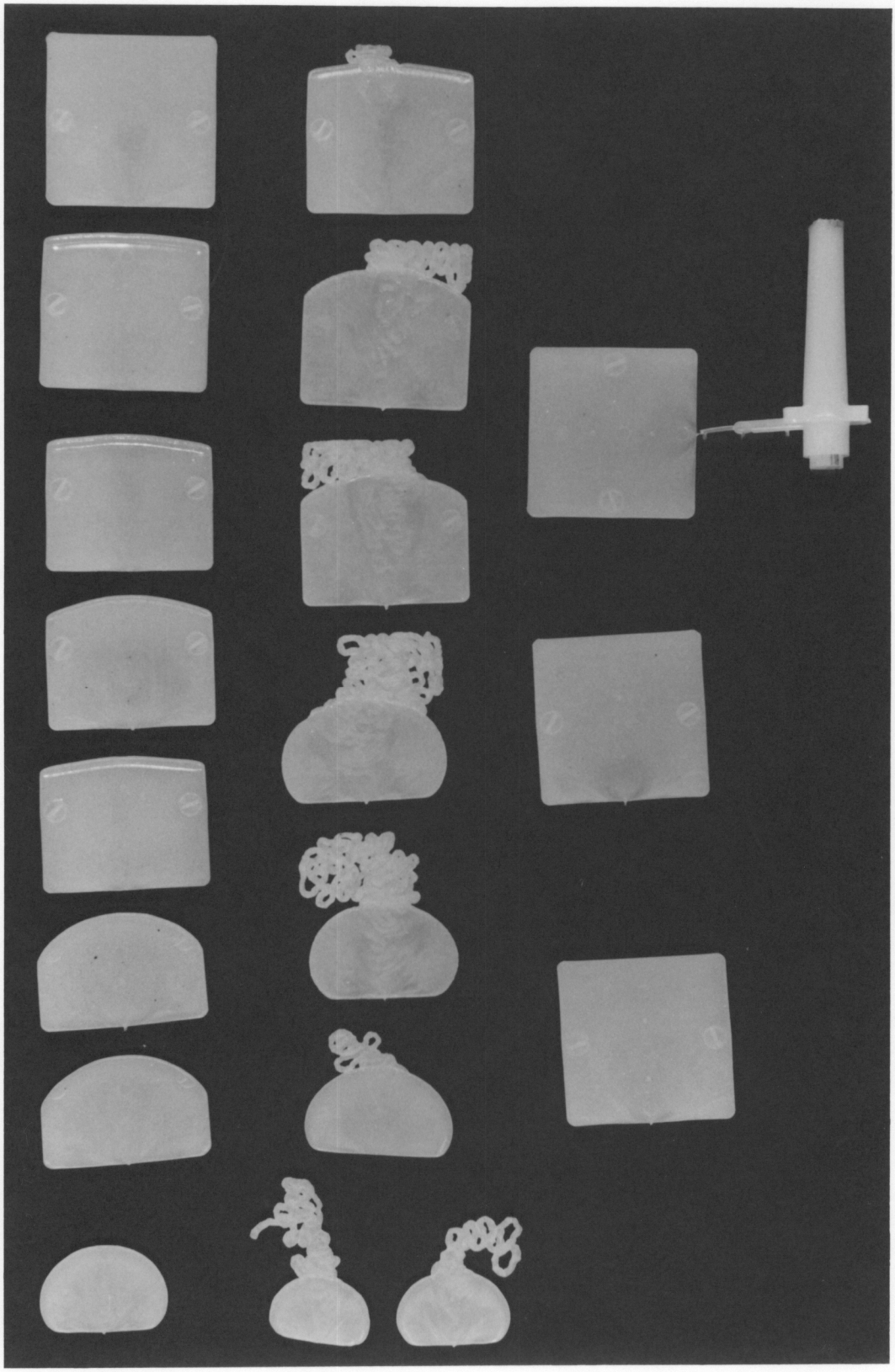

FIGURE 35. JETTING AND FLOW FRONT AXIAL DISPLACEMENT SEQUENCES.

VI. CONCLUSIONS AND RECOMMENDATIONS

Generally, the model developed in this investigation predicted quite well the values of the parameters measured experimentally. In certain cases, deviations were observed, but these were due to known factors which have been described in the previous section.

This model represents the first link in a chain that is just beginning. The end use of the program will be in DDC feed-forward control applications for injection molding cycles.

Several improvements can be made on this model. First, a more detailed analysis should yield a better relationship between the volumetric flow rate and the pressure at a given point. This is necessary because the volumetric flow rate should be smoothly decreased in order to keep the runner entrance pressure at the constant preset injection pressure. In this investigation, a power law relationship was used. This exponential relationship proved to decrease the volumetric flow rate faster than it should have. This caused some oscillations in the predicted temperature and pressure values. It was observed from the experimental data that a linear relationship could do the job, and that the volumetric flow rate should be decreased at each time interval as the pressure increased, instead of waiting until the preset injection pressure was reached as it was done in this investigation. Second, a non-linear regression fit should be performed on the experimental data available for heat capacity and thermal conductivity. The regression equations could be used in the model. This will reduce the consistently high temperatures predicted by the model.

Third, the model should be extended to take into account the heat transferred to the wall of the channels. In this investigation a constant wall temperature was assumed in order to simplify the initial development of the model. At this point the finite difference grid used in the model could be extended to include the metal containing the cooling channels where the temperature is known. The inclusion of this feature could be accomplished with a small programming effort.

Finally better packing and cooling models could be developed. The cooling model proved to be the poorest of the proposed models. An extra effort to develop a better cooling model was not considered to be necessary, because this investigation was more concerned with the filling and packing stages, which are the critical stages for gate design purposes.

VII. BIBLIOGRAPHY

1. Arden Bruce W., An Introduction to Digital Computing, Massachusetts: Addison-Wesley Publishing Co., Inc., 1963.

2. Arpaci Vedat S., Conduction Heat Transfer, Massachusetts: Addison-Wesley Publishing Co., Inc., 1966.

3. Bagley E., B., "End Corrections in the Capilary Flow of Polyethylene." J. Appl. Phys., (May, 1957) p. 624.

4. Bainbridge Robert W., "Design Hints on Vents, Runners and Gates". Advanced Methods in Tooling or Molding, SPE Regional Tech. Conf., February 1972, p. 69.

5. Bayley J., F., Owen J., M., and Tuner A., R., Heat Transfer, New York: Barnes and Noble Publishers, 1972.

6. Berger J., L., and Gogos C., G., "Simulation of the Mold Filling Process". SPE Tech. Conf., (May, 1971), p. 8.

7. Bernhart Ernest C., Processing of Thermoplastic Materials, New York: Robert E. Krieger Publishing Co., Inc., 1959.

8. Bird R., B., Steward W., E., and Lightfoot E., N., Transport Phenomena, New York: John Wiley & Sons, Inc., 1960.

9. Bostwick R., and Joslin C., A., "Restricted Gating". Plastic Engineering, (October, 1953), p. 125.

10. Briers D., G., "Feeding Techniques for Injection Molds". International Plastics Engineering, (May, 1961), p. 102.

11. Briers D., G., "Feeding Techniques for Injection Molds Part II". International Plastics Engineering, (May 1961), p. 166.

12. Broyer E., Gutfinger C., and Tadmor Z., "A Theoretical Model for the Cavity Filling Process in Injection Molding". Trans. Soc. Rheol., 19:3 (1975), p. 423.

13. Brydson A., J., Flow Properties of Polymer Melts, London: Iliffe Books, 1970.

14. Bueche F., "Derivation of the NFL Equation for the Mobility of Molecules in Molten Glasses." J. Che. Phys., 24, (February, 1956) p. 418.

15. Bueche F., and Harding S., W., "A New Molecular Weight Method for Linear Polymers". J. Polym. Sci. 32, (October, 1958) p. 177.

16. Carnahan Brice, Luther H., A., and Wilkes James O., Applied Numerical Methods, New York: John Wiley and Sons, Inc., 1969.

17. Carslaw H., S., and Jaeger J., C., Conduction of Heat in Solids, London: Oxford University Press, 1948.

18. Chapman Alan J., Heat Transfer, New York: The MacMillan Company, 1967.

19. Cress Paul, Dirksen Paul, and Graham J., Wesley, Fortran IV with Watfor and Watfiv, New Jersey: Prentice-Hall, Inc., 1970.

20. Donovan R., C., "A Theoretical Melting Model for a Reciprocating-Screw Injection Molding Machine". Polymer Eng. Sci., 11,5 (Sept. 1971), p. 361.

21. Donovan R., C., "The Plasticating Process in Injection Molding". Polymer Eng. Sci., 14,2 (Feb. 1974) p. 101.

22. Dubois J., H., and Prible W., I., Plastic Mold Engineering, New York: Van Nostrand Reinhold Company, 1965.

23. Dusinberre G., M., Numerical Analysis of Heat Flow, New York: McGraw-Hill Book Co., Inc., 1949.

24. Dusinberre G., M., Heat Transfer Calculations by Finite Differences, Scranton, Pa: International Text Book Co., 1961.

25. Duvdebani LLan J., and Klein Imrich, "Analysis of Polymer Melt Flow in Capilaries Including Pressure Effects". SPE Journal (Dec. 1967) p. 41.

26. Echenagucia Jorge E., "Injection Molding of Shot-Gun Shells". Master's Thesis, Virginia Polytechnic Institute and State University, (January 1975).

27. Eckert E., R., G., and Drake Robert M., Heat and Mass Transfer, New York: McGraw-Hill Book Co., Inc., 1959.

28. Engman James C., "Gates for Injection Molding". Plastic Technology, (Oct. 1962) p. 209.

29. Gutfinger V., Broyer E., and Tadmor Z., "Melt Solidification in Polymer Processing". Polymer Eng. Sci., 15, 7 (July 1975) p. 515.

30. Harry David H., and Parrott Richard G. Numerical Simulation of Injection Mold Filling". Polymer Eng. Sci., 10, 4 (July 1970) P. 23.

31. "Injection Moulding with Film Gating". International Plastics Engineering, (Nov. 1974) p. 347.

32. Kamal M., R., and Keing S., "Cooling Molded Parts--A Rigorous Analysis". SPE-Journal, 26, (July 1970) p. 50.

33. Kamal M., R., and Keing S., "Heat Transfer in the Cooling of Thermoplastic Melts under Pressure". The Canadian Journal of Chemical Engineering, 49, (April 1971) p. 210.

34. Kamal M., R., and Keing S., "The Injection Molding of Thermoplastics Parts I and II". Polymer Eng. Sci., 12,4 (July 1972) p. 294.

35. Kamal M., R., and Kuo Y., "The Injection Behavior of Thermoplastics in Thin Rectangular Cavities". Polymer Eng. Sci., 15,12 (Dec. 1975) p. 863.

36. Kays W., M., Convective Heat and Mass Transfer. New York: McGraw-Hill Book Co., Inc., 1966.

37. Kennedy Michael and Solomon Martin B., Ten Statement Fortran Plus Fortran IV, New Jersey: Prentice-Hall, Inc., 1975.

38. Klein Imrich and Marshall Donald, Computer Programs for Plastic Engineers, New York: Reinhold Book Co., 1968.

39. Kuo Y., and Kamal M., R., "The Fluid Mechanics and Heat Transfer of the Injection Mold Filling of Thermoplastic Materials". AICHE Journal, 22,4 (July 1976) p. 661.

40. Lord, H. A., and Williams G., "Mold Filling Studies for the Injection Molding of Thermoplastic Materials Parts I and II". Polymer Eng. Sci., 15, 8 (Aug. 1976) pp. 553-569.

41. Lloyd Scott R., "Monitoring and Control of Systems for Cavity Fill". Injection Molding 1974, SPE Regional Conf., (March 1974) p. 1.

42. McKelvey James M., Polymer Processing. New York: John Wiley & Sons, Inc., 1962.

43. Robinson J., D., "Gating and Cooling Techniques for Polypropylene". Plastics. (Aug. 1965) p. 47.

44. Rubin Irvin I., Injection Molding Theory and Practice. New York: John Wiley & Sons, Inc., 1973.

45. Spencer R., S., and Gilmore G., D., "Equation of State for High Polymers". J. Appl. Phys., 21, (June 1950) p. 523.

46. Spencer R., S., and Gilmore G., D., "Role of Pressure, Temperature and Time in Injection Molding Process". Modern Plastics, 27 (April 1950) p. 143.

47. Spencer R., S., and Gilmore G., D., "Some Flow Phenomena in the Injection Molding of Polystyrene". J. Coll. Sci., 6, (1951) p. 118.

48. Tadmor Z., Broyer E., and Gutfinger C., "Flow Analysis Network (FAN) a Method of Solving Flow Problems in Polymer Processing". Polymer Eng. Sci., 14,9 (Sept. 1974) p. 660.

49. White James L., "Fluid Mechanical Analysis of Injection Mold Filling". Polymer Eng. Sci., 15,1 (Jan. 1975) p. 44.

50. Williams C., M., "Stresses in Concentrated Polymer Solutions: Part 1". AICHE Journal, 12 (Nov. 1966) p. 1064.

51. Williams L., M., Landel F., R., Ferry D., J., "The Temperature Dependence of Relaxation Mechanisms in Amorphous Polymers and Other Glass-Forming Liquids". J. Am. Chem. Soc., 77 (July 1975) p. 3701.

52. Williams L., M., "The Temperature Dependence of Mechanical and Electrical Relaxations in Polymers". J. Phys. Chem., 59 (Jan. 1955) p. 95.

53. Wu P., C., Huang C., F., and Gogos C., G., "Simulation of the Mold Filling Process". Polymer Eng. Sci., 14, 3 (March 1974) p. 223.

APPENDIX

As mentioned on page 23, the experimental data, stored on the computer disc, could be plotted through the line printer or through the digital plotter. The plots presented in the Results and Discussion section were obtained through the digital plotter. The computer generated plots obtained through the line printer are included in this Appendix. In these figures the dimensional variables (dimensions are in accordance with table V) are plotted against time in seconds. Ram position (in) vs time and ram velocity (in/sec) vs time are also included.

In order to provide a starting point for further research on the computer simulation developed in this investigation, the computer generated Fortran code is included in this appendix.

```
//QUICKE SMART,WATFIV
      //WATFIV       JORGE
C
C
C     SIMULATION OF INJECTION MOLDING PROCESS
C     ***************************************
C
C     BY JORGE ECHENAGUCIA
C     ********************
C
      REAL TIM(50),P1(50),P2(50),P3(50),P4(50),P5(50),DIS(30)
      REAL T1(50),T2(50),T3(50),T4(50),QC(50),PR(10),PRT(20)
      REAL TAU(40),D1(40),TP(40,12),TAV(40),RLEND(4),RG(4)
      REAL SOLIN(40),Q1(20),Q2(20),Q3(20),DPA1(40),TAUP(30)
      REAL PAV1(20),PAV2(20),PAV3(20),RA1(20),RA2(20),RA3(20)
      COMMON /AREA1/ CPR
      COMMON /AREA2/ ROR,FLG,RA31,ROA3
      COMMON /AREA3/ TCONR
      COMMON QA,R1(40),U(40,12),GAMA(40,12),T(40,12),TR,FL,EPS,R(12)
      COMMON B1(40),NP1,VSCR,N,UC(40,12),Q,DP(40),NP2,UP(40),IW(4),W
      COMMON X(40),DT,TP1(40,12),TSTAR(40,12),VISCR,GAMAR,PE(40)
      COMMON TM
      READ, N,PID,TID,TR,QO,EPS,TMD,RLEND(1),RLEND(2),RLEND(3),NS,IZ
      READ, GAMAR,ROR,CPR,TCONR,RG(1),RG(2),RG(3),PATD,TSOLID,W,IX
      FLG=0.
      TOTLN=RLEND(1)+RLEND(2)+RLEND(3)
      WRITE(6,7) TID,PID,QO,TMD,TOTLN
    7 FORMAT('1',/,10X,'INITIAL TEMPERATURE= ',F9.2,/,
     1 10X,'PRESSURE SETTING= ',F9.2,/,
     2 10X,'INITIAL FLOW RATE= ',F9.2,/,
     3 10X,'METAL TEMPERATURE= ',F9.2,/,
     4 10X,'TOTAL CAVITY LENGTH= ',F9.2,/)
      PIS=20000
      TIM(1)=0.0
      IW(2)=0
      IW(3)=1000
      IW(4)=0
      L1=1
      TI=(TID-TR)/TR
      TM=(TMD-TR)/TR
      TSOL=(TSOLID-TR)/TR
      CUP=QO/(3.1416*RG(1)**2.)
      UP(1)=CUP
      VISCR=VISC(TR,GAMAR)
      PAT=(TCONR*(PATO-14.7))/(2.0*ROR*CUP**2.*CPR*VISCR)
      PA=(TCONR*(PID-PATD))/(2.0*ROR*CUP**2.*CPR*VISCR)
      NK=NS*IZ+1
      DO 59 K1=1,NK
      PE(K1)=PATD
      SOLIN(K1)=0.0
      DO 52 J=1,N
   52 T(K1,J)=TM
   59 CONTINUE
      TMU=(TMD-32.)/1.8
      P1(1)=PATD
      P2(1)=PATD
      P3(1)=PATD
      P4(1)=PATD
      P5(1)=PATD
      T1(1)=TMU
      T2(1)=TMU
      T3(1)=TMU
      T4(1)=TMU
      NP1=N+1
```

```
      FL1=0.
      DPA1(1)=0.
      D1(1)=0.0
      R(NP1+1)=1.+1./N
      R(1)=0.0
      TAU(1)=0.0
      X(1)=0.0
      RLEN=0.0
      R1(1)=RG(1)
      I=1
      DTP=RLEND(L1)/(NS*UP(1))
      DO 1 J=1,N
      T(I,J)=TI
    1 R(J+1)=R(J)+1./N
      Q=1.0
      QA=Q*QO
      QC(1)=QA
      T(1,NP1)=TM
      WRITE(6,204)
  204 FORMAT(12X,'LENGTH',15X,'TIME',18X,'NODES',10X,
     1 'SOLIDIFICATION LOCATION IN GATE CHANNEL',/,12X,6('*'),15X,
     2 4('*'),18X,5('*'),10X,39('*'),//)
      CALL POWLAW(I)
      KP=0
   55 CALL TMOM(I)
      IF(FL .NE. 1) GO TO 58
      KP=KP+1
      IF(KP .LT. 10) GO TO 55
      WRITE(6,100) I
  100 FORMAT(//,10X,'NO CONVERSION IN 100 ITERATIONS',
     1' AT BEGINNING',I2)
      GO TO 500
   58 DT=(TCONR*DTP)/(RG(L1)**2.*ROR*CPR)
      IF(I .EQ. IW(2))DTG=DT
      VAVP=Q*CUP
      DELXP=VAVP*DTP
      DELX=(TCONR*DELXP)/(ROR*CPR*CUP*RG(L1)**2)
      RLEN=RLEN+NS*DELX
   50 D1(I+1)=D1(I)+DELX
      TAU(I+1)=TAU(I)+DT
      UP(I+1)=CUP
      IF(D1(I+1) .GT. RLEN) GO TO 200
      I=I+1
      B1(I)=(UP(I)**2.*VISCR*1.070E-4)/(TR*TCONR)
      R1(I)=RG(L1)
      X(I)=D1(I)
      NP2=I-1
      T(I,NP1)=TM
      TSTAR(I,NP1)=TM
      TIM(I)=TAU(I)*R1(I)**2.*ROR*CPR/TCONR
      P1(I)=PE(4)
      P2(I)=PE(11)
      P3(I)=PE(13)
      P4(I)=PE(15)
      P5(I)=PE(10)
      T1(I)=((T(2,10)*TR+TR)-32.)/1.8
      T2(I)=((T(10,10)*TR+TR)-32.)/1.8
      T3(I)=((T(12,10)*TR+TR)-32.)/1.8
      T4(I)=((T(14,10)*TR+TR)-32.)/1.8
      QC(I)=QA
      DIS(I)=D1(I)*ROR*CPR*CUP*RG(L1)**2/TCONR
      WRITE(6,205)(SOLIN(I3),I3=6,11),TIM(I)
  205 FORMAT(59X,6(5X,F4.2),5X,F6.3)
```

```
111           IF(I .GE. NK) GO TO 200
112           KU=1
113           PR(1)=1.E6
114           WRITE(6,202) DIS(I),TIM(I),I
115       202 FORMAT(10X,E10.3,10X,E10.3,15X,I3,/)
116           DO 78 K5=1,NP2
117           V6=0.0
118           IF(I .GE. IW(3)) GO TO 77
119           DO 73 J=1,N
120           V9=(UC(K5,J)*T(K5,J)*R(J)+UC(K5,J+1)*T(K5,J+1)*R(J+1))
             1*(R(J+1)-R(J))
121        73 V6=V6+V9
122           GO TO 78
123        77 DO 79 J=1,N
124           V9=(UC(K5,J)*T(K5,J)+UC(K5,J+1)*T(K5,J+1))*(R(J+1)-R(J))
125        79 V6=V6+V9
126        78 TAV(K5)=V6
127           TAV(I)=TAV(NP2)
128           DO 74 J=1,N
129           TSTAR(I,J)=TAV(NP2)
130        74 T(I,J)=TAV(NP2)
131           KP=0
132           IP=0
133           CALL POWLAW(I)
134        61 CALL TMOM(I)
135           IF(FL .NE. 1) GO TO 63
136           KP=KP+1
137           IF(KP .LT. 10) GO TO 61
138           PRINT,'     NO CONVERSION IN 10 ITERATIONS AT FRONT ',I
139           GO TO 500
140        63 KP=0
141           IF(I .EQ. 2)PE(1)=-(DP(I-1)+DP(I))*(X(I)-X(I-1))*ROR*CPR*VISCR
             1 *UP(1)**2/TCONR +PATD
142           DO 65 K1=1,I
143           PRT(K1)=PE(K1)
144           DO 69 K2=1,NP1
145        69 TP(K1,K2)=T(K1,K2)
146        65 CONTINUE
147        64 CALL ALTDIR(I)
148           DO 41 K4=2,I
149           CALL TMOM(K4)
150           IF(FL .NE. 1) GO TO 41
151           KP=KP+1
152        41 CONTINUE
153           IF(KP .LT. 1) GO TO 62
154           IP=IP+1
155           KP=0
156           DO 67 K1=1,I
157           DO 68 K2=1,NP1
158        68 T(K1,K2)=TP(K1,K2)
159        67 CONTINUE
160           IF(IP .LT. 30) GO TO 64
161           WRITE(6,102) I,DPA,PA
162       102 FORMAT(//,10X,'NO CONVERSION IN 30 ITERATIONS
             1 AFTER TEMPERATURE CORECTION',/,12X,I2,3(2X,E14.7))
163           GO TO 500
164        62 DPA=0.0
165           DO 42 I4=2,I
166           IF(I4.GE.IW(3)) GO TO 8
167           DPE=(DP(I4-1)*RG(1)**4/R1(I4-1)**4+DP(I4)*RG(1)**4/R1(I4)**4)
             1 *(X(I4)-X(I4-1))/2.0
168           GO TO 9
169         8 DPE=(DP(I4-1)*RG(1)**4/R1(I4-1)**3+DP(I4)*RG(1)**4
```

```
     1 /R1(I4)**3)*3.1416/W*(X(I4)-X(I4-1))/4.
170    9 DPA=DPA+DPE
171   42 DPA1(I4)=DPA
172      A4=DPA1(I-1)-DPA1(I)
173      DO 83 K1=2,I
174      K=I-K1
175   83 PE(K1-1)=PAT-DPA1(K+2)+A4
176      PE(I)=DPA1(I)+PE(1)
177      DO 85 K1=1,I
178   85 PE(K1)=(PE(K1)*2.*ROR*CPR*VISCR*UP(1)**2.)/TCONR+PATD
179      IF(PE(1) .LT. PID)GO TO 56
180      PR(KU+1)=PE(1)-PID
181      IF(PR(KU+1)-PR(KU))91,91,94
182   91 KU=KU+1
183      S=TAV(NP2)*TR+TR
184      QB=Q
185      QA=EXP(-(KU-1)/10.)*QA*(PID/PE(1))**(1./FLP(S))
186      Q=QA/QO
187      VAVP=Q*CUP
188      WRITE(6,800) Q,QA,TIM(I),PE(1),VAVP
189  800 FORMAT(//,64X,'FLOW RATE REDUCED TO= ',F5.3,
     1 1X,'DIMENSIONAL FLOW RATE= ',F5.3,1X,'TIME= ',F6.4,/64X,
     2 'PE(1)=',E10.3,2X,'VAVP=',F5.2,/)
190      DT=DT*QB/Q
191      IF(VAVP .LE. .01)GO TO 201
192      DO 36 K1=1,I
193      PE(K1)=PRT(K1)
194      DO 37 K2=1,N
195   37 T(K1,K2)=TP(K1,K2)
196   36 CONTINUE
197      DO 44 I3=2,I
198      CALL POWLAW(I3)
199   44 CALL TMOM(I3)
200      IP=0
201      KP=0
202      GO TO 64
203   94 DO 95 K1=1,I
204      PE(K1)=PRT(K1)
205      DO 96 K2=1,NP1
206   96 T(K1,K2)=TP(K1,K2)
207   95 CONTINUE
208      GO TO 201
209   56 CALL SOLID(I,T,SOLIN,FL1,TSOL,N)
210      IF(FL1 .GE. I) GO TO 305
211      GO TO 50
212  200 IF(I .EQ. 2) GO TO 302
213      L1=L1+1
214      IF(L1 .NE. 4) GO TO 84
215      QC(I)=QA
216      IM(4)=I
217      TAV(I)=TM
218   38 WRITE(6,805)
219  805 FORMAT('1',//,10X,'PACKING STAGE',/,10X,13('*'),/)
220      WRITE(6,806)
221  806 FORMAT(/,10X,'VOL.FLOW R',2X,'AV.TEMP.',2X,'AV.DENSITY',2X,
     1'INIT.DENS',2X,'AV.PRESS.',2X,'AV.PRESS.',2X,'AV.PRESS.',2X,
     2'ENTRANCE',/,10X,2(10('*'),2X),9('*'),2X),2X,'RUNNER',5X,'GATE'
     3,5X,'CAVITY',4X,'PRESSURE',/,55X,9('*'),2X,9('*'),2X,9('*')
     4,2X,9('*'),/)
222      DT=DTG/(20.*Q)
223      Q1(1)=PE(1)
224      IN=0
225      TAUP(1)=TAU(I)
```

```
226           TL3=(TCONR*RLEND(3))/(ROR*CPR*UP(IW(4))*RG(3)**2.)
227           DO 103 I1=1,I
228           DO 104 J=1,NP1
229       104 UC(I1,J)=0.0
230       103 CONTINUE
231           Q3(1)=Q
232           DO 10 KS=1,NP2
233           V6=0.
234           DO 11 J=1,N
235           V9=T(KS,J)
236        11 V6=V9+V6
237        10 TAV(KS)=V6/N
238           KS=1
239           PA=0.
240           TA=0.
241           NA=IW(2)
242           DO 105 I1=1,NA
243           TA=TA+TAV(I1)
244       105 PA=PA+PE(I1)
245           TA=TA/IW(2)
246           PA=PA/IW(2)
247           TAP=TA*TR+TR
248           ROA1=DEN1(TAP,PA)
249           PAV1(KS)=PA
250           PA=0.
251           TA=0.
252           NA=IW(2)+1
253           NB=IW(3)
254           NW=NB-NA+1
255           DO 106 I1=NA,NB
256           TA=TA+TAV(I1)
257       106 PA=PA+PE(I1)
258           TA=TA/NW
259           PA=PA/NW
260           TAP=TA*TR+TR
261           ROA2=DEN1(TAP,PA)
262           PAV2(KS)=PA
263           PA=0.
264           TA=0.
265           NB=IW(3)+1
266           NC=IW(4)
267           NW=NC-NB+1
268           DO 107 I1=NB,NC
269           TA=TA+TAV(I1)
270       107 PA=PA+PE(I1)
271           TA=TA/NW
272           PA=PA/NW
273           TAP=TA*TR+TR
274           ROA3=DEN1(TAP,PA)
275           PAV3(KS)=PA
276           RA3(KS)=1.0
277           Q2(1)=TAP
278           S=TAP
279           Q3(KS+1)=Q*((PE(1)-PA)/(PE(1)-PATD))**(1./FLP(S))
280           WRITE(6,807) Q3(KS),Q2(KS),RA3(KS),ROA3,PAV1(KS),PAV2(KS),PAV3(KS)
             1,Q1(KS)
281       807 FORMAT(/,10X,8(E10.3,'1'))
282           UT3=0.
283       118 UT=RA3(KS)*(Q3(KS)+Q3(KS+1))*DT/2.
284           UT3=UT3+UT
285           RA3(KS+1)=1.+UT3/TL3
286           KS=KS+1
287           TAUP(KS)=TAUP(KS-1)+DT
```

```
288           CALL ALTDIR(NP2)
289           CALL SOLID(I,T,SOLIN,FL1,TSOL,N)
290           DO 29 I2=6,11
291        29 TP1(KS,I2)=SOLIN(I2)
292           IF(FL1 .LT. IW(2)) GO TO 130
293           IN=1
294       130 DO 113 K5=1,I
295           V6=0.
296           DO 114 J=1,N
297           V9=T(K5,J)
298       114 V6=V9+V6
299       113 TAV(K5)=V6/N
300           TA=0.0
301           DO 117 I1=NB,NC
302       117 TA=TA+TAV(I1)
303           TA=TA/NA
304           TAP=TA*TR+TR
305           Q2(KS)=TAP
306           PAP=PRESS(TAP,RA3(KS),ROA3,PAV3(KS-1))
307           PAV3(KS)=PAP
308           PIP=PAV3(KS)-PAV3(KS-1)
309           Q1(KS)=Q1(KS-1)+PIP
310           IF(PID .LE. Q1(KS)) GO TO 35
311           PAV1(KS)=PAV1(KS-1)+PIP
312           PAV2(KS)=PAV2(KS-1)+PIP
313           DO 26 I1=1,I
314        26 PE(I1)=PE(I1)+PIP
315           S=TAP
316           GO TO 6
317        35 DIFF=PID-Q1(KS-1)
318           PAV3(KS)=PAV3(KS-1)+DIFF
319           RA3(KS)=DEN1(TAP,PAV3(KS))/ROA3
320           NA=IW(2)
321           TA=0.0
322           DO 115 I1=1,NA
323           PE(I1)=PE(I1)+DIFF*(1-I1/IW(4))
324       115 TA=TA+TAV(I1)
325           TA=TA/IW(2)
326           TAP=TA*TR+TR
327           PAV1(KS)=PAV1(KS-1)+DIFF
328           RA1(KS)=DEN1(TAP,PAV1(KS))/ROA1
329           NA=IW(2)+1
330           NB=IW(3)
331           TA=0.0
332           DO 116 I1=NA,NB
333           PE(I1)=PE(I1)+DIFF*(1-I1/IW(4))
334       116 TA=TA+TAV(I1)
335           TA=TA/(NB-NA+1)
336           TAP=TA*TR+TR
337           PAV2(KS)=PAV2(KS-1)+DIFF
338           RA2(KS)=DEN1(TAP,PAV2(KS))/ROA2
339           NB=NB+1
340           DO 27 I1=NB,NC
341        27 PE(I1)=PE(I1)+DIFF*(1-I1/IW(4))
342           IN=1
343         6 Q3(KS+1)=Q*((PE(1)-PAV3(KS))/(PE(1)-PATD))**(1./FLP(S))
344           QPW=Q3(KS)*QA
345           WRITE(6,807) QPW,Q2(KS),RA3(KS),ROA3,PAV1(KS),PAV2(KS),PAV3(KS)
             1,PE(1)
346           TIM(I+KS-1)=TAUP(KS)*RG(3)**2.*ROR*CPR/TCONR
347           P1(I+KS-1)=PE(4)
348           P2(I+KS-1)=PE(11)
349           P3(I+KS-1)=PE(13)
```

```
350           P4(I+KS-1)=PE(15)
351           P5(I+KS-1)=PE(10)
352           T1(I+KS-1)=((T(2,10)*TR+TR)-32.)/1.8
353           T2(I+KS-1)=((T(10,10)*TR+TR)-32.)/1.8
354           T3(I+KS-1)=((T(12,10)*TR+TR)-32.)/1.8
355           T4(I+KS-1)=((T(14,10)*TR+TR)-32.)/1.8
356           QC(I+KS-1)=Q3(KS)*QA
357           IF(Q3(KS+1) .LE. 1.0E-4) IN=1
358           IF(IN .GE.1) GO TO 119
359           DT=DT+DTG/(10.*Q)
360           GO TO 118
361       119 DTPC=DT
362           WRITE(6,809)
363       809 FORMAT(11(/))
364           DO 30 I1=2,KS
365        30 WRITE(6,205)(TP1(I1,K5),K5=6,11),TIM(I+I1-1)
366           WRITE(6,810)
367       810 FORMAT('1',/,10X,'COOLING STAGE',/,10X,13('*'),//)
368           FLG=1.
369           RA31=(RA3(KS)+RA2(KS)+RA1(KS))/3.
370           IA=KS+I-1
371           TAUP(1)=0.
372           DO 20 K1=1,NP2
373           TAP=TAV(K1)*TR+TR
374        20 Q3(K1)=DEN1(TAP,PE(K1))
375           DO 121 I1=1,IX
376           I0=I1-1
377           TAUP(I1+1)=TAUP(I1)+DT
378           CALL ALTDIR(NP2)
379           CALL SOLID(I,T,SOLIN,FL1,TSOL,N)
380           IF(FL1 .GE. I) PRINT,'      SOLIDIFICATION COMPLETED AT COOLING'
381           V9=0.
382           V10=0.
383           DO 21 K1=1,NP2
384           V6=0.
385           DO 22 J=1,N
386        22 V6=T(K1,J)/N+V6
387           V6=V6*TR+TR
388           V9=V9+V6/NP2
389           PE(K1)=PRESS(V6,Q3(K1),1.,PE(K1))
390        21 V10=V10+PE(K1)/NP2
391           P1(I1+IA)=PE(4)
392           P2(I1+IA)=PE(11)
393           P3(I1+IA)=PE(13)
394           P4(I1+IA)=PE(15)
395           P5(I1+IA)=PE(10)
396           TIM(I1+IA)=TIM(IA)+TAUP(I1+1)*RG(3)**2.*ROR*CPR/TCONR
397           T1(IA+I1)=((T(2,10)*TR+TR)-32.)/1.8
398           T2(IA+I1)=((T(10,10)*TR+TR)-32.)/1.8
399           T3(IA+I1)=((T(12,10)*TR+TR)-32.)/1.8
400           T4(IA+I1)=((T(14,10)*TR+TR)-32.)/1.8
401           QC(IA+I1)=0.0
402           WRITE(6,205)(SOLIN(K1),K1=6,11),TIM(I1+IA)
403           DT=DT+10.*DTPC
404           RA31=DEN1(V9,V10)/ROA3
405       121 CONTINUE
406           WRITE(6,811)
407       811 FORMAT(10X,'CYCLE HAS BEEN COMPLETED',/,10X,24('*'))
408           IX=IA+IX
409           WRITE(6,308)
410       308 FORMAT('1',//,14X,'T1',8X,'T2',8X,'T3',8X,'T4',8X,'P1',8X,'P2',
              1 8X,'P3',8X,'P4',8X,'P5',7X,'TIME',3X,'FLOW RATE',/7X,
              2 9(6X,4('*')),5X,6('*'),2X,10('*'))
```

```
411           DO 99 K=1,IX
412            99 WRITE(6,300) T1(K),T2(K),T3(K),T4(K),P1(K),P2(K),
                 1P3(K),P4(K),P5(K),TIM(K),QC(K)
413          300 FORMAT(/,9X,9(1X,F9.3),2(2X,F8.4))
414           WRITE(6,306)
415          306 FORMAT('1')
416           GO TO 500
417            84 R1(I+1)=RG(L1)
418           IW(L1)=I
419           WRITE(6,203) IW(L1),L1
420          203 FORMAT(10X,'CHANNEL TRANSITION:',5X,'NODE=',I3,5X,
                1 'ZONE=',I3,/,10X,18('*'),6X,4('*'),9X,4('*'),/)
421           CUPP=CUP
422           CUP=QQ/(3.1416*RG(L1)**2.)
423           IF(I .GE. IW(3))CUP=QQ/(2.*W*RG(L1))
424           DTP=RLEND(L1)/(NS*Q*CUP)
425           RLEN=RLEN*RG(L1-1)**2*CUPP/(RG(L1)**2*CUP)
426           D1(I)=D1(I)*RG(L1-1)**2*CUPP/(RG(L1)**2*CUP)
427           TAU(I)=TAU(I)*R1(I)**2./R1(I+1)**2.
428           GO TO 58
429          201 TOTL=D1(I)*ROR*CPR*CUP*RG(L1)**2/TCONR
430           TIM(I)=TAU(I)*RG(L1)**2*ROR*CPR/TCONR
431           QA=QC(I)
432           Q=QA/QQ
433           WRITE(6,301) TOTL,PE(1),TIM(I)
434          301 FORMAT(/////,10X,'SHORT SHOT',/,10X,10('*'),//,10X,'LENGTH=
                1 F6.3,/,10X,'ENTRANCE PRESSURE= ',F9.2,/,10X,'TIME= ',F8.4)
435           IF(IW(4) .EQ. 0) IW(4)=I
436           IF(IW(3) .EQ. 1000) IW(3)=I
437           IF(IW(2) .EQ. 0) IW(2)=I
438           PID=PE(1)
439           GO TO 38
440          302 WRITE(6,303) RLEN,D1(I)
441          303 FORMAT(//,10X,'RUNNER FULL AT FIRST TIME INTERVALL,',
                1 ' DECREASE TIME INTERVAL',/,'RLEN= ',F6.3,'D1= ',F6.3)
442           GO TO 500
443          305 TOTL=D1(I)*ROR*CPR*CUP*RG(L1)**2/TCONR
444           TIM(I)=TAU(I)*RG(L1)**2*ROR*CPR/TCONR
445           QA=QC(1)
446           Q=QA/QQ
447           PRINT,'   SOLIDIFICATION COMPLETED',TIM(I),TOTL
448           IF(IW(4) .EQ. 0) IW(4)=I
449           IF(IW(3) .EQ. 1000) IW(3)=I
450           IF(IW(2) .EQ. 0) IW(2)=I
451           GO TO 38
452          500 STOP
453           END

454           SUBROUTINE TRIDAG(I1,L,A,B,C,D,V)
455           DIMENSION A(40),B(40),C(40),D(40),V(40),BETA(40),GAMMA(40)
456           BETA(I1)=B(I1)
457           GAMMA(I1)=D(I1)/BETA(I1)
458           IFP1=I1+1
459           DO 1 I=IFP1,L
460           BETA(I)=B(I)-A(I)*C(I-1)/BETA(I-1)
461            1 GAMMA(I)=(D(I)-A(I)*GAMMA(I-1))/BETA(I)
462           V(L)=GAMMA(L)
463           LAST=L-I1
464           DO 2 K=1,LAST
465           I=L-K
466            2 V(I)=GAMMA(I)-C(I)*V(I+1)/BETA(I)
467           RETURN
```

```
468           END

469           SUBROUTINE POWLAW(I)
470           COMMON QA,R1(40),U(40,12),GAMA(40,12),T(40,12),TR,FL,EPS,R(12)
471           COMMON B1(40),NP1,VSCR,N,UC(40,12),Q,DP(40),NP2,UP(40),IW(4),W
472           COMMON X(40),DT,TP1(40,12),TSTAR(40,12),VISCR,GAMAR,PE(40)
473           COMMON TM
474           NA=NP1
475           NB=N
476           NC=NP1+1
477           U(I,NA)=0.
478           U(I,NC)=0.
479           IF(I .GE. IW(3)) GO TO 4
480           DO 1 J=1,NA
481           S=T(I,J)*TR+TR
482         1 GAMA(I,J)=-QA*(3.0*FLP(S)+1.0)*R(J)**(1.0/FLP(S))/
              1 (3.1416*R1(I)**3.0*FLP(S))
483           GO TO 6
484         4 DO 5 J=1,NA
485           S=T(I,J)*TR+TR
486         5 GAMA(I,J)=-(2.*FLP(S)+1.)*QA*R(J)**(1./FLP(S))/
              1 (2.*W*FLP(S)*R1(I)**2)
487         6 DO 2 K=1,N
488           J=NA-K
489         2 U(I,J)=U(I,J+1)-(R(J+1)-R(J))/2.*(GAMA(I,J+1)+GAMA(I,J))*
              1 R1(I)/(Q*UP(I))
490           RETURN
491           END

492           SUBROUTINE TMOM(I)
493           REAL VI(40,12),V(40,12)
494           COMMON QA,R1(40),U(40,12),GAMA(40,12),T(40,12),TR,FL,EPS,R(12)
495           COMMON B1(40),NP1,VSCR,N,UC(40,12),Q,DP(40),NP2,UP(40),IW(4),W
496           COMMON X(40),DT,TP1(40,12),TSTAR(40,12),VISCR,GAMAR,PE(40)
497           COMMON TM
498           NB=N
499           NA=NP1
500           NC=NP1+1
501           UC(I,NA)=0.
502           UC(I,NC)=0.
503           FL=0.
504           DO 1 J=1,NA
505           TV=T(I,J)*TR+TR
506           GA=-GAMA(I,J)
507         1 VI(I,J)=VISC(TV,GA)/VISCR
508           IF(I .LT. IW(3)) GO TO 15
509           CALL TMOMC(R,VI,Q,N,DP,UC,I)
510           GO TO 16
511        15 DO 2 K=1,NB
512           V2=0.0
513           DO 3 J=K,NB
514           V1=(R(J)/VI(I,J)+R(J+1)/VI(I,J+1))*(R(J+1)-R(J))
515         3 V2=V2+V1
516         2 V(I,K)=0.5*V2
517           V(I,NA)=0.0
518           F=0.0
519           DO 4 J=1,NB
520           F1=(V(I,J)*R(J)+V(I,J+1)*R(J+1))*(R(J+1)-R(J))/2.0
521         4 F=F+F1
522           DP(I)=-Q/(2.0*F)
523           DO 5 J=1,NB
```

```
524         5 UC(I,J)=-V(I,J)*DP(I)/Q
525        16 K1=0
526           DO 6 J=1,NA
527         6 IF (ABS(UC(I,J)-U(I,J)).LE.EPS)K1=K1+1
528           IF(K1-NA)11,12,12
529        11 DO 13 J=1,NA
530        13 U(I,J)=UC(I,J)
531           FL=1.
532        12 DO 14 J=2,NA
533        14 GAMA(I,J)=(UC(I,J+1)-UC(I,J-1))*Q*UP(I)/((R(J+1)-R(J-1))*R1(I))
534           GAMA(I,1)=0.0
535           RETURN
536           END

537           SUBROUTINE TMOMC(R,VI,Q,N,DP,UC,I)
538           REAL R(12),VI(40,12),V(40,12),DP(40),UC(40,12)
539           NB=N
540           DO 2 K=1,NB
541           V2=0.
542           DO 3 J=K,NB
543           NA=N+1
544           V1=(R(J)/VI(I,J)+R(J+1)/VI(I,J+1))*(R(J+1)-R(J))
545         3 V2=V2+V1
546         2 V(I,K)=.5*V2
547           V(I,NA)=0.0
548           F=0.0
549           DO 4 J=1,NB
550           F1=(V(I,J)+V(I,J+1))*(R(J+1)-R(J))/2.0
551         4 F=F+F1
552           DP(I)=-Q/(2.*F)
553           DO 5 J=1,NB
554         5 UC(I,J)=-2.*V(I,J)*DP(I)/Q
555           RETURN
556           END

557           SUBROUTINE SOLID(I,T,SOLIN,FL1,TSOL,N)
558           REAL T(40,12),UC(40,12),SOLIN(40)
559           FL1=0.
560           TOP=TSOL
561           SIP=N
562           NA=N+1
563           DO 65 K1=1,I
564           DO 69 K2=1,NA
565           IF(T(K1,K2) .GT. TOP) GO TO 69
566           GO TO 3
567        69 CONTINUE
568           GO TO 65
569         3 SOLIN(K1)=ABS(1.-(K2-1)/SIP)
570           IF(SOLIN(K1) .GT. 0.9) FL1=FL1+1.
571        65 CONTINUE
572           RETURN
573           END

574           SUBROUTINE ALTDIR(I1)
575           COMMON QA,R1(40),U(40,12),GAMA(40,12),T(40,12),TR,FL,EPS,R(12)
576           COMMON B1(40),NP1,VSCR,N,UC(40,12),Q,DP(40),NP2,UP(40),IW(4),W
577           COMMON X(40),DT,TP1(40,12),TSTAR(40,12),VISCR,GAMAR,PE(40)
578           COMMON TM
579           REAL AP(40,12),A1(40,12),A2(40,12),A(40),B(40),C(40)
580           REAL A3(40,12),TPRIME(40),D(40),BETA(40,12)
```

```
      DO 1 I=2,I1
      DO 2 J=1,N
      IF(J .NE. 1) GO TO 3
      AP(I,1)=0.
      BETA(I,1)=0.
      GO TO 4
    3 AP(I,J)=(R(J+1)*TCD(T(I,J+1))-R(J-1)*TCD(T(I,J-1)))*
     1 DT/(2.*DE(T(I,J),PE(I),TR)*CPP(T(I,J))*R(J)
     2 *(R(J+1)-R(J-1))**2)
      BETA(I,J)=B1(I)*R(J)*Q*DP(I)*(UC(I,J+1)-UC(I,J-1))*DT
     1 /(2.*DE(T(I,J),PE(I),TR)*CPP(T(I,J))*(R(J+1)-R(J-1)))
    4 A2(I,J)=-(Q*UC(I,J)*DT)/(2.*(X(I)-X(I-1)))
      A1(I,J)=(TCD(T(I,J))*DT)/(2.*(R(J+1)-R(J))**2.
     1 *DE(T(I,J),PE(I),TR)*CPP(T(I,J)))
      IF(J .EQ. 1) GO TO 2
      IF(I .LT. IM(3)) GO TO 2
      AP(I,J)=(TCD(T(I,J+1))-TCD(T(I,J-1)))*DT
     1 /(2.*DE(T(I,J),PE(I),TR)*CPP(T(I,J))*(R(J+1)-R(J-1))**2.)
      BETA(I,J)=2.*BETA(I,J)
    2 CONTINUE
    1 CONTINUE
      DO 5 I=2,I1
      DO 6 J=1,N
      A(J)=AP(I,J)-A1(I,J)
      B(J)=2.*A1(I,J)+1.
      C(J)=-(AP(I,J)+A1(I,J))
      C(1)=-2.*A1(I,1)
    6 D(J)=A2(I,J)*(T(I,J)-T(I-1,J))+T(I,J)+BETA(I,J)
      D(N)=D(N)+(AP(I,N)+A1(I,N))*TSTAR(I,NP1)
      CALL TRIDAG(1,N,A,B,C,D,TPRIME)
      DO 7 J=1,N
    7 TSTAR(I,J)=TPRIME(J)
    5 CONTINUE
      DO 8 I=2,I1
      DO 9 J=1,N
      IF(J .NE. 1) GO TO 10
      D(I)=2.*A1(I,J)*(TSTAR(I,2)-TSTAR(I,1))+TSTAR(I,1)+BETA(I,1)
      GO TO 11
   10 D(I)=AP(I,J)*(TSTAR(I,J+1)-TSTAR(I,J-1))+A1(I,J)*(TSTAR(I,J-1)
     1 -2.*TSTAR(I,J)+TSTAR(I,J+1))+TSTAR(I,J)+BETA(I,J)
   11 T(I,J)=(D(I)-A2(I,J)*T(I-1,J))/(1.-A2(I,J))
      IF(T(I,J) .LE. TM) T(I,J)=TM
    9 CONTINUE
    8 CONTINUE
      RETURN
      END

      REAL FUNCTION DEN1(T,P)
      DEN1=53.76+.000252*P-.0165*T
      IF(T .LE. 214.9) DEN1=57.1
      RETURN
      END

      REAL FUNCTION PRESS(T,RA,RO,PU)
      RM=RA*RO
      PRESS=(RM-53.76+.0165*T)/.000252
      IF(PRESS .LT. 0.0) PRESS=PU
      RETURN
```

```
      END

      REAL FUNCTION FLP(S)
      FLP=.835-.126E-2*S+.179E-5*S**2.+.277E-9*S**3.
      RETURN
      END

      REAL FUNCTION VISC(TV,GA)
      IF(GA.GT.1) GO TO 1
      SA=(-0.57483 +( 4.402E-4)*TV)/.038924
      SA=EXP(SA)
      IF(GA .GT. SA) GO TO 1
      SA=ALOG(SA)
      GO TO 2
    1 SA=ALOG(GA)
    2 VISC=EXP(3.3568-0.57483*SA-0.019462*SA*SA-0.010242*TV
     1 +4.186E-6*TV*TV+4.402E-4*TV*SA)
      RETURN
      END

      REAL FUNCTION DE(T,P,TR)
      COMMON /AREA2/ ROR,FLG,RA31,ROA3
      IF(FLG .NE. 1.) GO TO 3
      DE=RA31*ROA3/ROR
      GO TO 2
    3 IF(T .LE. -.452) GO TO 1
      RAR=ROR*1728.
      TF=T*TR+TR
      DE=(53.76+.000252*P-.0165*TF)/RAR
      GO TO 2
    1 DE=.03304/ROR
    2 RETURN
      END

      REAL FUNCTION CPP(XX)
      COMMON /AREA1/ CPR
      CPP=.62/CPR
      IF(XX .LE. -.452) CPP=.55/CPR
      RETURN
      END

      REAL FUNCTION TCD(XX)
      COMMON /AREA3/ TCONR
      TCD=2.43E-6/TCONR
      IF(XX .LE. -.452) TCD=4.63E-6/TCONR
      RETURN
      END
```

RESULTS FOR THE INJECTION CYCLE RUN AT

$T' = 388\ ^{o}F$; $P' = 13500$ Psig ; $Q_o' = 1.30\ \frac{in^3}{sec}$

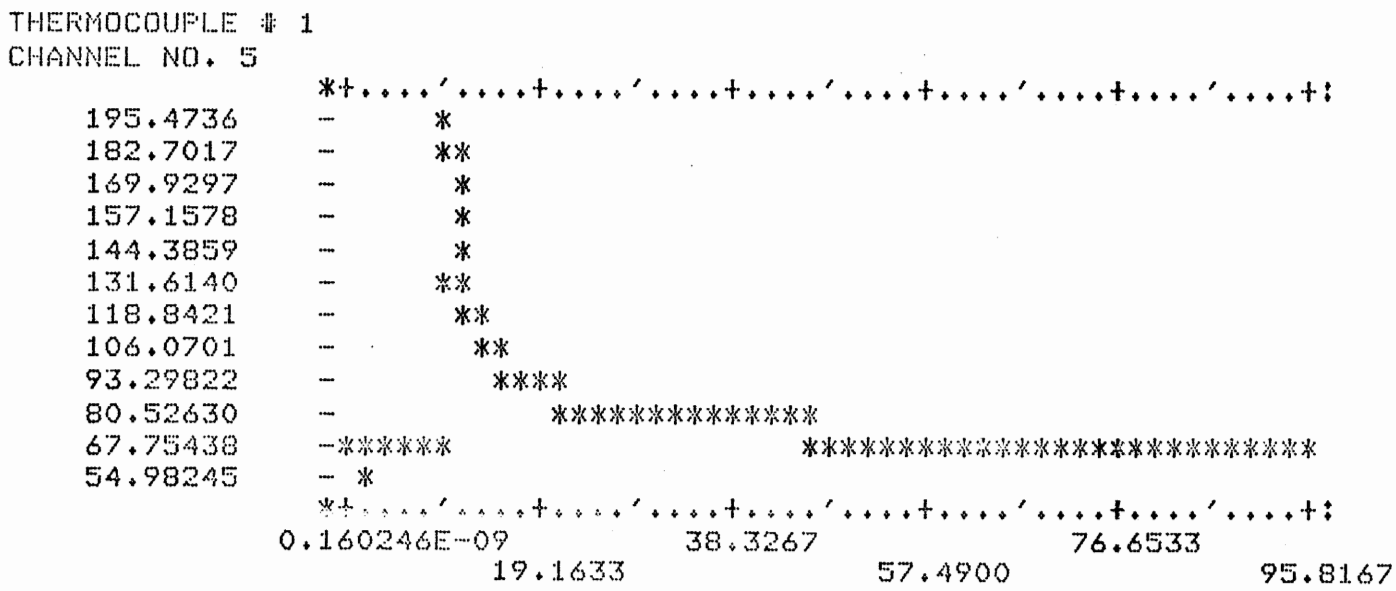
THERMOCOUPLE # 1
CHANNEL NO. 5
195.4736
182.7017
169.9297
157.1578
144.3859
131.6140
118.8421
106.0701
93.29822
80.52630
67.75438
54.98245
0.160246E-09
19.1633
38.3267
57.4900
76.6533
95.8167

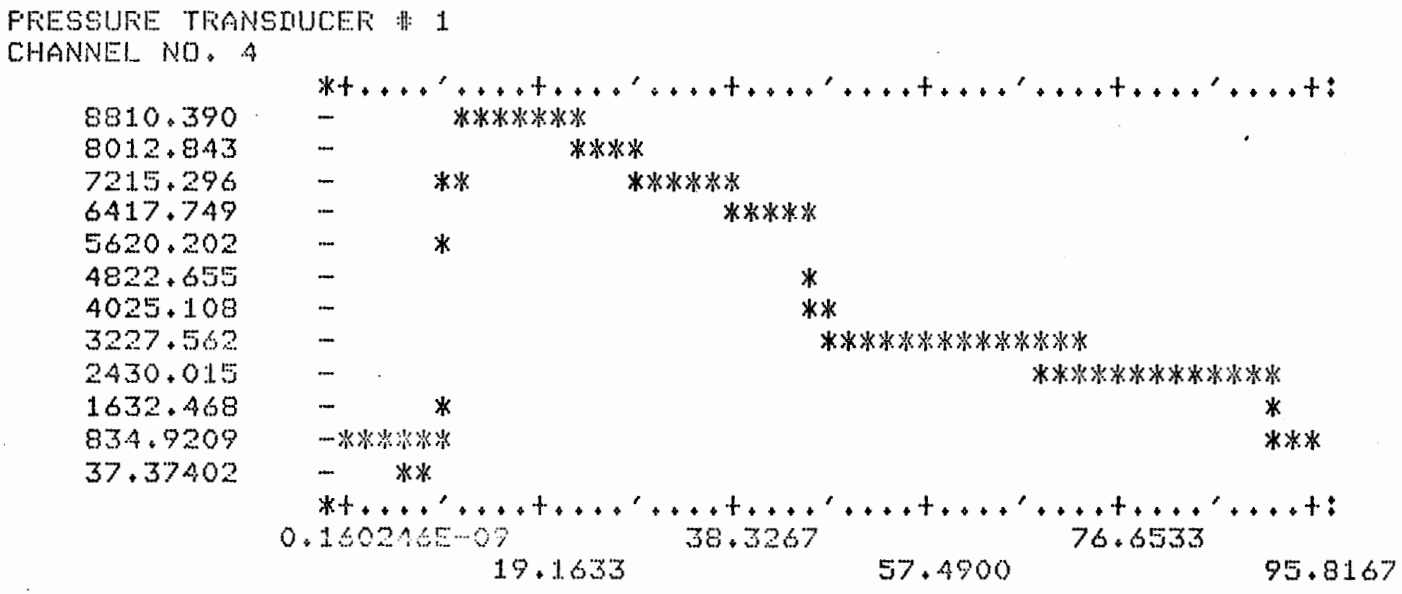
PRESSURE TRANSDUCER # 1
CHANNEL NO. 4
8810.390
8012.843
7215.296
6417.749
5620.202
4822.655
4025.108
3227.562
2430.015
1632.468
834.9209
37.37402
0.160246E-09
19.1633
38.3267
57.4900
76.6533
95.8167

THERMOCOUPLE # 2
CHANNEL NO. 6

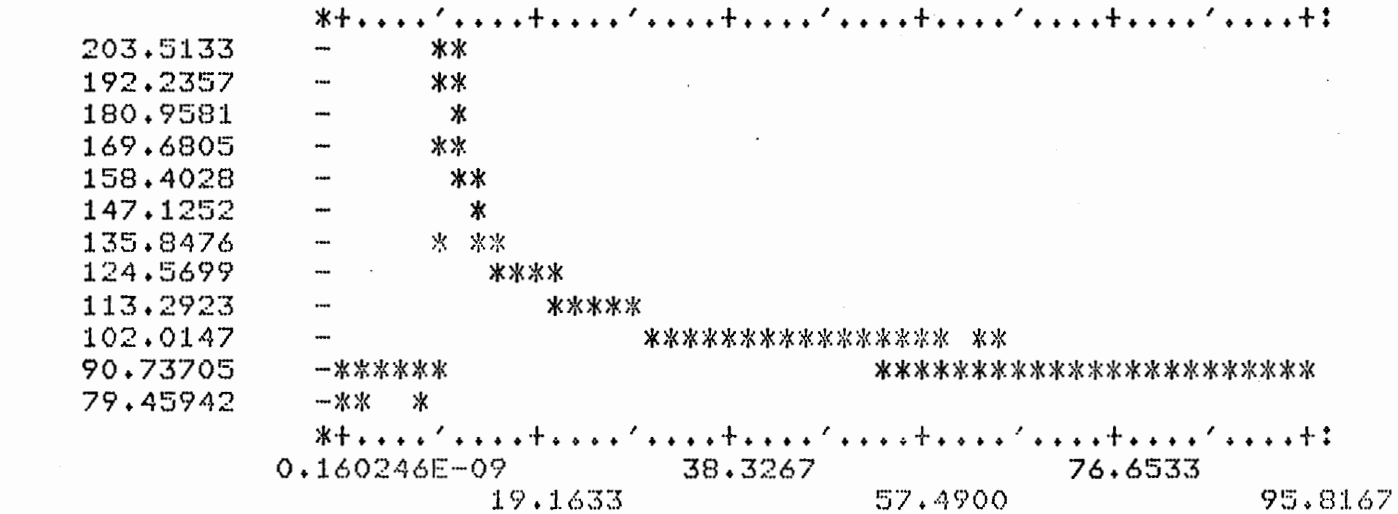

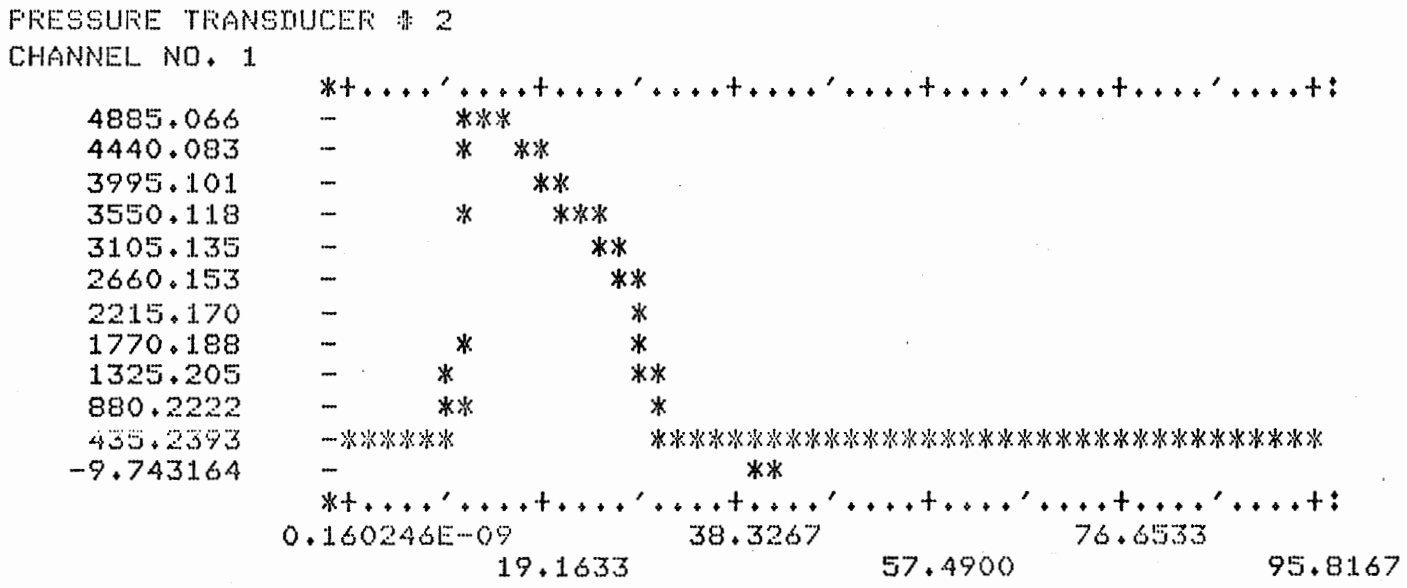
PRESSURE TRANSDUCER # 2
CHANNEL NO. 1
4885.066
4440.083
3995.101
3550.118
3105.135
2660.153
2215.170
1770.188
1325.205
880.2222
435.2393
-9.743164
0.160246E-09
19.1633
38.3267
57.4900
76.6533
95.8167

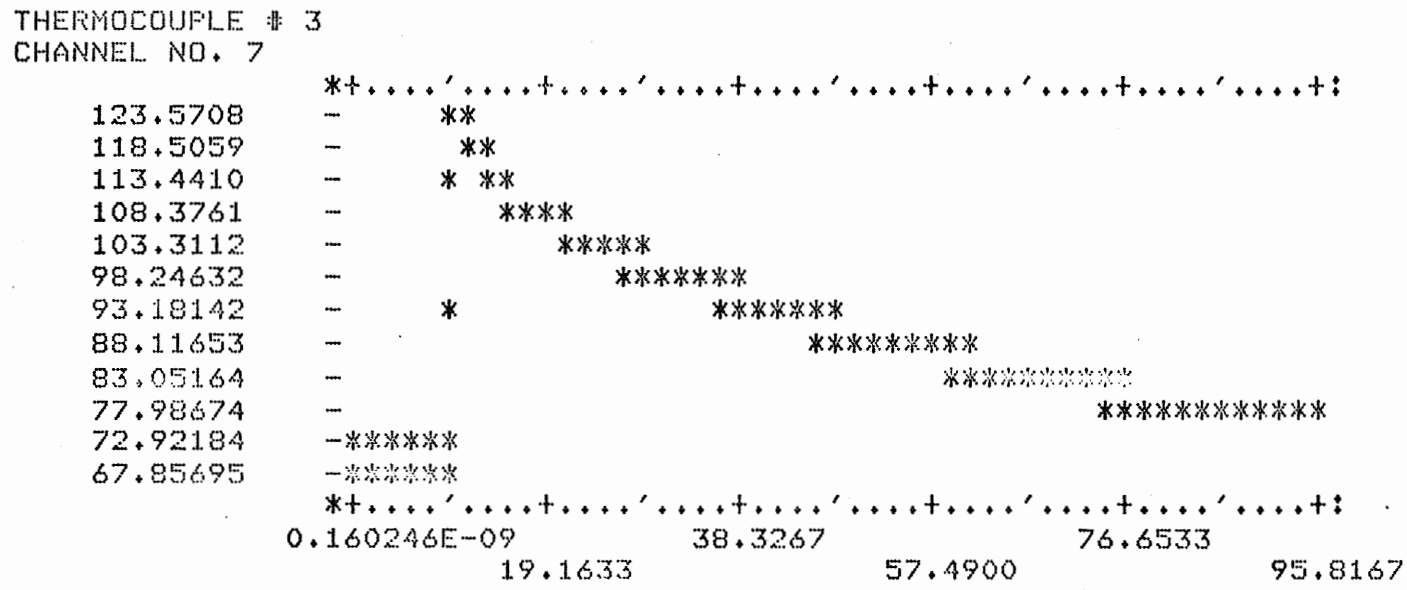
THERMOCOUPLE # 3
CHANNEL NO. 7
123.5708
118.5059
113.4410
108.3761
103.3112
98.24632
93.18142
88.11653
83.05164
77.98674
72.92184
67.85695
0.160246E-09
19.1633
38.3267
57.4900
76.6533
95.8167

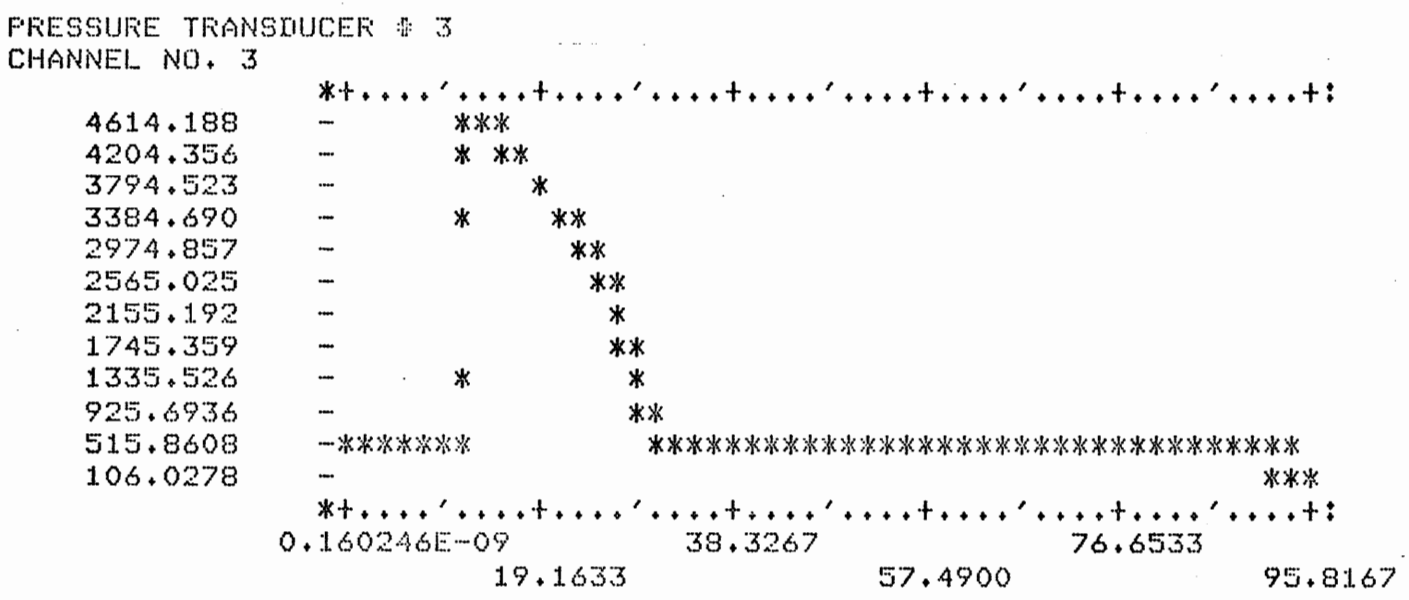
PRESSURE TRANSDUCER # 3
CHANNEL NO. 3
4614.188
4204.356
3794.523
3384.690
2974.857
2565.025
2155.192
1745.359
1335.526
925.6936
515.8608
106.0278
0.160246E-09
19.1633
38.3267
57.4900
76.6533
95.8167

THERMOCOUPLE # 4
CHANNEL NO. 8

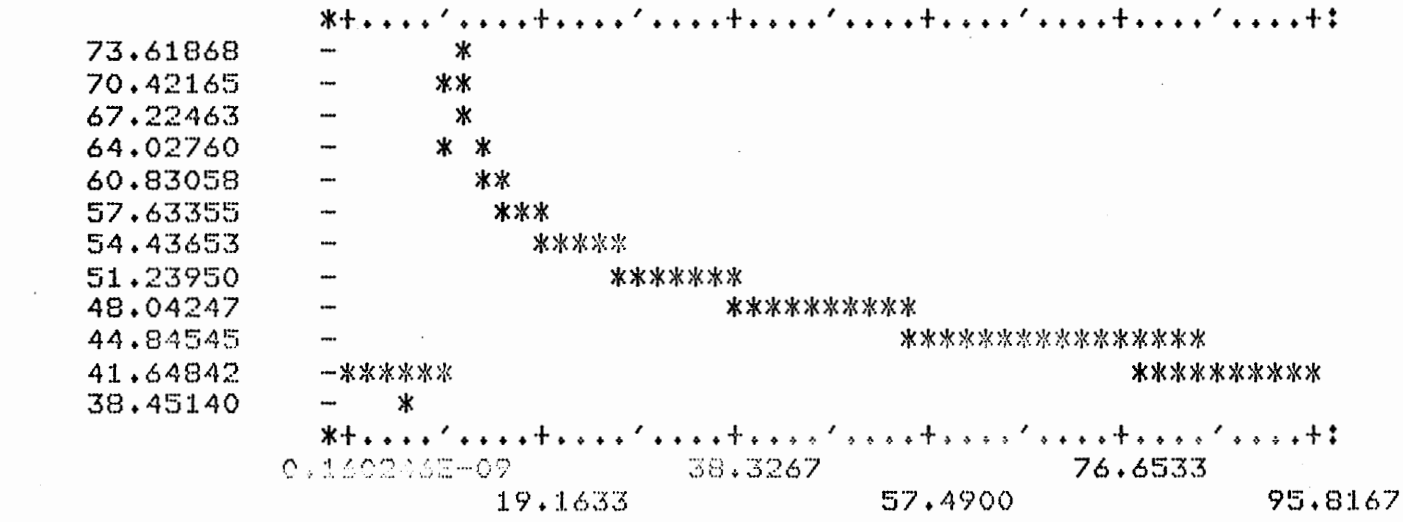

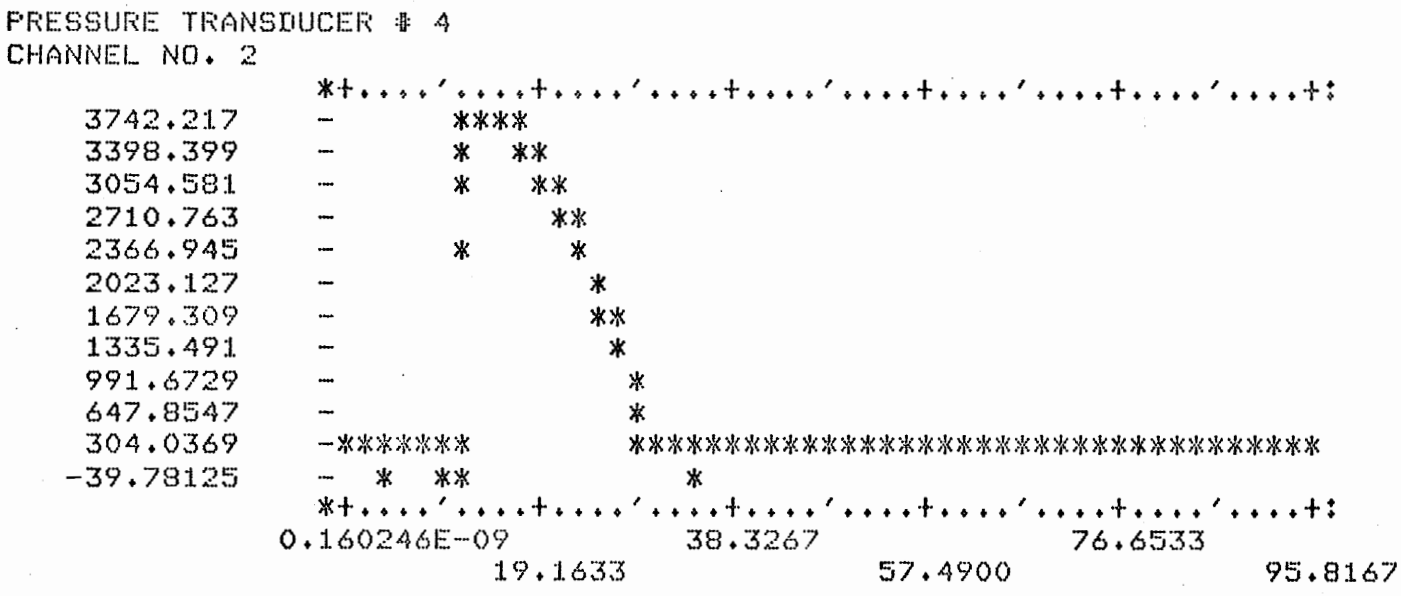
PRESSURE TRANSDUCER # 4
CHANNEL NO. 2
3742.217
3398.399
3054.581
2710.763
2366.945
2023.127
1679.309
1335.491
991.6729
647.8547
304.0369
-39.78125
0.160246E-09
19.1633
38.3267
57.4900
76.6533
95.8167

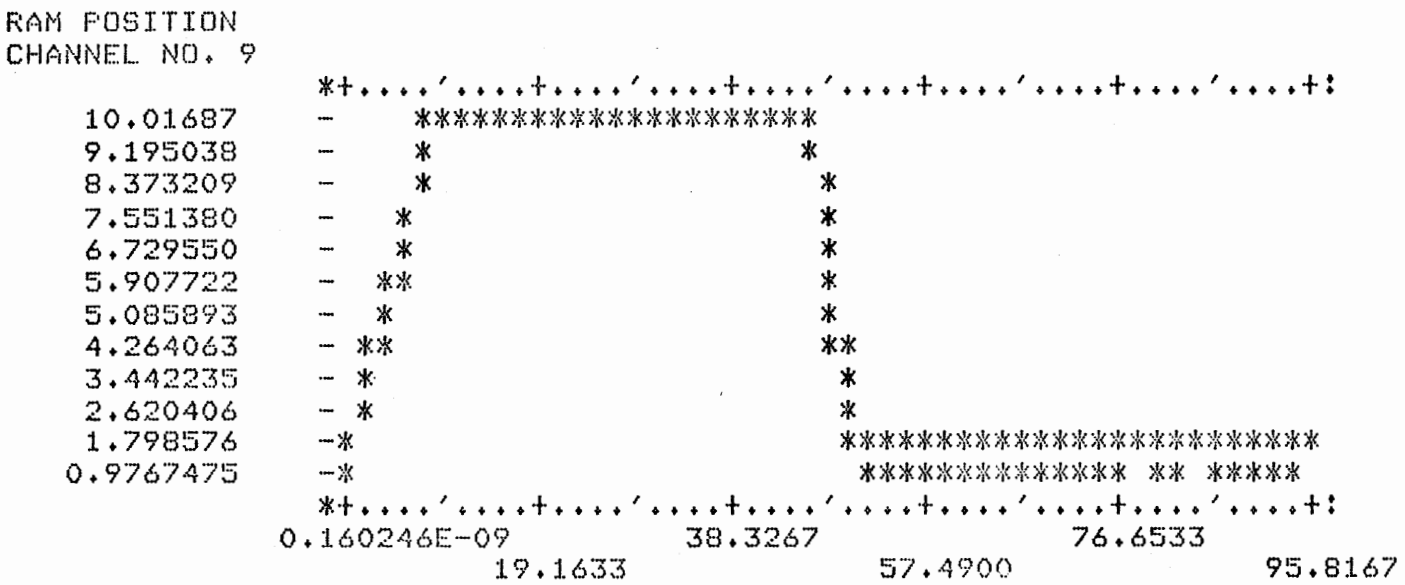
RAM POSITION
CHANNEL NO. 9
10.01687
9.195038
8.373209
7.551380
6.729550
5.907722
5.085893
4.264063
3.442235
2.620406
1.798576
0.9767475
0.160246E-09
19.1633
38.3267
57.4900
76.6533
95.8167

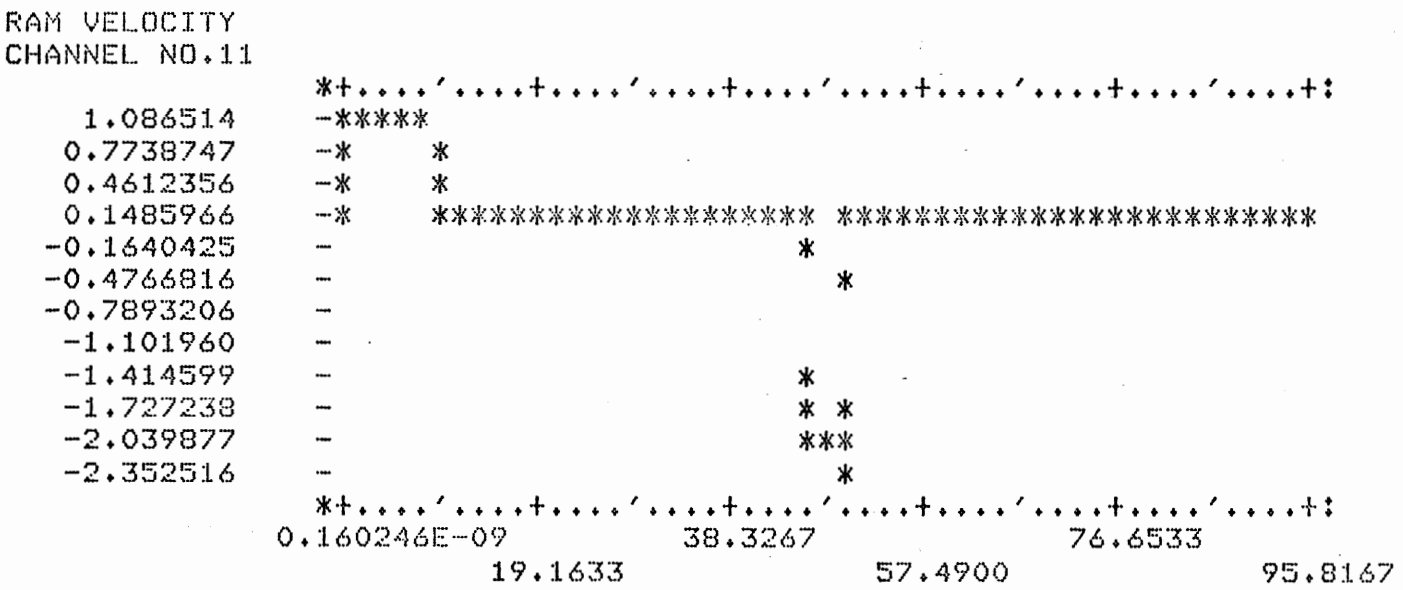
RAM VELOCITY
CHANNEL NO.11
1.086514
0.7738747
0.4612356
0.1485966
-0.1640425
-0.4766816
-0.7893206
-1.101960
-1.414599
-1.727238
-2.039877
-2.352516
0.160246E-09
19.1633
38.3267
57.4900
76.6533
95.8167

RESULTS FOR THE INJECTION CYCLE RUN AT

$T'=400\ ^{o}F$; $P'=12000$ Psig ; $Q_o'=1.83\ \frac{in^3}{sec}$

THERMOCOUPLE # 1
CHANNEL NO. 5

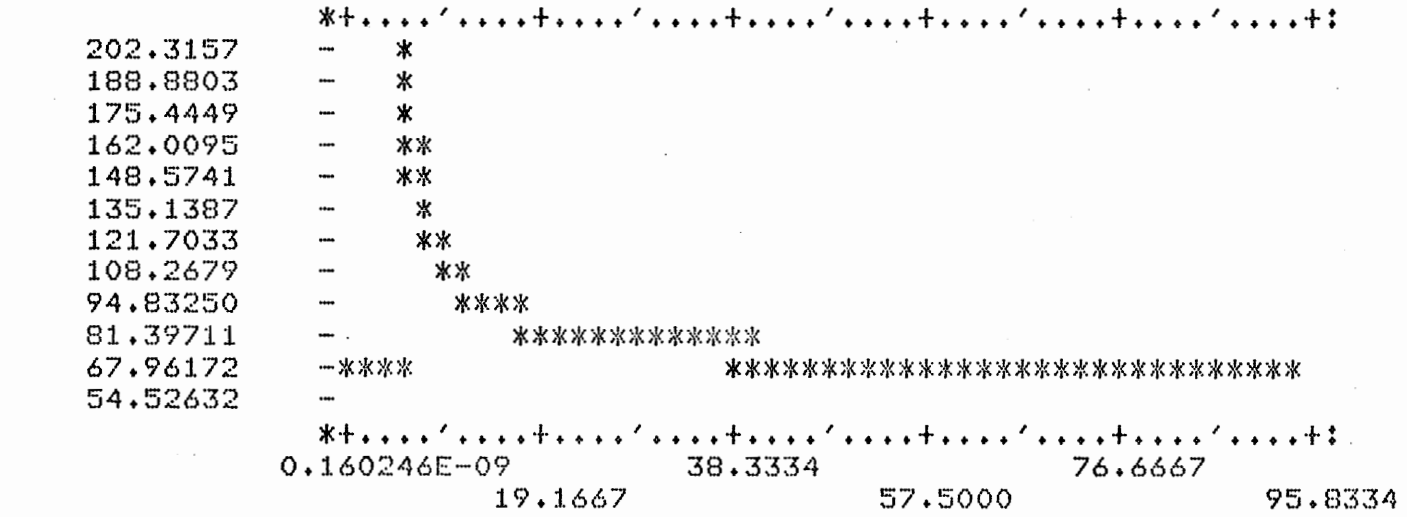

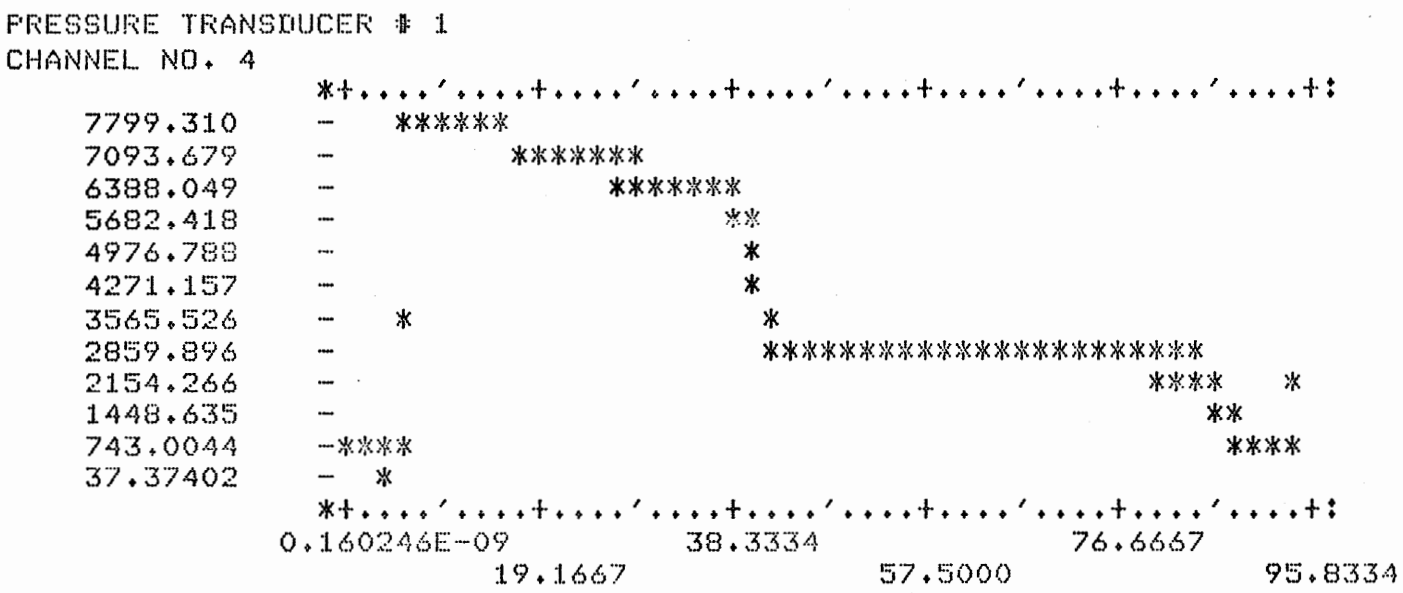
PRESSURE TRANSDUCER # 1
CHANNEL NO. 4
7799.310
7093.679
6388.049
5682.418
4976.788
4271.157
3565.526
2859.896
2154.266
1448.635
743.0044
37.37402
0.160246E-09
19.1667
38.3334
57.5000
76.6667
95.8334

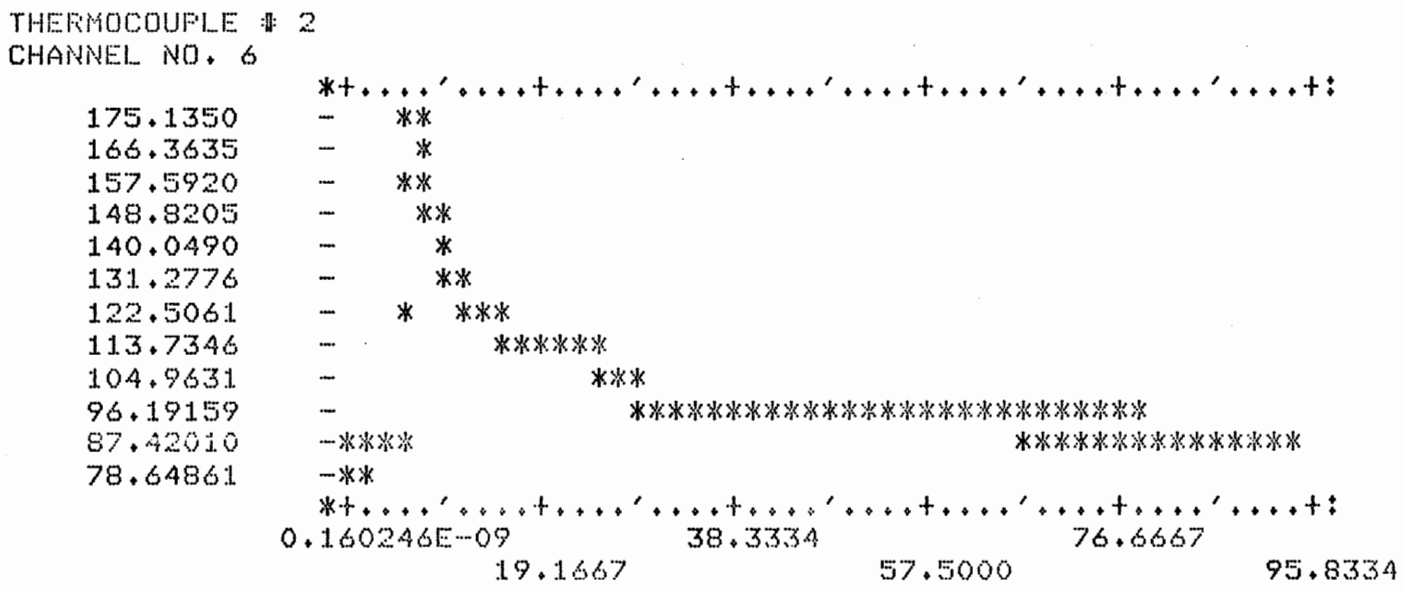
THERMOCOUPLE # 2
CHANNEL NO. 6
175.1350
166.3635
157.5920
148.8205
140.0490
131.2776
122.5061
113.7346
104.9631
96.19159
87.42010
78.64861
0.160246E-09
19.1667
38.3334
57.5000
76.6667
95.8334

PRESSURE TRANSDUCER # 2
CHANNEL NO. 1

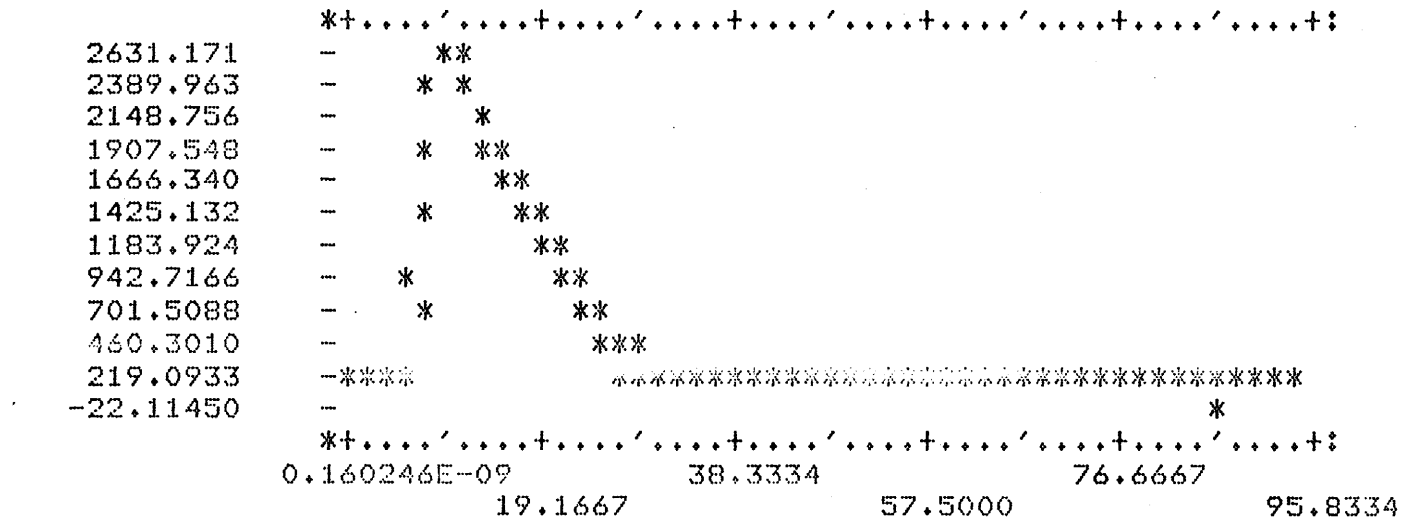

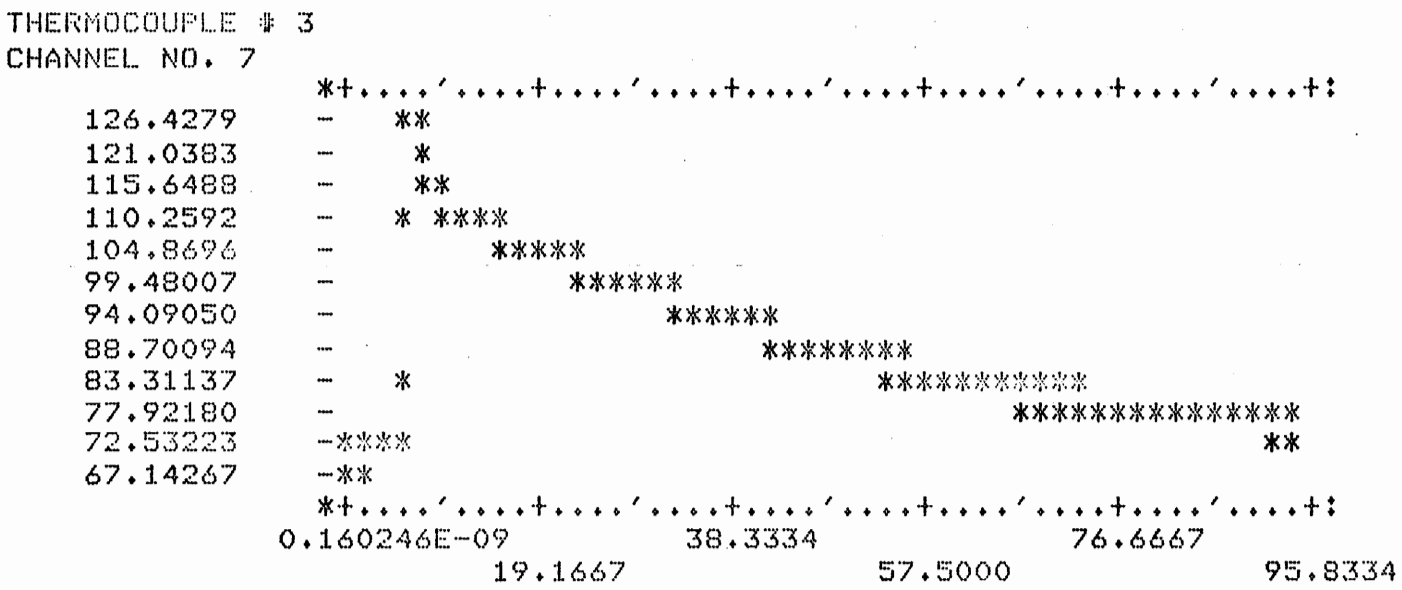
THERMOCOUPLE # 3
CHANNEL NO. 7
126.4279
121.0383
115.6488
110.2592
104.8696
99.48007
94.09050
88.70094
83.31137
77.92180
72.53223
67.14267
0.160246E-09
19.1667
38.3334
57.5000
76.6667
95.8334

PRESSURE TRANSDUCER # 3
CHANNEL NO. 3

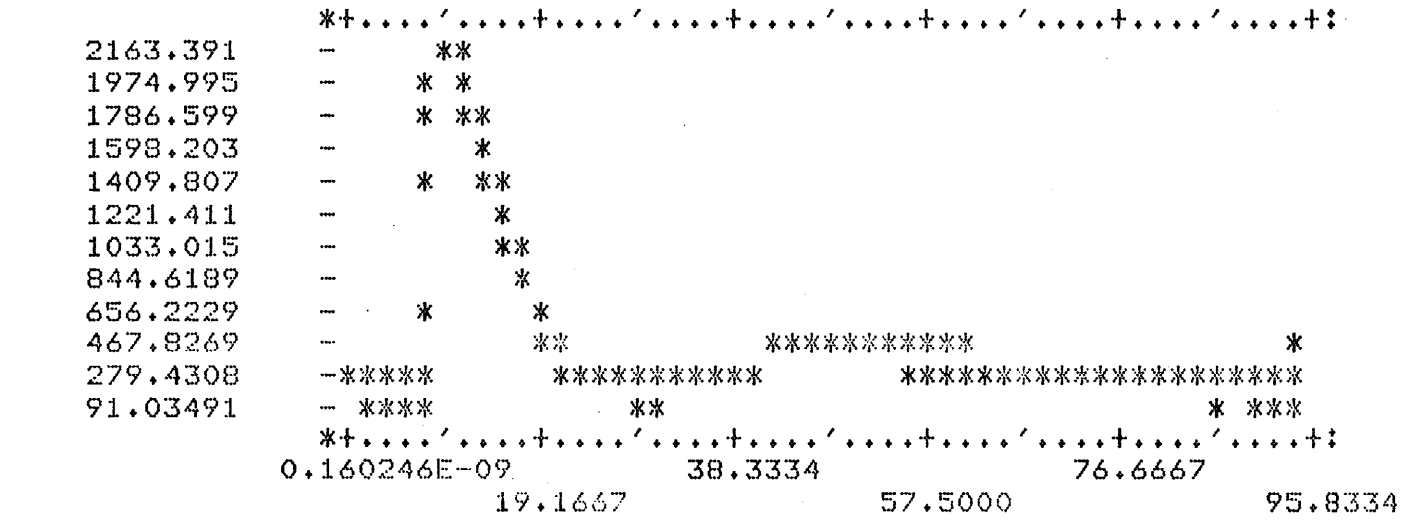

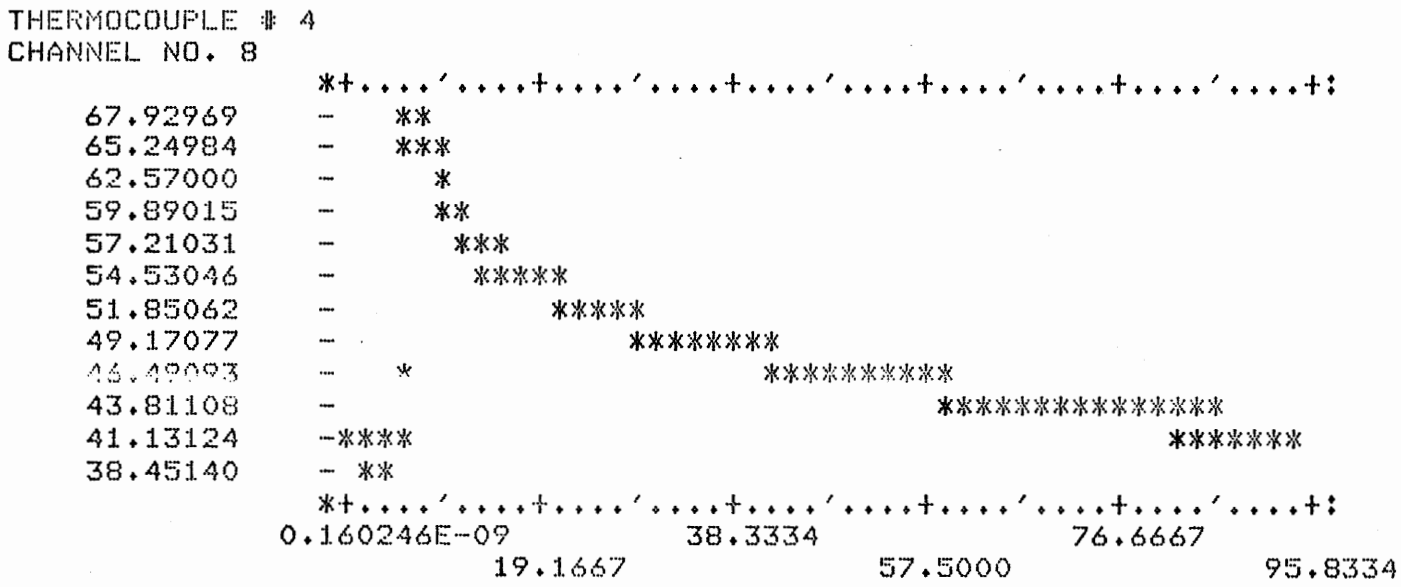
THERMOCOUPLE # 4
CHANNEL NO. 8
67.92969
65.24984
62.57000
59.89015
57.21031
54.53046
51.85062
49.17077
46.49093
43.81108
41.13124
38.45140
0.160246E-09
19.1667
38.3334
57.5000
76.6667
95.8334

PRESSURE TRANSDUCER # 4
CHANNEL NO. 2

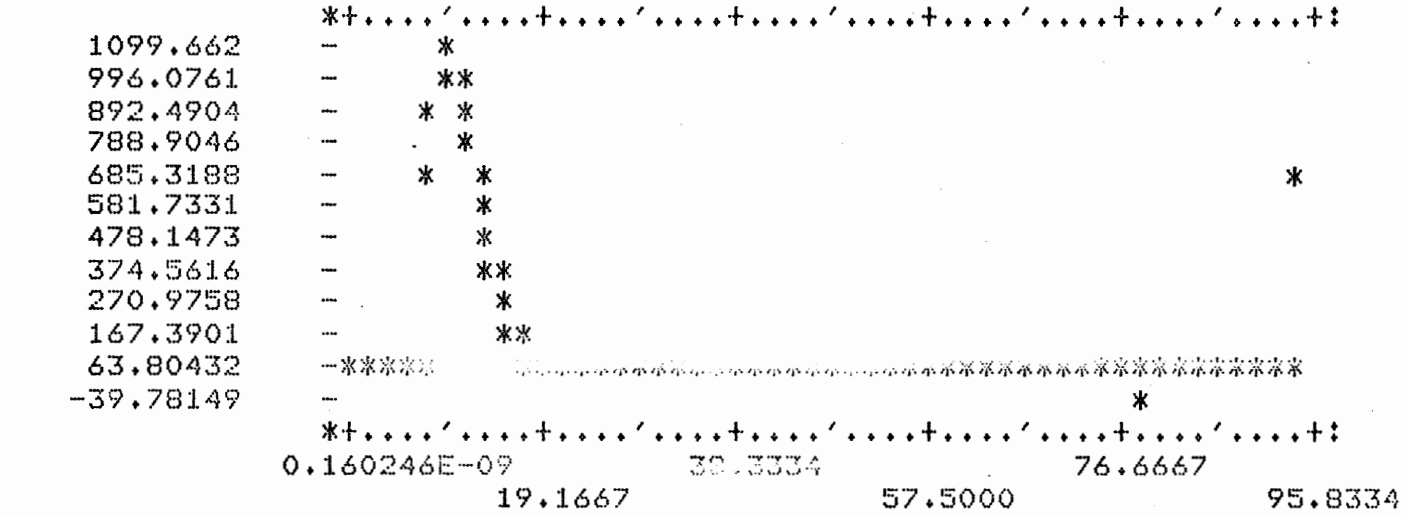

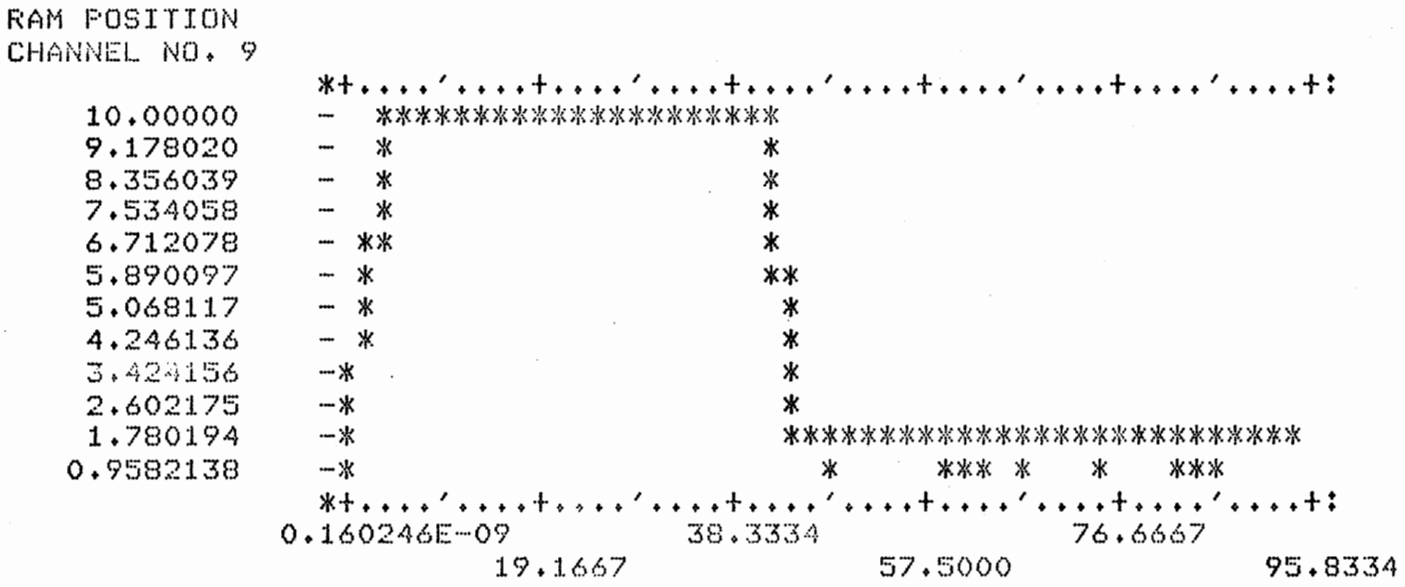
RAM POSITION
CHANNEL NO. 9
10.00000
9.178020
8.356039
7.534058
6.712078
5.890097
5.068117
4.246136
3.424156
2.602175
1.780194
0.9582138
0.160246E-09
19.1667
38.3334
57.5000
76.6667
95.8334

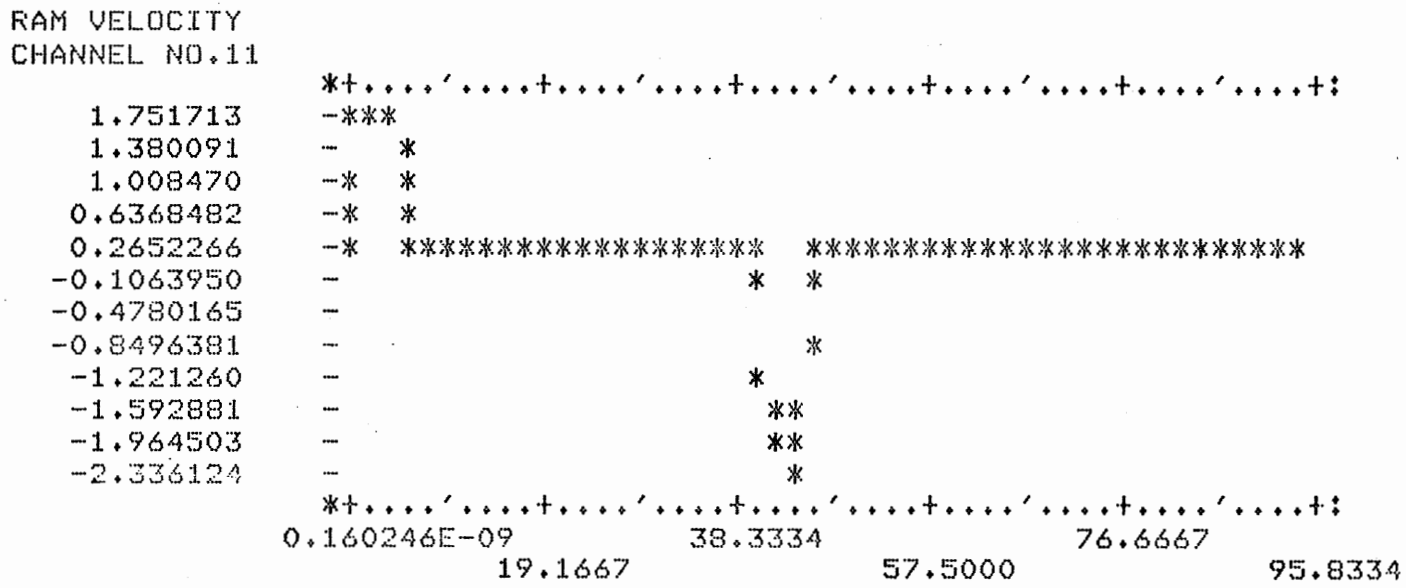
RAM VELOCITY
CHANNEL NO.11
1.751713
1.380091
1.008470
0.6368482
0.2652266
-0.1063950
-0.4780165
-0.8496381
-1.221260
-1.592881
-1.964503
-2.336124
0.160246E-09
19.1667
38.3334
57.5000
76.6667
95.8334

RESULTS FOR THE INJECTION CYLE RUN AT

$T' = 290\ ^{o}F$; $P' = 11000$ Psig ; $Q'_{o} = 0.63\ \frac{in^3}{sec}$

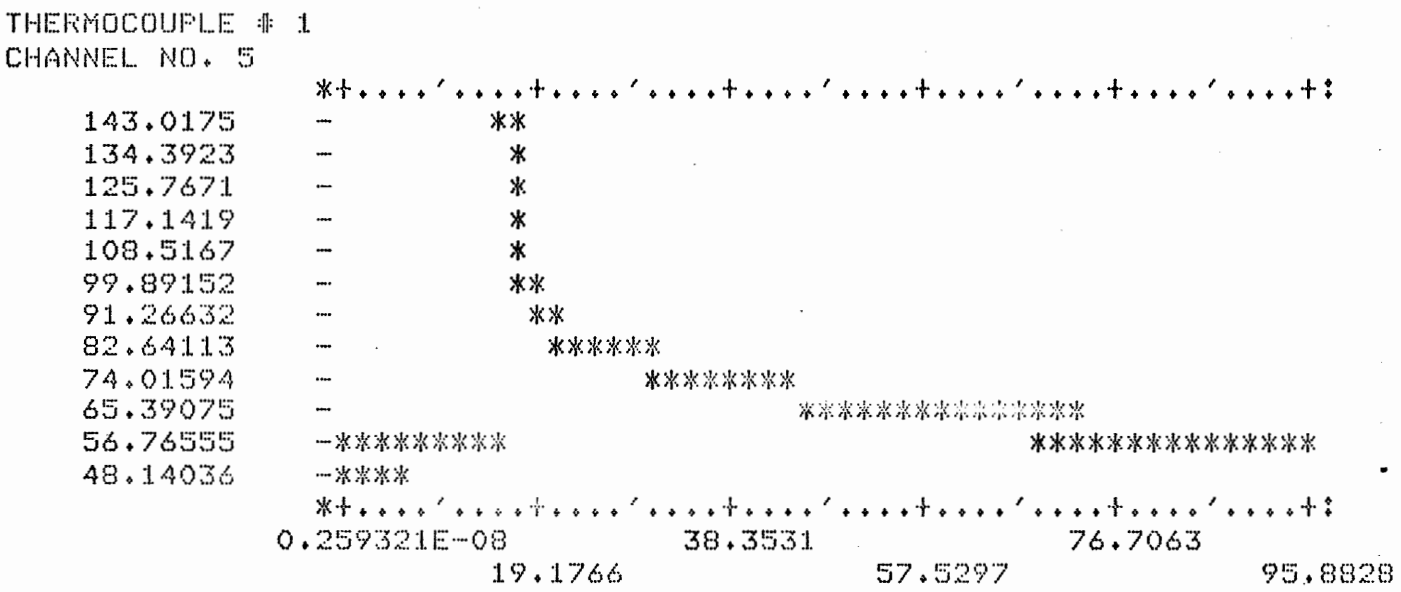
THERMOCOUPLE # 1
CHANNEL NO. 5
143.0175
134.3923
125.7671
117.1419
108.5167
99.89152
91.26632
82.64113
74.01594
65.39075
56.76555
48.14036
0.259321E-08
19.1766
38.3531
57.5297
76.7063
95.8828

PRESSURE TRANSDUCER # 1
CHANNEL NO. 4

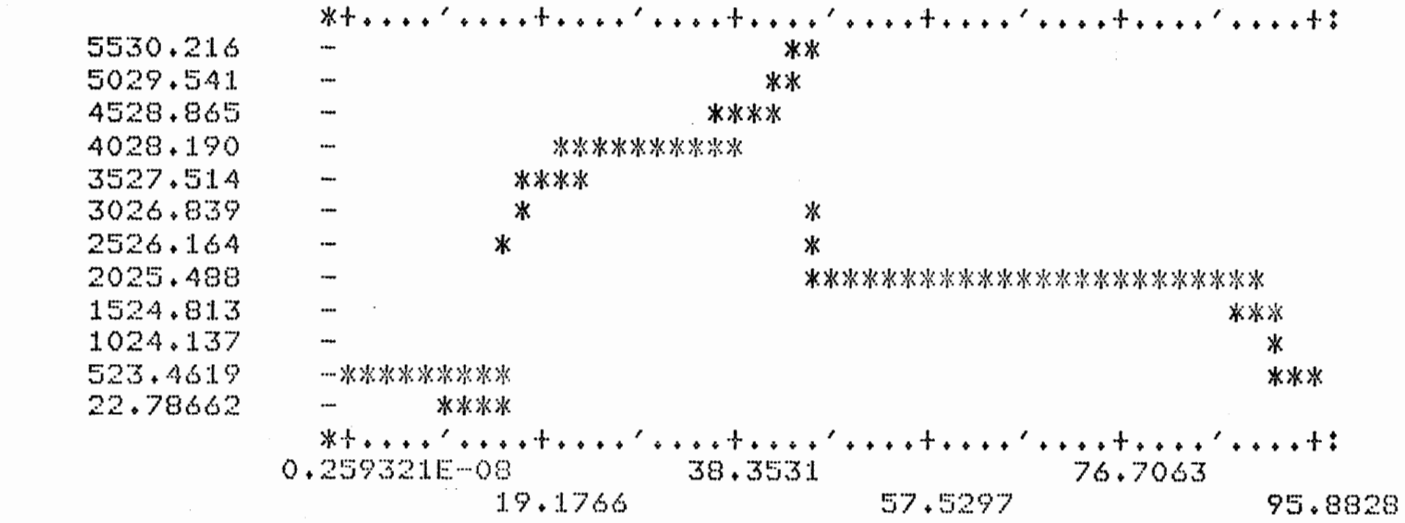

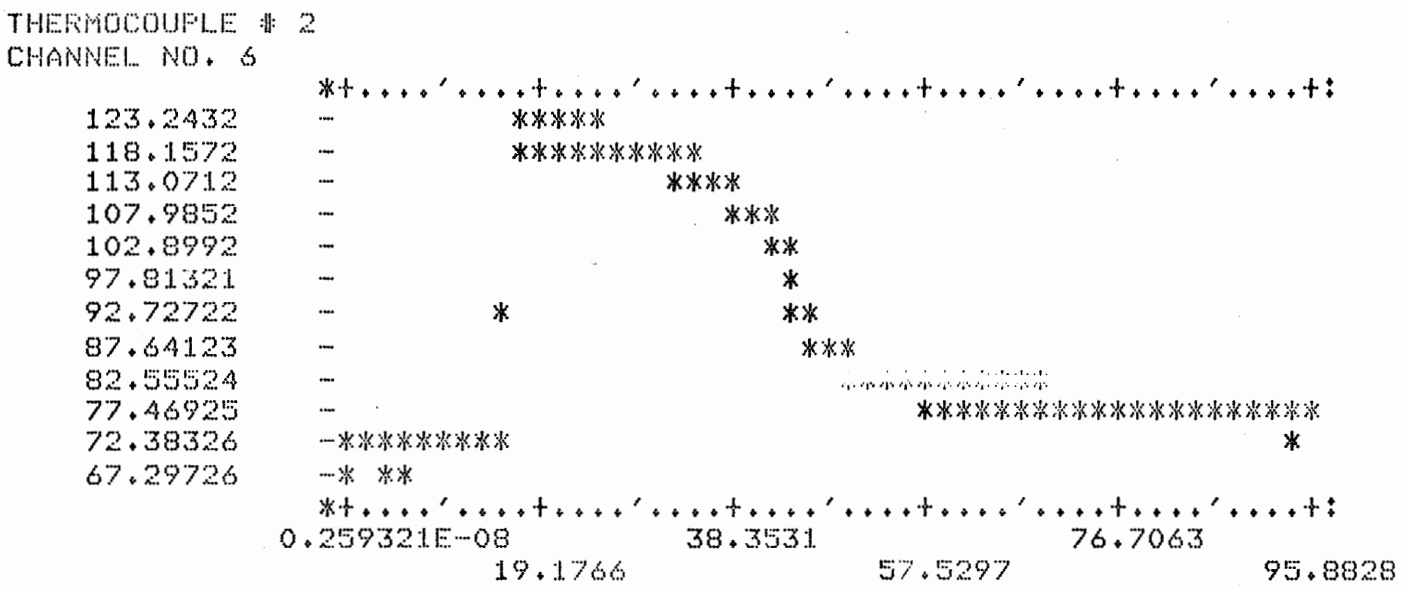
THERMOCOUPLE # 2
CHANNEL NO. 6
123.2432
118.1572
113.0712
107.9852
102.8992
97.81321
92.72722
87.64123
82.55524
77.46925
72.38326
67.29726
0.259321E-08
19.1766
38.3531
57.5297
76.7063
95.8828

PRESSURE TRANSDUCER # 2
CHANNEL NO. 1

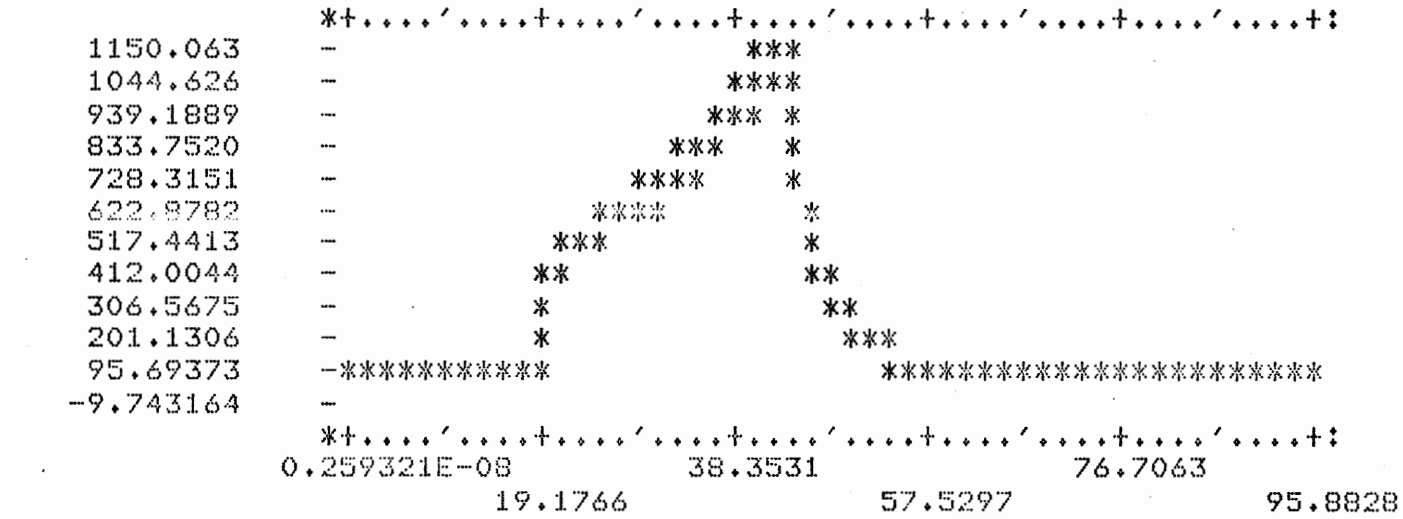

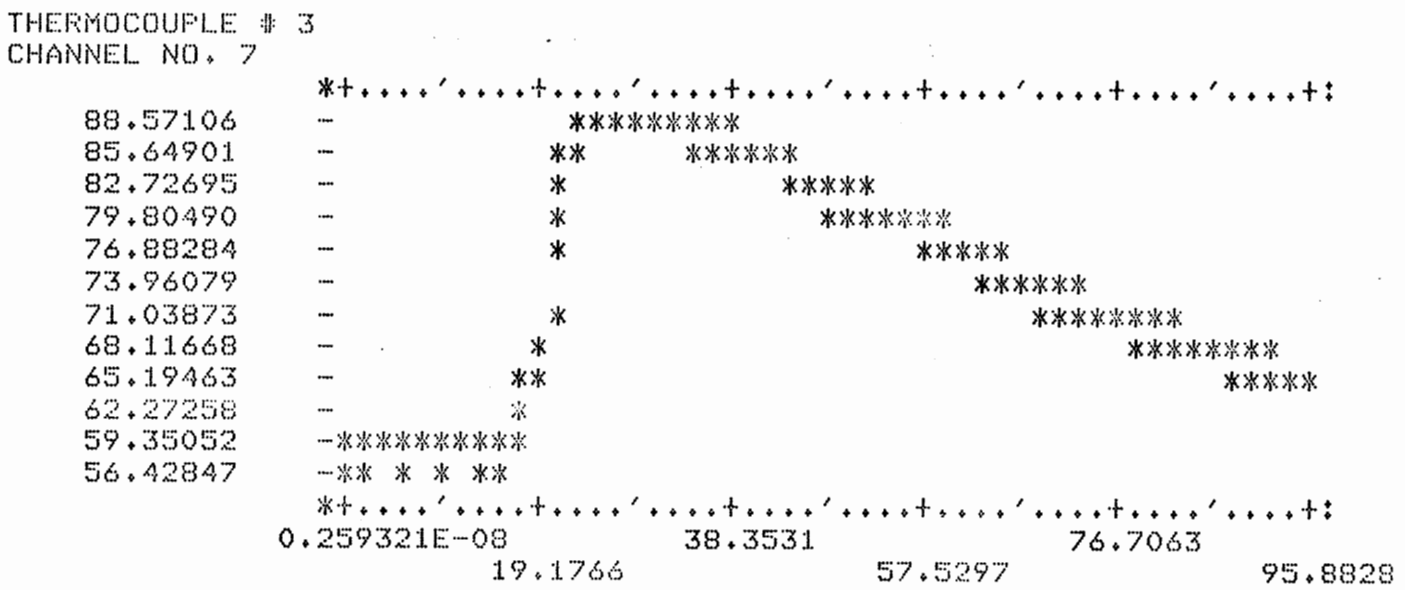
THERMOCOUPLE # 3
CHANNEL NO. 7
88.57106
85.64901
82.72695
79.80490
76.88284
73.96079
71.03873
68.11668
65.19463
62.27258
59.35052
56.42847
0.259321E-08
19.1766
38.3531
57.5297
76.7063
95.8828

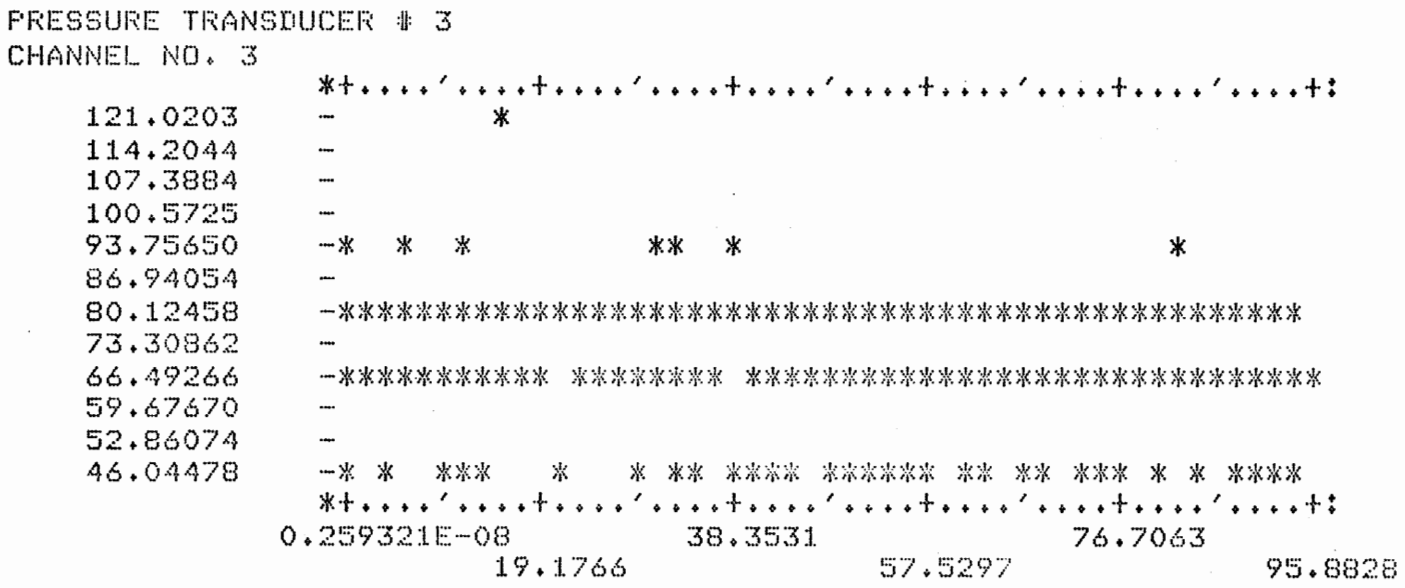
PRESSURE TRANSDUCER # 3
CHANNEL NO. 3
121.0203
114.2044
107.3884
100.5725
93.75650
86.94054
80.12458
73.30862
66.49266
59.67670
52.86074
46.04478
0.259321E-08
19.1766
38.3531
57.5297
76.7063
95.8828

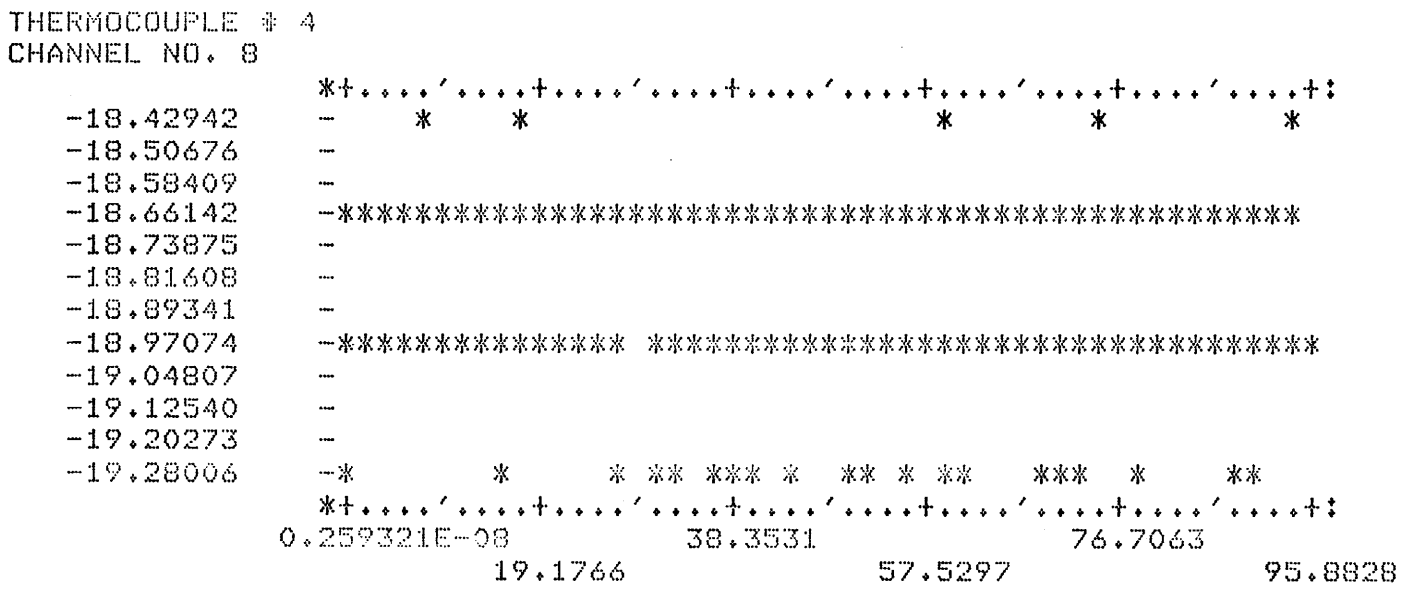
THERMOCOUPLE # 4
CHANNEL NO. 8
-18.42942
-18.50676
-18.58409
-18.66142
-18.73875
-18.81608
-18.89341
-18.97074
-19.04807
-19.12540
-19.20273
-19.28006
0.259321E-08
19.1766
38.3531
57.5297
76.7063
95.8828

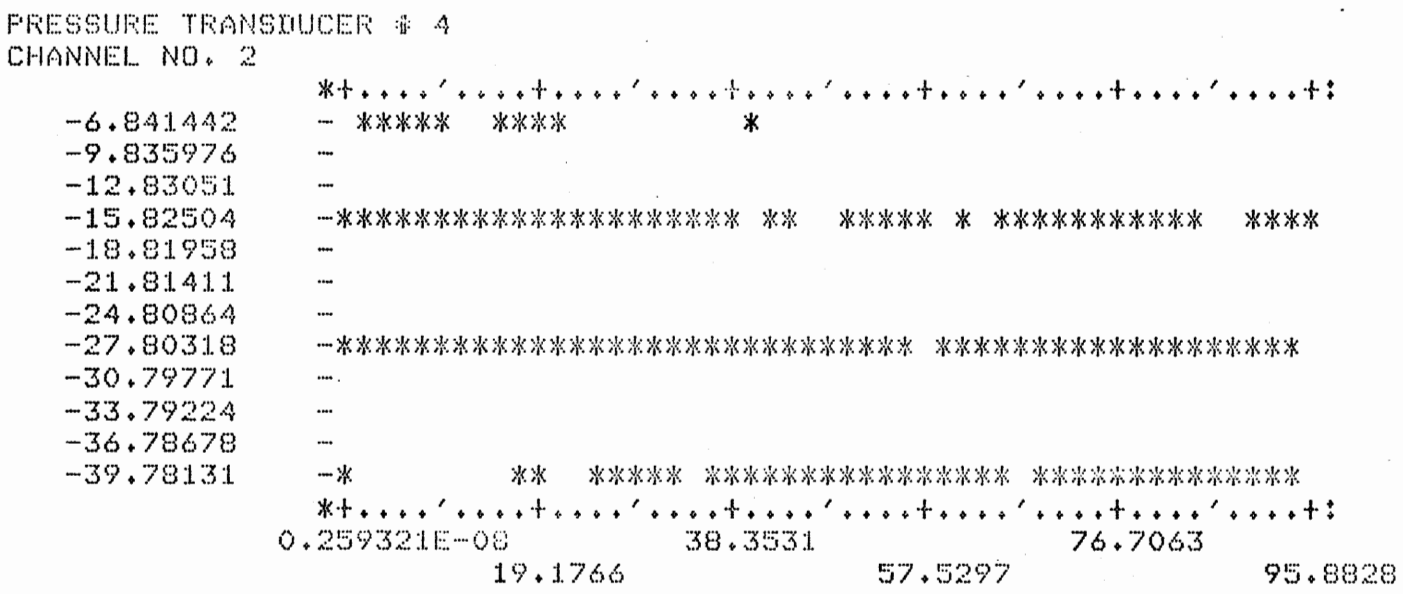
PRESSURE TRANSDUCER # 4
CHANNEL NO. 2
-6.841442
-9.835976
-12.83051
-15.82504
-18.81958
-21.81411
-24.80864
-27.80318
-30.79771
-33.79224
-36.78678
-39.78131
0.259321E-08
19.1766
38.3531
57.5297
76.7063
95.8828

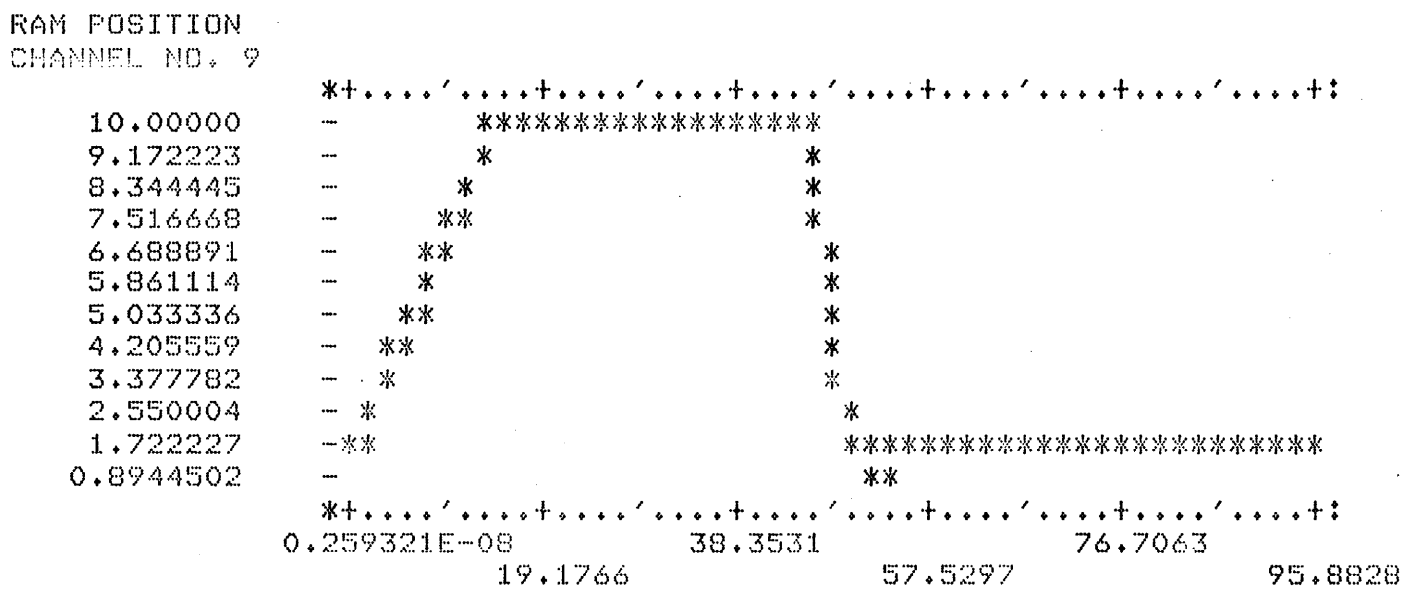
RAM POSITION
CHANNEL NO. 9
10.00000
9.172223
8.344445
7.516668
6.688891
5.861114
5.033336
4.205559
3.377782
2.550004
1.722227
0.8944502
0.259321E-08
19.1766
38.3531
57.5297
76.7063
95.8828

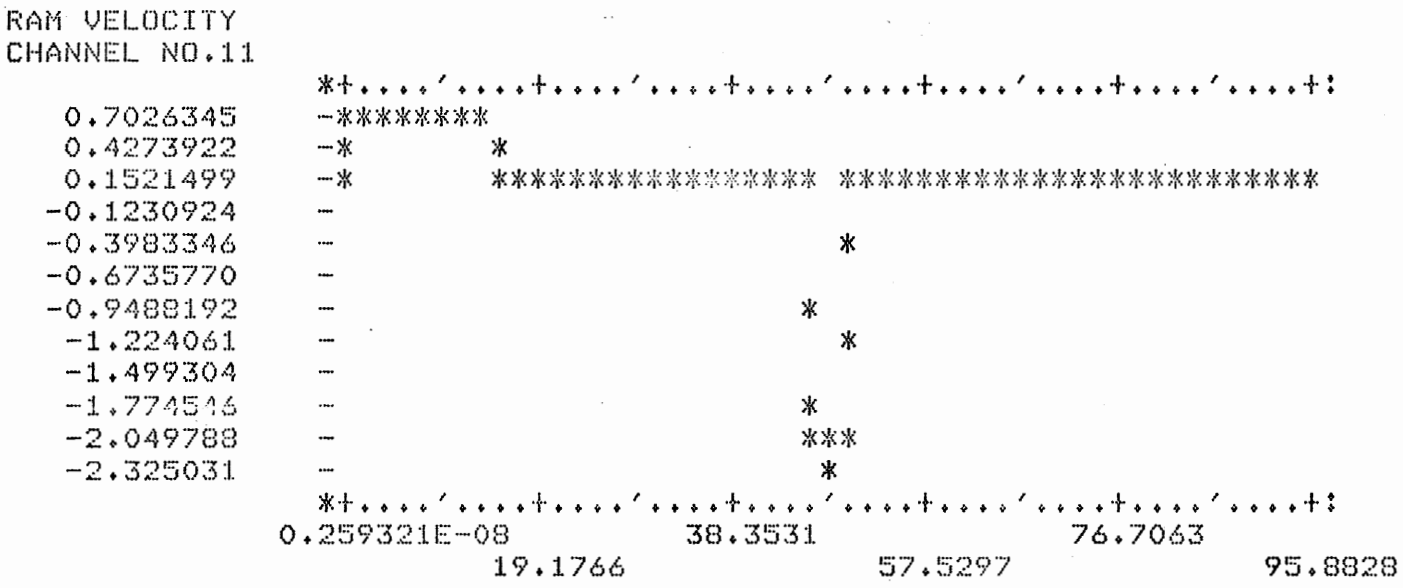
RAM VELOCITY
CHANNEL NO.11
0.7026345
0.4273922
0.1521499
-0.1230924
-0.3983346
-0.6735770
-0.9488192
-1.224061
-1.499304
-1.774546
-2.049788
-2.325031
0.259321E-08
19.1766
38.3531
57.5297
76.7063
95.8828

VITA

The author was born on April 23, 1948, in Caracas, Venezuela. He is the oldest son of Mr. and Mrs. Jacobo Echenagucia. He graduated from elementary and high school in Caracas. Mr. Echenagucia entered the Universidad Central of Venezuela in July 1965. After the completion of eight semesters at that institution, he transferred to the University of Texas at Austin in January 1972, where he received his B.S. in Chemical Engineering in August 1973. While in high school and college in Caracas, he participated and lettered in varsity level baseball and soccer.

In the Fall of 1973 he enrolled in the Chemical Engineering Department at Virginia Polytechnic Institute and State University, where he has served as a Graduate Teaching Assistant and as a student representative to the Graduate Assembly. During his studies at the University of Texas, Mr. Echenagucia was awarded two scholarships by the University of Texas and the Venezuelan Government respectively. In February of 1975 he received his M.S. in Chemical Engineering. During the summer of 1975 Mr. Echenagucia went to Venezuela to work for Exxon Co. There, he was awarded a scholarship to continue graduate studies in Chemical Engineering leading to the Ph.D. degree.

Upon graduation the author will work as a consultant for

the Venezuelan plastic industry and as a chief process engineer for a Venezuelan firm.

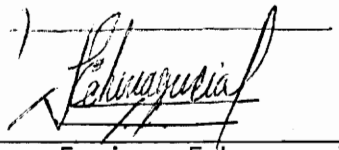

Jorge Enrique Echenagucia

GATE DESIGN FOR INJECTION MOLDS

by

Jorge Enrique Echenagucia

(ABSTRACT)

The design of gates for injection molds is a subject too often neglected when consideration is being given to the various problems related to product quality. The effect which gate design has on the properties of the molded part is as important as its effect on the molding cycle. Despite of the great advances in mold design techniques, gates are still designed by a trial and error procedure.

In this investigation a design procedure for gates and runner systems for injection molds of pseudoplastic materials was developed. The steps followed in this study included: (1) Selection of a suitable polymer for molding purposes. In this instance, low density polyethylene was selected because of the large amount of literature published on its processing, mechanical and physical properties, (2) Determination of a viscosity-shear rate-temperature relationship for polyethylene, (3) Development of a mathematical model of the complete injection molding cycle. This model was used to predict the effect of the gate dimensions on the properties of the polymer being molded, (4) Design and construction of an injection mold and monitoring system to validate the proposed model, (5) Development of a gate design procedure based on the predictions of the model.

The temperature and pressure data from four thermocouples and pressure transducers, located in the runner, gate and cavity respectively, were taken every 80 milliseconds by the monitoring system. The experimental data for each molding cycle was then stored on a disc unit. Using a software package developed in this investigation, the data could be immediately printed or plotted.

Comparison of the experimental and model predicted data show that they are in good agreement. Some discrepancies were observed, but they were explained in terms of: (1) the impossibility of accurately determining the initial volumetric flow rate, (2) the fact that the viscosity equation applies for a narrow range of shear rates, (3) the use of constant physical properties for polyethylene as a first approximation, (4) the difficulties experienced to keep the thermocouples from being pushed inside their cavity due to the high pressures developed during the molding process, (5) the non-constant feed rate delivered by the injection molder, (6) the use of average, instead of local, pressures and temperatures in the packing and cooling models.

The results of the model were used to develop a graphical optimization technique to determine optimum gate dimensions.